

ISTANBUL TECHNICAL UNIVERSITY ★ GRADUATE SCHOOL OF SCIENCE
ENGINEERING AND TECHNOLOGY

**DESIGN, SIMULATION AND ANALYSIS OF PIEZORESISTIVE
MICROCANTILEVER FOR BIOSENSING APPLICATIONS**

M.Sc. THESIS

Amal AHMED

Department of Nano Science and Nano Engineering

Nano Science and Nano Engineering Programme

December 2016

ISTANBUL TECHNICAL UNIVERSITY ★ GRADUATE SCHOOL OF SCIENCE
ENGINEERING AND TECHNOLOGY

**DESIGN, SIMULATION AND ANALYSIS OF PIEZORESISTIVE
MICROCANTILEVER FOR BIOSENSING APPLICATIONS**

M.Sc. THESIS

**Amal AHMED
(513131026)**

Department of NanoScience and NanoEngineering

Nano Science and NanoEngineering Programme

Thesis Advisor: Prof. Dr. Levent TRABZON

December 2016

ISTANBUL TEKNİK ÜNİVERSİTESİ ★ FEN BİLİMLERİ ENSTİTÜSÜ

**BİYOLOJİK TESPİT UYGULAMALARI İÇİN PIEZORESİSTİVE
MİKROKANTİLEVER TASARIM, SİMÜLASYON VE ANALİZİ**

YÜKSEK LİSANS TEZİ

**Amal AHMED
(513131026)**

Nano Bilim ve Nano Mühendisliği Anabilim Dalı

Nano Bilim ve Nano Mühendisliği Programı

Tez Danışmanı: Prof. Dr. Levent TRABZON

Aralık 2016

Amal Ahmed, a M.Sc. student of İTÜ Graduate School of Science Engineering and Technology student ID 513131026, successfully defended the thesis entitled “DESIGN, SIMULATION AND ANALYSIS OF PIEZORESISTIVE MICROCANTILEVER FOR BIOSENSING APPLICATIONS”, which she prepared after fulfilling the requirements specified in the associated legislations, before the jury whose signatures are below.

Thesis Advisor : **Prof. Dr. Levent TRABZON**
Istanbul Technical University

Jury Members : **Doç. Dr. Turgut GÜLMEZ**
Istanbul Technical University

Doç. Dr. Erdem ALACA
Koç University

Date of Submission : 25 November 2016
Date of Defense : 20 December 2016

To my Father's Soul, May he rest in peace

FOREWORD

Alhamdulillah for giving me uncountable blessings including giving me this masters degree opportunity, the strength and the patience to complete my project despite all the challenges and difficulties.

First I would like to thank my supervisor Prof. Levent Trabzon. I would also like to thank my caring and loving mom who raised me to be as good as I'm right now, and my dad who was impatiently waiting for me to get my masters degree and come back home but he passed away before this day has come. May he rest in peace.

My sincere thanks also goes to my sisters and brothers who surrounded me with their love and support.

I also would like to thank my friends for their support and prayers. They believed in me more than I did in myself.

Last but not least, I would like to thank Turkey scholarship team (Türkiye Bursları) for granting me this life changing opportunity.

November 2016

Amal AHMED

TABLE OF CONTENTS

	<u>Page</u>
FOREWORD	ix
TABLE OF CONTENTS	xi
ABBREVIATIONS	xv
SYMBOLS	xvii
LIST OF TABLES	xix
LIST OF FIGURES	xxi
SUMMARY	xxv
ÖZET	xxix
1. INTRODUCTION	1
1.1 BioMEMS	1
1.1.1 Introduction to BioMEMS	1
1.1.2 The Overlap between Bio-MEMS, LOC and μ TAS	2
1.1.3 BioMEMS Applications	3
1.1.3.1 BioMEMS for Detection, Analysis, and Diagnosis	3
1.1.3.2 BioMEMS for therapeutics	3
1.1.3.3 BioMEMS for Drug Delivery	4
1.1.3.4 BioMEMS for Cell culture and tissue engineering	4
1.1.3.5 Bio-MEMS for medical implants and surgery	4
1.2 Bio-MEMS as Miniaturized Biosensors	5
1.2.1 Introduction to Biosensors	5
1.2.2 Detection methods	5
1.2.2.1 BioMEMS and electrical detection	5
1.2.2.2 BioMEMS and optical detection	6
1.2.2.3 BioMEMS and mechanical detection	6
1.3 Microcantilever-Based Biosensors	6
2. THEORY	9
2.1 Introduction	9
2.2 Cantilever Working Modes	10
2.2.1 Static mode	10
2.2.2 Dynamic mode	11
2.2.3 Heat mode	12
2.2.4 Lorentz force based cantilever actuation	12
2.3 Cantilever Transducing Mechanisms	13
2.3.1 Optical	14
2.3.1.1 Detection mechanism	14
2.3.1.2 Advantages	14
2.3.1.3 Disadvantages	14
2.3.2 Capacitive	15
2.3.2.1 Detection mechanism	15
2.3.2.2 Advantages	15
2.3.2.3 Disadvantages	15
2.3.3 Piezoelectric	15

2.3.3.1	Detection mechanism	15
2.3.3.2	Advantages	16
2.3.3.3	Disadvantages.....	16
2.3.4	Piezoresistive.....	16
2.3.4.1	Detection mechanism	16
2.3.4.2	Advantages	16
2.3.4.3	Disadvantages.....	17
2.3.5	Comparison.....	17
2.4	Piezoresistive Microcantilever Theory.....	17
2.4.1	Strain effect on crystal materials	18
2.4.2	Piezoresistive effect.....	19
2.4.3	Microcantilever based piezoresistive sensors.....	23
2.4.4	Piezoresistance Temperature and Doping Dependency	25
3.	SENSOR DESIGN AND SIMULATION.....	27
3.1	General Optimization Procedure	27
3.1.1	Optimization parameters	28
3.1.2	Optimization flowchart	29
3.2	Starting Piezoresistive Microcantilever.....	31
3.2.1	Sensor definition	31
3.2.2	Multiphysics setup.....	32
3.2.3	Mesh and solver studies	33
3.3	Piezoresistor Material Selection	33
3.4	Choosing the Piezoresistor Doping level	34
3.5	Cantilever Material Optimization.....	34
3.6	Optimizing Cantilever Shape	34
3.6.1	Rectangular.....	34
3.6.2	Pi-shape from cantilever (Double legged)	35
3.6.3	T shape cantilever (one legged)	36
3.6.4	Trapezoid shape cantilever.....	36
3.6.5	Stepped Trapezoid shape cantilever.....	37
3.6.6	Triangular shape cantilever	38
3.7	Stress Concentration Region	39
3.8	Range of Force	40
3.9	Fabrication.....	40
4.	RESULTS AND DISCUSSION.....	43
4.1	Starting Sensor.....	43
4.2	Piezoresistor Material Selection	45
4.3	Choosing the Piezoresistor Doping Level	46
4.4	Cantilever Material Optimization.....	48
4.5	Optimizing Cantilever Shape	49
4.5.1	Rectangular.....	49
4.5.2	Pi shape cantilever (Double legged).....	53
4.5.3	T shape cantilever (one legged)	54
4.5.4	Trapezoid shape cantilever.....	55
4.5.5	Stepped Trapezoid shape cantilever.....	57
4.5.6	Triangular shape cantilever	59
4.6	Comparison between different shapes.....	60
4.7	Stress Concentration Region (SCR)	61
4.8	Final Sensor Design.....	64
4.9	Comparison with Prior Works Available in Open Literature.....	66

5. CONCLUSIONS, RECOMMENDATIONS AND FUTURE WORK.....	69
5.1 Conclusions	69
5.2 Recommendations and Future Work.....	70
REFERENCES.....	71
CURRICULUM VITAE.....	81

ABBREVIATIONS

AFM	: Atomic Force Microscopy
AC	: Alternating Current
BioMEMS	: Biomedical (or biological) Microelectromechanical Systems
CAGR	: Compound Annual Growth Rate
DNA	: Deoxyribonucleic Acid
FEA	: Finite Element Analysis
GF	: Gauge Factor
LOC	: Lap-on-chip
MEMS	: Microelectromechanical Systems
MOSFET	: Metal–Oxide–Semiconductor Field-Effect Transistor
μTAS	: Micro total analysis systems
NeuroMEMS	: Neural MEMS probes
SCR	: Stress concentration Region
SPR	: Surface Plasmon Resonance
PSD	: Position-Sensitive Detector

SYMBOLS

δ	: Cantilever displacement
ν	: Poisson's ratio,
E	: Young's modulus,
σ	: Stress
l	: Length
w	: Width
h	: Height
t	: Thickness
k	: Spring constant
f_n	: Resonance frequency
m	: Mass
F	: Force
q	: Charged particle
v	: Velocity
E	: Electric Field
B	: Magnetic field
I	: Current
V	: Voltage
ε, e	: Strain
τ, T	: Stress
$C_{ij\alpha\beta}$: Elastic stiffness constants
R	: Resistance
ΔR	: The change of resistance
ρ	: Resistivity
ν	: Poisson ratio
GF	: Gauge factor
π_{ik}	: The piezoresistance coefficients
P	: Piezoresistance factor
N	: Doping Level
T	: Temperature

LIST OF TABLES

	<u>Page</u>
Table 2.1: Normalized piezoresistance under some combination of stress and current directions.....	21
Table 2.2: π -Coefficients for bulk Si and Ge (10^{-11}Pa^{-1}).....	22
Table 3.1: Starting Sensor Specifications.....	31
Table 3.2: Material properties.....	31
Table 4.1: longitudinal (π_l) and transverse piezoresistive coefficients (π_t) of a Polysilicon material.....	44
Table 4.2: The Starting Sensor Simulation Results...../.....	44
Table 4.3: Longitudinal (π_l) and transverse piezoresistive coefficients (π_t) of a silicon $\langle 100 \rangle$ wafer for a doping level of 10^{16}cm^{-3}	46
Table 4.4: Polysilicon Transverse piezoresistance coefficient (π_t) for different doping level calculated from the piezoresistance factor plot (T=300K)....	47
Table 4.5: Simulation Results when Different Piezoresistor Doping levels were used	47
Table 4.6: Simulation results when Different Cantilever materials were used.....	48
Table 4.7: Simulation results when Different Cantilever thicknesses were used.....	50
Table 4.8: Simulation Results when Different Cantilever Lengths were Used.....	51
Table 4.9: Simulation Results when Different Cantilever Widths were used.....	53
Table 4.10: Simulation Results for Pi-shape cantilever variations.....	54
Table 4.11: Simulation Results for T-shape cantilever variations.....	55
Table 4.12: Simulation Results for Trapezoid Shape Cantilever variations.....	56
Table 4.13: Simulation Results for Stepped-Trapezoid Shape Cantilever variations... ..	58
Table 4.14: Simulation Results for Triangular Shape Cantilever variations.....	60
Table 4.15: Comparison between the Simulation Results for the Different Cantilever Shapes.....	61
Table 4.16: Effect of Adding Stress Concentration Region (SCR) at different positions.....	63
Table 4.17: Optimized Sensor results when Different Forces Are Applied.....	66

LIST OF FIGURES

	<u>Page</u>
Figure 1.1: Some aspects of the fields of bio-MEMS, lab-on-a-chip, μ TAS and the overlapping between them.....	2
Figure 2.1 : Piezoresistance coefficients and corresponding stress-current configuration.....	22
Figure 2.2: Two cases of rectangular piezoresister orientations with respect to stress, T : (a) Longitudinal current, (b) transverse current.....	23
Figure 2.3: Wheatstone Bridge.....	24
Figure 2.4: Longitudinal and transverse π -coefficients for p-type Si in the (100) plane.....	24
Figure 2.5: Attenuation factor for bulk p-type Si piezoresistance coefficients as a function of boron concentration.....	25
Figure 3.1: Sensor Optimization procedure flowchart.....	30
Figure 3.2: Starting Sensor.....	32
Figure 3.3: Starting Sensor's mesh.....	33
Figure 3.4: Pi-Shape sensor (a) Structure (b) Mesh.....	36
Figure 3.6: T-Shape sensor (a) Structure (b) Mesh.....	36
Figure 3.6 : Trapezoid Shape sensor (a) 1:1 (b) 1:2 (c) 1:3 and (d) 1:4.....	37
Figure 3.7 : Stepped-Trapezoid Shape sensor (a) 1:1 (b) 1:2 (c) 1:3 and (d) 1:4.....	38
Figure 3.8: Triangular Shape sensor (a) $100\mu\text{m}\times 100\mu\text{m}$ Gold layer (b) $100\mu\text{m}\times 100\mu\text{m}$ Gold layer mesh (c) $200\mu\text{m}\times 50\mu\text{m}$ Gold layer (d) $200\mu\text{m}\times 50\mu\text{m}$ Gold layer mesh.....	39
Figure 3.9 : Cross-section view of the Sensor Fabrication sequence : (a) DSP wafer (b) Wafer covered with SiO_2 in both sides (c) Polysilicon deposition and patterning (d) Reversed photoresist and Gold deposition (e) Gold Liftoff (f) Reversed photoresist and Aluminum deposition (g)Aluminum Lift-off, (h) SiO_2 patterning (i) Final sensor cross section.....	42
Figure 3.10: Fabrication Masks (a) Piezoresistor mask (b) Gold Mask (c) Aluminum connections mask (d) Cantilever shape mask (e) Cantilever holes backside mask.....	42
Figure 4.1: Starting Sensor Results (a) Von Mises stress plot, (b) Piezoresistor potential plot and (c) Deflection plot.....	43
Figure 4.2: Von Mises stress plot (a) Single crystal silicon piezoresistor (b) Polysilicon piezoresistor.....	45
Figure 4.3: The piezoresistance factor of p-type silicon plotted as a function of dopant concentration for several operating temperatures.....	46
Figure 4.4: The $\frac{\Delta R}{R}$ Sensitivity of the sensor when Different Doping Level was used for the p-type Polysilicon piezoresistor.....	48
Figure 4.5: Maximum Von Mises Stress and Maximum deflection values for various cantilever materials.....	49
Figure 4.6: The $\frac{\Delta R}{R}$ Sensitivity of the Sensor when the Cantilever was Built from	

Different Materials.....	49
Figure 4.7: Maximum Von Mises Stress and Maximum Deflection Values for Different Rectangular Cantilever Thicknesses.....	50
Figure 4.8: The $\Delta R/R$ Sensitivity of the Sensor when for Different Cantilever Thicknesses.....	51
Figure 4.9: Maximum Von Mises Stress and Maximum Deflection Values for Different Rectangular Cantilever Lengths.....	52
Figure 4.10: The $\Delta R/R$ Sensitivity of the Sensor for Different Rectangular Cantilever Lengths.....	52
Figure 4.11: Maximum Von Mises Stress and Maximum Deflection Values for Different Rectangular Cantilever Widths.....	53
Figure 4.12: The $\Delta R/R$ Sensitivity of the Sensor for Different Rectangular Cantilever Widths.....	53
Figure 4.13: Optimized Rectangular Cantilever (a) Von Mises stress plot, (b) Deflection Plot.....	54
Figure 4.14: Optimized Pi-shape Cantilever (a) Von Mises stress plot, (b) Deflection Plot.....	55
Figure 4.15: Optimized T-shape Cantilever (a) Von Mises stress plot, (b) Deflection Plots.....	56
Figure 4.16: Maximum Von Mises Stress and Maximum Deflection Values for Different Trapezoid cantilevers designs.....	57
Figure 4.17: The $\Delta R/R$ Sensitivity of the Sensor for Different Trapezoid cantilevers designs.....	57
Figure 4.18: Optimized Trapezoid Cantilever (a) Von Mises stress plot, (b) Deflection Plot.....	58
Figure 4.19: Maximum Von Mises Stress and Maximum Deflection Values for Different Stepped-Trapezoid cantilevers designs.....	59
Figure 4.20: The $\Delta R/R$ Sensitivity of the Sensor for Different Stepped-Trapezoid cantilevers designs	59
Figure 4.21: Optimized Stepped-Trapezoid Cantilever (a) Von Mises stress plot, (b) Deflection Plot.....	60
Figure 4.22: Optimized Triangular Cantilever (a) Von Mises stress plot, (b) Deflection Plot.....	61
Figure 4.23: Maximum Von Mises Stress and Maximum Deflection Values for Different Cantilever shapes.....	62
Figure 4.24: The $\Delta R/R$ Sensitivity of the Sensor for Different Cantilever shapes.	62
Figure 4.25: Final Optimized Sensor (a) Geometry, (b) Von Mises stress plot and (C) Deflection Plot.....	63
Figure 4.26: Trapezoid Cantilever with 90 degrees Oriented SCR hole (a) Geometry (b) Von Mises Stress Plot.....	64
Figure 4.27: Final Optimized Sensor Mode Shapes (a) 4.86KHz, (b) 42.66KHz, (c)54.73KHz, (d) 0.16MHz, (e) 0.17MHz and (f) 0.248MHz.....	65
Figure 4.28: The $\Delta R/R$ Sensitivity of the Sensor for Different Cantilever shapes..	66
Figure 4.29: The biosensor's Whinstone bridge circuit.....	67

DESIGN, SIMULATION AND ANALYSIS OF PIEZORESISTIVE MICROCANTILEVER FOR BIOSENSING APPLICATIONS

SUMMARY

In the past decade, several research works demonstrated the ability of Biological Microelectromechanical System (Bio-MEMS) biosensors to detect of biomolecules such as Deoxyribonucleic Acid (DNA), proteins, Bacteria and Antigens. But due to the low concentration of the analytes that need to be detected in the samples, a minuscule signal results in the output of the sensor.

In response to this, a need arisen for an optimized biosensor capable of giving high output signal in response the detection of few analytes in the sample; the ultimate goal is being able to convert the attachment of a single biomolecule into a measurable quantity.

For this purpose, MEMS microcantilevers based biosensors have emerged as a promising sensing solution because it is simple, cheap, highly sensitive and more importantly does not need analytes optical labeling (Label-free). Among the different microcantilever transducing techniques, piezoresistive based microcantilever biosensors seem to be a more attractive solution being cheap, high sensitive, miniature, works well in liquid environments and having integrated readout system.

Even though there are many publications in literature that concentrated on increasing the piezoresistive microcantilevers sensitivity, they only considered in optimizing few design and process parameters thus the resultant sensitivity enhancements are not good enough for practical applications.

After the analyzation of the work found in literature, it was found that the parameters/approaches that be can be optimized/used to enhance the sensitivity of Piezoresistive microcantilever-based sensors are: Cantilever dimensions, Cantilever Material, Cantilever Shape, Piezoresistor's material, Piezoresistor's doping level, Piezoresistor's Dimensions, Piezoresistor's position, Stress concentration Region's (SCR) shape and position.

In this study, after a systematic analyzation of the effect of each design and process parameters on the sensitivity, a step-wise optimization approach was developed in which almost all these parameters were variated one at each step while fixing the others to get the maximum possible sensitivity at the end. Throughout this work, COMSOL Multiphysics 5.0, a commercial Finite Element Analysis (FEA) tool, was used to simulate the sensor performance.

At each optimization step, the goal was to optimize the parameter in such a way that it maximizes and concentrates the stress in piezoresistors region for the same applied force thus get the higher sensitivity. In total, almost 46 different simulations were done to get the final optimized sensor.

Starting with a rectangular cantilever, the piezoresistor material and doping level were optimized in two steps. When the piezoresistor material was varied (single crystal silicon and Poly-silicon), it was found that the $\Delta R/R$ sensitivity is higher in the case of single crystal silicon.

But for this sensor design, polysilicon has been chosen as the piezoresistor material because its sensitivity does not depend on the crystal orientation, the sensor fabrication is easier, cheaper and can be realized in ITUnano laboratory.

Next, by changing the doping level in the range between $1 \times 10^{15} \text{ cm}^{-3}$ to $1 \times 10^{20} \text{ cm}^{-3}$ and calculating the $\Delta R/R$ sensitivity, the doping level that will be used throughout the following simulations was determined. It was found that, $1 \times 10^{18} \text{ cm}^{-3}$ doping level is high enough to reduce the thermal noise effect, at the same time it does not be affected the sensitivity that much. Thus this doping level was chosen and used throughout the following simulations.

Afterward, the cantilever material is varied to find the material that gives maximum stress and deflection for the same applied force. It was found that SiO_2 resulted into almost 2.5x higher deflection and 1.7x higher sensitivity when compared to single crystal silicon (the starting cantilever material) case thus SiO_2 has been selected as the cantilever material for this biosensor and it is used in the following optimization steps.

Next, various cantilever shapes (Rectangular, Pi-shape, T-shape, Trapezoid, Stepped-Trapezoid, and Triangular) were introduced, and for each shape, the dimensions were varied bearing in mind the process and device limits. The results from all these simulations were compared to find the optimized shape which gives the maximum sensitivity.

During the rectangular shape microcantilever optimization step, it was found that the cantilever thickness has the highest effect on the sensor sensitivity when compared to the change in cantilever length and width. In addition to that, after the different rectangular microcantilever dimensions were optimized (length, width and thickness), the sensitivity increased 18.3x folds.

Also, adding two side holes to the rectangular cantilever structure (T-shape) increased the sensitivity by 1.6 factor. Overall, for the same applied force, the trapezoid-shaped microcantilever design gave higher sensitivity (more than 46x times greater than the starting sensor sensitivity) whereas the stepped-trapezoid shaped gave the highest maximum deflection.

Afterward, Stress Concentration Region (SCR) was introduced in the optimized trapezoid structure in different locations and orientations seeking for further sensitivity enhancement. From the simulations, it was found that adding a $30\mu \times 10\mu\text{m}$ SCR rectangular hole to the optimized trapezoid structure $15\mu\text{m}$ away from the clamped cantilever edge, resulted in almost 1.6x times sensitivity enhancement which gave the best sensitivity value compared to the other positions.

Regarding the normalized change in resistance to the applied force the final sensor's sensitivity equals to $-1.5 \times 10^{-8} \Omega/\Omega / \text{pN}$; this means that for each 1pN (10^{-10} g) biomolecules attach to this biosensor; the piezoresistor resistivity will decrease by $1.5 \times 10^{-8} \Omega$. When compared to the starting sensor, the final sensor design gave 73.5x times better $\Delta R/R$ sensitivity and it is more sensitive than the other sensor designs previously reported in the literature.

The fabrication sequence for this sensor was prepared, but due to technical problems in some of the devices found in ITUnano laboratory, the sensor has not been fabricated.

BİYOLOJİK TESPİT UYGULAMALARI İÇİN PIEZORESİSTİVE MİKROKANTİLEVER TASARIM, SİMÜLASYON VE ANALİZİ

ÖZET

Son on yılda, çeşitli araştırma çalışmaları, Biyolojik Mikroelektromekanik Sistem (Bio-MEMS) biyosensörlerinin Deoksiribonükleik Asit (DNA), proteinler, Bakteri ve Antijenler gibi biyomolekülleri belirleme yeteneğini ortaya koydu. Ancak, numunelerde tespit edilmesi gereken analitlerin düşük konsantrasyonundan dolayı, sensörün çıktısına ufak bir sinyal neden olur.

Buna cevap olarak, numunedeki birkaç analitin bulgulanmasına yanıt olarak yüksek çıktı sinyali verebilen optimize edilmiş bir biyosensör için bir ihtiyaç ortaya çıkmıştır; Nihai hedef tek bir biyomoleküle yapışmayı ölçülebilir bir miktara dönüştürmektir.

Bu amaçla, basit, ucuz, oldukça hassas ve daha önemlisi analitlerin optik etiketlenmesine ihtiyaç duymadığı için (Etiketsiz), MEMS mikrokantilever tabanlı biyosensörler umut verici bir algılama çözümü olarak ortaya çıkmıştır.

Farklı mikrokantilever ileten teknikler arasında, piezoresistif tabanlı mikrokantilever biyosensörler, ucuz, yüksek hassasiyetli, minyatür olan, sıvı ortamlarda iyi çalışan ve entegre okuma sistemi olan cazip bir çözüm gibi gözükmektedir.

Literatürde piezoresistif mikrokantileverlerin hassasiyetini arttırmaya odaklanan birçok yayın olmasına rağmen, sırf birkaç tasarım ve işlem parametresini optimize etmeyi düşündükleri için sonuçta elde edilen hassaslık arttırmaları pratik uygulamalar için yetersiz kalıyordu.

Literatürde yapılan çalışmanın analizinden sonra, Piezoresistif mikrokantileverlere dayalı sensörlerin hassasiyetini arttırmak için optimize edilebilen / kullanılabilen parametreler / yaklaşımlar: kantilever boyutları, kantilever Malzemesi, kantilever şekli, Piezoresistör malzemesi, Piezoresistör Doping seviyesi, Piezoresistör Boyutları, Piezoresistörün konumu, Stres konsantrasyon Bölgesinin (SCR) şekli ve konumu.

Bu çalışmada, tüm tasarım ve işlem parametrelerinin duyarlılık üzerindeki etkisini analizi yapıldıktan sonra, kademeli optimizasyon yaklaşımı geliştirilmiş. Bu yaklaşımda neredeyse tüm parametreleri, her adımda biri olmak üzere, değiştirilerek optimizasyon yapılmış ve böylece hassasiyet maksimum düzeyde olmasını sağlamıştır.

Bu çalışma boyunca, sensör performansını simüle etmek için ticari bir Sonlu Elemanlar Analizi (FEA) aracı olan COMSOL Multiphysics 5.0 kullanıldı.

Her bir optimizasyon adımında, aynı uygulanan kuvvet için piezoresistör bölgelerindeki gerilimi en üst düzeye çıkaracak ve yoğunlaştıracak şekilde parametrenin optimize edilmesi hedefi daha yüksek duyarlılık elde etmektir. Toplamda, son optimize edilmiş sensörü elde etmek için neredeyse 46 farklı simülasyon yapıldı.

Biyolojik uygulamalarında kullanılan etkileşimli kuvvetler onlarca ila yüzlerce pN arasında olduğu için, bu sensörde kullanılacak 25 ila 250 pN aralığı seçilmiştir. Optimizasyon işlemindeki tüm simülasyonlar sırasında 250 pN'lik bir toplam

dağıtılmış kuvvet, analitlerin sensöre bağlanmasını temsil eden Altın katmanın üzerine uygulanır.

Başlangıç olarak sırasıyla uzunluk, genişlik ve kalınlık için boyutları ($200\mu\text{m} \times 120\mu\text{m} \times 1.5\mu\text{m}$) olan dikdörtgen bir tek kristal Silicon Microcantilever kullanılmıştır.

Konsolun üst kısmında, analitlerin tutturulması için $100\mu\text{m} \times 100\mu\text{m} \times 0.2\mu\text{m}$ Gold katmanı kullanılırken, piezo rezistanslı algılama için $20\mu\text{m} \times 5\mu\text{m} \times 0.5\mu\text{m}$ dikdörtgen polisilik piezoresistor kullanılır. Burada kullanılan piezoresistor, $1 \times 10^{16} \text{ cm}^{-3}$ lük bir p-tipi dopant yoğunluğuna, 400 nm'lik bir kalınlığa ve 1V'lık uyarılma voltajına sahiptir.

Dikdörtgen bir konsoldan başlamak üzere piezoresistor malzemesi ve doping seviyesi iki aşamada optimize edilmiştir. Piezoresistor malzemesi değiştiğinde (tek kristal silikon ve Poly-silikon), tek kristal silikon durumunda $\Delta R / R$ duyarlılığının daha yüksek olduğu bulundu. Fakat bu sensör tasarımı için, hassasiyet kristal yönüne bağlı olmayan, sensör imalatı daha kolay, daha ucuz ve ITUNano laboratuvarında gerçekleştirilebildiğinden, piezoresistor malzemesi olarak polisilikon seçilmiştir.

Sonra, doping düzeyini $1 \times 10^{15} \text{ cm}^{-3}$ ile $1 \times 10^{20} \text{ cm}^{-3}$ aralığında değiştirerek ve $\Delta R / R$ hassasiyetini hesaplayarak, aşağıdaki simülasyonlar boyunca kullanılacak doping seviyesi belirlendi. $1 \times 10^{18} \text{ cm}^{-3}$ doping seviyesinin, termal gürültü etkisini azaltacak kadar yüksek olduğu, aynı zamanda duyarlılığın da o kadar fazla etkilemediği görülmektedir. Böylece, bu doping seviyesi tüm sonraki simülasyonlar boyunca seçildi ve kullanıldı.

Daha sonra konsol malzemesi, aynı uygulanan kuvvet için maksimum gerilme ve sapma sağlayan malzeme bulmak için çeşitlendirilir.

Beklendiği gibi, farklı konsol malzemeler, farklı maksimum sapma ve gerilme değerleri verdi. Elde edilen bulgulara göre, Silikon Dioksit (SiO_2) düşük genç modül değerleri nedeniyle diğer malzemelere kıyasla en yüksek azami sapma ve gerilme değerlerine sahip olduğu bulundu. Tekli kristal silikon (başlangıç konsol malzemesi) durumunda olduğu gibi SiO_2 'nin neredeyse 2.5 kat daha yüksek sapma ve 1.7 kat daha yüksek hassaslık ile sonuçlandı ve böylece bu biyosensörün konsol malzemesi olarak SiO_2 seçildi ve aşağıdaki optimizasyon adımlarda kullanıldı.

Daha sonra, çeşitli konsol şekilleri (Dikdörtgen, Pi-şekli, T-şekli, Trapezoid, Kademeli-Trapezoid ve Üçgen) tanıtıldı ve her şekil için boyutlar, işlem ve cihaz sınırlamaları göz önünde bulundurularak değiştirildi. Bütün bu simülasyonların sonuçları, maksimum hassaslığı veren optimize şekli bulmak için karşılaştırıldı.

Dikdörtgen şekil mikrokantilever optimizasyon adımı sırasında konsol kalınlığının konsol uzunluğu ve genişliğindeki değişimle karşılaştırıldığında sensör hassasiyeti üzerinde en yüksek etkiye sahip olduğu bulunmuştur.

Konsol kalınlığı $3\mu\text{m}$ ve $1.5\mu\text{m}$ arasında değiştiğinde, konsol kalınlığı azaldığında duyarlılık arttığı bulundu. $1.5\mu\text{m}$ kalınlıktaki konsolun kullanılması, $3\mu\text{m}$ kalınlıktaki konsoldan 4 kat daha fazla yüksek hassasiyet göstermiştir. Böylece, $1.5\mu\text{m}$ son optimize konsol kalınlığı olarak seçildi.

Konsol uzunluğu $150\mu\text{m}$ ila $350\mu\text{m}$ arasında değiştirildiğinde, konsol uzunluğu arttıkça hassasiyet artmaktadır. Elde edilen sonuçlara göre, $350\mu\text{m}$ uzunluğunda konsolun $150\mu\text{m}$ uzunluğundaki konsoldan yaklaşık 3.5 kat daha yüksek bir

hassaslık verdiđini görüyoruz. Böylece, 350µm son optimize konsol uzunluđu olarak seçildi.

Konsol genişliđi 120µm ve 250µm arasında deđiştirildiđinde, konsol genişliđi arttıkça hassasiyet azalmaktadır. Elde edilen sonuçlara göre, 120µm genişlikli konsolun 250µm genişliğinde konsoldan 2.4 kat daha yüksek bir hassaslık verdiđini görüyoruz. Böylece, 120µm son optimize konsol genişliđi olarak seçildi.

Buna ek olarak, farklı dikdörtgen mikrokantilever boyutları optimize edildikten sonra (uzunluk, genişlik ve kalınlık), duyarlılık 18.3x kat arttı.

Ayrıca, dikdörtgen konsol yapısına (T şekli) iki yan delik eklenmesi, duyarlılıđı 1,6 oranında arttırmıştır. Farklı trapezoid biçimli konsollardan elde edilen sonuçlardan, sıkıştırılmıř konsol kenarı ile serbest kenar arasındaki 1:4 oranındaki yapının en yüksek maksimum von Mises stresini ve en yüksek duyarlılıđı verdiđini görülebilir. Bunların 1:1'lik durumundan (optimize edilmiř dikdörtgen konsol) neredeyse 2.5 kat daha fazla hassasiyet vardır. Böylece, bu tasarım optimize edilmiř yamuk şeklinde konsol tasarımı olarak seçildi.

Farklı basamaklı trapezoid şekilli konsollardan elde edilen sonuçlara göre, sıkıştırılmıř konsol kenarı ile serbest kenara arasındaki oran 1: 4 olan yapıda, en yüksek maksimum von Mises gerilmesi ve en yüksek duyarlılık görüldükten, bunun neredeyse 2.5 kat arttıđı görülmektedir 1: 1'den daha büyüktür (optimize edilmiř dikdörtgen konsol). Böylece, bu tasarım optimize edilmiř basamaklı trapez şeklinde konsol tasarımı olarak seçildi.

Aynı uygulanan kuvvet için, trapez şeklinde mikrokantilever tasarımı, başlangıç sensöründen 46 kat daha fazla daha yüksek hassasiyet vermiřtir (Hassasiyet), Kademeli-Trapezoid şekli en fazla azami sapma göstermiřtir.

Ardından, daha fazla duyarlılık geliştirme arayışında olan farklı konum ve yönlerde optimize trapezoid yapıda Stres Yođunlařtırma Bölgesi (SCR) tanıtıldı. Simülasyonlardan, kelepçelenmiř konsol kenarından 15µm uzakta bulunan optimize edilmiř trapezoid yapıya 30µ × 10µm SCR dikdörtgen bir delik açılmasının, diđer konumlara kıyasla en iyi hassasiyet deđerini veren neredeyse 1.6x kat daha fazla hassasiyet artışı sađladıđı bulundu.

Nihai sensör duyarlılıđı, uygulanan kuvvete karřı dirençteki normalize edilmiř deđişim açısından $-1.5 \times 10^{-8} \Omega/\Omega /pN$ 'ye eşittir. Bu, her bir 1pN (10^{-10} g) için biyomoleküllerin bu biyosensöre tutunması için, piezoresistor direnci $1.5 \times 10^{-8} \Omega$ kadar azalacaktır. Başlangıç sensörüne kıyasla, son sensör tasarımı 73.5x kat daha iyi $\Delta R / R$ duyarlılıđı sađlamıř ve daha önce literatürde bildirilen diđer sensör tasarımlarına göre daha duyarlıdır.

Bu sensörün üretim sırası hazırlanmıř ancak ITUnano laboratuvarında bulunan bazı cihazlarda teknik problemler nedeniyle sensör üretilmemiřtir. Gelecekteki bir çalıřma olarak, önerilen imalat dizisi sensörü imal etmek ve sonuçları simülasyon sonuçları ile karřılařtırmak için kullanılacaktır.

Simülasyon sonuçlarına göre, konsol kalınlıđı ve piezoresistor kalınlıđı sensör hassasiyetini kolayca etkiler. Bu tasarımda silisyum dioksit konsol ve polisilikon piezoresistor için en düşük kalınlık sınırı olarak 1.5µm ve 0.5µm ayarlandı. Aynı tasarım için bu malzemelerin daha ince katmanlarının kullanılması duyarlılıđın daha da artmasına neden olacaktır.

1. INTRODUCTION

Microelectromechanical systems (MEMS) are the micro size electromechanical devices that are used for sensing or actuation. The term MEMS has been proposed since the 1960s, but these devices were not commercialized until 1980s [1]. Since then, they have been used in many consumer products and other areas (e.g., aerospace, agriculture, environmental) but the same devices are also found in medical devices.

Since the 1970s, a new branch of MEMS has emerged as biomedical (or biological) microelectromechanical systems (BioMEMS) that is specifically developed for medical and biological applications such as diagnostics, therapeutics, and tissue engineering. In some of them (biosensor), biological molecules are incorporated into the device to facilitate selective sensing of other biomolecules in liquid or air. BioMEMS has already come up with new promising and innovative solutions that rapidly improved the sensing and actuating functions for all of the healthcare fields.

While some of BioMEMS applications are still under development, some of these applications have already been commercialized. According to the “BioMEMS Market Size Report,” In 2014 the market size of BioMEMS was estimated to be around USD 2.5 billion and is anticipated to grow at Compound Annual Growth Rate (CAGR) of over 25% from 2016 to 2023 [2]. A more detailed overview of the BioMEMS components and applications, market share and future perspectives can be found in Yole Développement’s BioMEMS report [3].

1.1 BioMEMS

1.1.1 Introduction to BioMEMS

BioMEMS refers to the use of microfabrication techniques to fabricate microelectromechanical systems/devices to be used for biological and biomedical

applications such as processing, detecting, delivery, manipulation, analysis, or construction of biological or chemical entities . BioMEMS are now heavily researched since it already started to revolutionize medicine especially after the start of using polymer materials resulting in cost-effective solutions to biomedical problems [4]. BioMEMS can be utilized as a stand-alone system themselves or may be the key component of a much larger medical device. In addition to that, having the biocompatibility property, they may operate in vivo or in vitro (inside or outside a living system).

1.1.2 The Overlap between Bio-MEMS, LOC and μ TAS

BioMEMS have a huge overlap and is sometimes considered synonymous, with lab-on-a-chip (LOC) and micro total analysis systems (μ TAS), as shown in the Venn diagram in Figure 1.1. Despite that, the primary focus of each one of these technologies is different. BioMEMS concentrate on developing mechanical parts and making microfabrication techniques suitable for biological applications. Whereas LOC focuses on the miniaturization and integration of the processes and experiments done in laboratories into a single chip (mostly includes microfluidics [5]) . μ TAS are more concerned on including all necessary steps for a sample chemical analysis in one chip. Which means that unlike BioMEMS, LOC and μ TAS do not necessarily have a biological application.

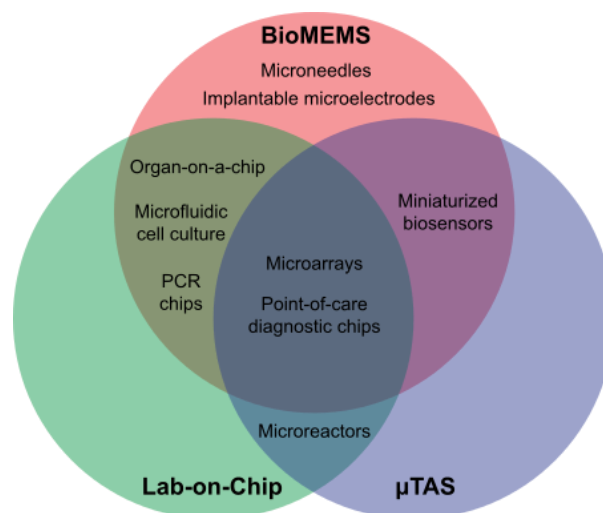


Figure 1.1

Figure 6.1: Some aspects of the fields of bio-MEMS, lab-on-a-chip, μ TAS and the overlapping between them [6]

1.1.3 BioMEMS Applications

1.1.3.1 BioMEMS for Detection, Analysis, and Diagnosis

The use of BioMEMS for diagnostic applications is the largest and most researched BioMEMS segment [7]. These BioMEMS devices differ significantly in their designs and fabrication techniques and also in the areas of their applications such as detecting viruses, proteins, cells, microorganisms, DNA and related nucleic acids, and small molecules of biochemical importance and interest.

The main advantage of BioMEMS diagnosis platforms lies in the fact that large numbers of analytes/genes/proteins can be analyzed identified in parallel such as in chemical sensor arrays [8], DNA microarrays [9] and protein microarrays[10].

In addition to that, Bio-MEMS are now one of the reasons behind the advances of endoscopes such as Single-fiber Micro-optical scanner [11] and capsule endoscopy which revolutionizes the diagnosis technology [12,13].

BioMEMS biosensors can be used for the purpose of identifying the presence of diseases, antibodies or collecting the needed information to prescribe appropriate drugs for personalized medicine. BioMEMS based biosensors (such as Glucose [14], Lactate [15], and Alcohol [16] biosensors) and point-of-care [17]/ lap-on-chip (LOC) systems are widely researched because they resemble small, portable, low-cost, easy to use, yet extremely versatile and capable diagnostic instruments.

1.1.3.2 BioMEMS for therapeutics

Many BioMEMS based therapeutic devices are currently being researched and developed, and some of them have already been commercialized.

Among these devices, the artificial retinal prosthesis called the Argus™ Retinal Prosthesis System which has already been demonstrated to be a safe, reliable, and efficient method that significantly improves visual function and quality of life for people blinded by retinitis pigmentosa [18].

1.1.3.3 BioMEMS for Drug Delivery

Over the past decade, BioMEMS have received considerable attention in the drug delivery field as both internal and external drug delivery devices [19]. One of the already commercial internal BioMEMS drug delivery system is the MiniMed Paradigm® 522 insulin pump [20]. The system is composed of the insulin pump, sensor, transmitter and infusion line thus not only it monitors the person's glucose levels 24/7 but can deliver insulin on an as needed basis.

Among the external drug delivery BioMEMS technologies, Microneedles are the most extensively developed to be used for transdermal drug delivery to deliver the drugs that exhibit poor bioavailability such as proteins [21].

1.1.3.4 BioMEMS for Cell culture and tissue engineering

BioMEMS are also used as cell culture using cell culture array which creates a microenvironment to grow cells in vitro and parallel thus enables the analysis of multiple cell growth conditions [22].

In addition to that, the use of Microfluidic-BioMEMS platforms led into advances in tissue engineering, harvesting and manipulation more information about tissue engineering using BioMEMS can be found in [23].

1.1.3.5 Bio-MEMS for medical implants and surgery

Another use of BioMEMS for diagnostic applications are the neural probes (NeuroMEMS) that have already had a considerable positive effect on the understanding of the brain by revealing the functioning of networks of biological neurons. NeuroMEMS are implanted in the brain to record and/or stimulate specific sites in the brain thus help the diagnosis of brain diseases such as seizures, epilepsy, migraine, Alzheimer's, and dementia [24].

Another use of BioMEMS is to build the microtools used in robotic-assisted surgery systems such as the da Vinci System that is employed in Minimally Invasive Surgery which results in reduced tissue damage, scarring and pain and shorter recovery time [25]. Furthermore, it may be used for testing the next generation of artificial organs (organs-on-a-chip), more about this can be found in [26].

1.2 Bio-MEMS as Miniaturized Biosensors

1.2.1 Introduction to Biosensors

According to Oxford dictionary definition, Biosensor is a device that uses biological molecules to detect and record the presence of chemicals in a substance [27]. It is composed of two parts, the biological receptor system, and the transducer system.

When an analyte attaches to the biosensor surface, it will change one of its properties thus producing ions, electrons, gasses, heat, mass or light which will be converted to an electrical measurement using the transducer.

For the biological sensing part, different biological interactions are used among which antibody–antigen interactions, enzymatic interactions, nucleic acid interactions, cellular interactions, and interactions using biomimetic materials are the most commonly used [28]. For transducing mechanical, electrical, and optical detection techniques are the most dominant. According to the device, the nature of the analyte molecules, and the precision required the appropriate detection method is chosen.

Nowadays, biosensors represent an analytically powerful and cheap alternative to the conventional technologies to measure glucose, ethanol, lidocaine, nerve gasses, creatinine, penicillin, sodium ions, gamma globulin, testosterone, theophylline, vitamin B12, and O₂ [29].

1.2.2 Detection methods

There are many ways to convert the attachment of biomolecules to BioMEMS into a measurable signal, but they are divided into electrical, optical and mechanical techniques.

1.2.2.1 BioMEMS and electrical detection

The electrical detection methods based biosensor includes amperometric biosensors, potentiometric biosensors, and conductometric biosensors. In the amperometric biosensors, an enzyme-catalyzed redox reaction results in a redox electron current that is measured by a working electrode. In potentiometric biosensors, on the other

hand, the electrical potential at one electrode is measured referring to another electrode. The conductometric biosensors work by measuring the electrical impedance between the two electrodes corresponding to the to the biomolecular reaction. When compared to optical techniques, electrical detection methods are advantages being portable and miniature.

1.2.2.2 BioMEMS and optical detection

Optical detection based BioMEMS including surface plasmon resonance (SPR), fluorescence-based techniques and chemiluminescence-based techniques requires bulky detectors. Thus it is hard to produce it in a miniaturized portable format.

Optical biosensors widely used in food quality and safety analysis since it shows a greater potential to detect pathogens, pesticide and drug residues, hygiene, heavy metals and other toxic that can be found in food [30].

1.2.2.3 BioMEMS and mechanical detection

The mechanical detection method in bio-MEMS refers to the use of micro-/nano-scale cantilevers (stress sensing and mass sensing) or micro-/nano-scale plates or membranes. In the stress sensing, one side of the microcantilever is functionalized, and when the analytes attach to the surface, the surface stress changes thus the cantilever bends. The bending of the microcantilever can be sensed using optical, capacitive and piezoresistive means. On the other hand, in mass sensing approach the cantilever is actuated in the resonance frequency which changes when analytes attach to the cantilever surface due to the mass change.

1.3 Microcantilever-Based Biosensors

Cantilever-based sensors emerged as a label-free sensing technique in the mid-1990s since the discovery of Atomic Force Microscopy (AFM) [31]. In the recent years, Microcantilever-based biosensors resulted in very exciting and significant advances in the biochemical detection. Using this technique, the detection of DNA, cells, antigens, virus, bacteria enzymes, and proteins have been demonstrated [32-34].

One of the attractive advantages of microcantilever-based BioMEMS biosensors is that no optical labeling is needed thus no specimens loss occurs (label-free

detection). Cantilever-based sensing became promise as a technique for cheap, portable, highly sensitive and parallel analysis systems, easy integration, greater portability, robustness and low power consumption [35].

The goal of this study is to design cheap, miniature, simple and highly sensitive microcantilever to be used in biosensing applications. Bearing in mind the ability of the sensor to work well in liquid mediums, because most of the biological samples are in liquid form (blood, urine, etc.), the piezoresistive sensing technique has been chosen. More details about microcantilevers and this sensor design is presented in the following sections.

2. THEORY

2.1 Introduction

Nowadays with the emergence of deadly diseases and the existence of toxic gases (volatile compounds e.g. HF vapor), a need has arisen for ultra-sensitive biosensors with an ultimate goal of detection and recognition of single bio/chemical molecules. The selectivity of these biosensors is achieved using a functionalized chemical layer on the sensor's surface that maximizes the sensor's sensitivity to that particular analyte. By the year 2020, It is expected that the global biosensors market will reach USD 21.17 billion [36].

According to the detection method used, the design art of biosensors can be broadly classified into label-free and label-based biosensors. In the Label-based techniques, the properties of labels like fluorescence, chemiluminescence, etc. help to detect a particular target. However, sample losses occur during the process of labeling and purification; this is even significant when sample quantity is limited. Another disadvantage of Label-based techniques is that Labeling processes can also affect the functionality and stability of molecules like proteins. Among these label-free techniques, Mass Spectrometry, Surface Plasmon Resonance (SPR) and microcantilever-based sensors [37].

Cantilevers are a basic mechanical structure that is clamped at one end while the other end is free. Microcantilevers are cantilevers with at least one dimension in the micrometer or the nanometer range [2]. Originally it was used in Atomic Force Microscopy (AFM) but in the recent years microcantilever-based MEMS sensors have been successful in many applications including diagnostics, switching applications, magnetic field sensing and label-free biochemical sensing applications [38-41]. The latest advances in Biosensors showed that compared with earlier used detection methods, microcantilevers biosensors has many attractive advantages being fast, reliable, cheap, easy-to-use and highly sensitive and selective for the recognition of biomolecules [42]. Microcantilever-based sensors allow rapid and reliable

detection of small amounts of analytes in air or solution. Nanomechanical sensors have even reached to the detection of femtomolar concentrations of analytes in few minutes [43]. Despite all that, still there is no commercial MEMS-based biosensor available in the market [44].

When microcantilever arrays are used, they enable the detection of several analytes simultaneously while solving the inherent problem of thermal drift found in single microcantilever sensors, this includes applications such artificial nose [45], gas flow sensor [46], DNA sensors [47] and Lap-on-chip (LOC) [48]. This is done by using some of the cantilevers for detection whereas reference cantilevers don't interact with the molecules to be detected, by comparing the signals from reference and sensor cantilevers the net cantilevers response is obtained. This way, even small sensor responses can be extracted from large cantilever deflections omitting the undesired effects [49].

2.2 Cantilever Working Modes

In biosensing applications, The attachment of the analytes to the functionalized cantilever surface results in a proportional change in one or more of the cantilevers properties, such as the surface stress, mass, displacement or resonant frequency. According to the property that has been changed, the cantilever's working mood is defined.

2.2.1 Static mode

In the static mood, one side of the cantilever is covered with a sensing layer, affinity to the targeted analyte, while the other is passive. The attachment of the analytes to the cantilever's surface results in a change in the surface stress thus bends the cantilever accordingly [50].

The deflection of the cantilever can be calculated using Stoney's formula [51] using the differential surface stress:

$$\delta = \frac{3L^2(1 - \nu)}{Et^2} (\sigma_1 - \sigma_2) \quad (2.1)$$

Where δ is the cantilever displacement, ν Poisson's ratio, E Young's modulus, $(\sigma_1 - \sigma_2)$ the differential surface stress, L , is the cantilever Length and t is the thickness of the cantilever.

The spring constant “ κ ” of the cantilever is related to the cantilever dimensions and material constants by the formula [52]:

$$\kappa = \frac{F}{\delta} = \frac{E w t^3}{4 L^3} \quad (2.2)$$

A more accurate formula for the deflection has been proposed by Tamayo et al. Which considers the clamping effect on the cantilever's deflection thus gives more accurate results in biosensing applications [53].

2.2.2 Dynamic mode

When using dynamic mode, the cantilever is actuated at its fundamental resonance frequency at the steady state and the attachment of the molecules to the sensing layer located near to the tip increases its total mass thus results in a shift in the resonance frequency correlated to some analytes attachment to the sensor [54]. Even though dynamic mode is more sensitive compared to static mode but when the cantilever is working in liquid mediums its sensitivity is severely affected due to the high viscous damping forces, this makes static mode is ideal for working in liquids [55,56].

Resonance frequency (f_n) is determined as vibrating frequency at which there is a maximum deflection of the cantilever. It can be calculated by [57]:

$$f_n = \frac{1}{2\pi} \sqrt{\frac{k}{m}} \quad (2.3)$$

Where k represents the spring constant and m stands for the cantilever mass. k and m of the cantilever are related to the geometrical dimensions (e.g. thickness, width, length) using the equation (2.2). By substituting m and k into to (2.3), then the final formula for resonance frequency:

$$f_n = \frac{1}{2\pi} \sqrt{\frac{E t^2}{4\rho L^4}} \quad (2.4)$$

2.2.3 Heat mode

Another working mode called heat mode was pioneered by Gimzewski et al. taking advantage of the bimetallic effect; When a metal-coated cantilever is heated it bends. Based on this effect they constructed a miniaturized calorimeter that has pico-joule sensitivity [58].

2.2.4 Lorentz force based cantilever actuation

Lorentz force-based electromagnetic actuation allows actuating a cantilever in both dynamic and static modes. Lorentz forces can be used for the actuation of a cantilever either by evaporating a magnetic layer on the cantilever and applying an external magnetic field or by using the interaction between an Alternating Current (AC) passing through a conductive pathway on top of the cantilever and an external magnetic field [59,60].

As defined in the Encyclopaedia Britannica [61], Lorentz force (F) is the force applied on a charged particle q that moves with velocity v in an electric E and magnetic field B . The whole electromagnetic force F on the charged particle is named the Lorentz force.

$$F = qE + qv \times B \quad (2.5)$$

The first term of equation (2.5) corresponds to the electric field whereas the second term corresponds to the magnetic force having a direction perpendicular to both the velocity and the magnetic field.

Since current consists of a stream of moving charges, thus when a current-carrying wire is placed in a magnetic field the combination of the forces exerted on each charge will result in a macroscopic force on the wire. The following equation (2.6) describes the Lorentz force exerted on a straight stationary wire with ℓ is a vector with magnitude equals to the length of wire that carries current I and it is placed in a magnetic field with density B [62].

$$F = I\ell \times B \quad (2.6)$$

Lorentz force based actuated microcantilever has gained lots of attention in the last few decades and has been used in a different application. Nowadays, the most preferred MEMS magnetometers are Lorentz force MEMS magnetometer; in addition to the fact that they are small, consumes low power, high functionality, and wide dynamic range magnetometers when compared with Hall Effect magnetometers they are free from hysteresis and they don't require magnetic materials [63-65].

For biosensing applications, even though measuring the frequency changes seems to be a better choice because it can quantify minute mass changes easily and it is much more stable, but this method has many disadvantages such as the complicated the measurement setup and the noise resulting from the electronics for the frequency feedback. Additionally, a change in the frequency can arise when the temperature changes and/or changes in the force constant [66].

2.3 Cantilever Transducing Mechanisms

When microcantilevers are used as a platform for biosensing applications, there are many mechanisms that can be used for transducing the attachment of the biomolecule to the cantilever into a measurable quantity [67]. The sensing mechanism to be used is chosen according to the nature of the analytes, the sensing medium (air or liquid) and level of sensitivity and selectivity required [68]. Each one of these mechanisms has advantages and disadvantages; they vary in the level of sensitivity, need for alignment and setup, robustness, ease of readout and the potential for further miniaturization. When designed for detecting and sensing specific biomolecules compromising between these mechanisms is done and further optimization is required to get the best performance for the specific biosensor.

The molecular interaction of the analytes with the sensitized cantilever surface changes the surface free energy thus results into stress which bends the cantilever with respect to the horizontal surface, the amount of deflection is proportional to the applied force or some analytes attach to the surface [69]. The vibrational amplitude and/or the deflection of a microcantilever can be sensed using various techniques such as optical, capacitive, piezoelectric and piezoresistive means.

2.3.1 Optical

2.3.1.1 Detection mechanism

The typical optical detection mechanism, which is the most effective method for detection [68], is based on a low power laser beam that is focused on a reflective layer on top of the microcantilever which reflects the beam to a Position-Sensitive Detector (PSD). When the cantilever has deflected this results in a change in the position of the light spot in the PSD.

2.3.1.2 Advantages

- Very sensitive; using this method sub-nanometer cantilever deflection can be detected [70].

2.3.1.3 Disadvantages

- high cost due to the need for highly sophisticated instrumentation.
- Complicated and time-consuming optical setup and alignment. Thus it is not ideal for rapid or simultaneous detection on large microcantilever arrays.
- The laser spot size in most commercially available optical lever systems is several micrometers, which is difficult to measure sub-micrometer sized structures [70].
- Optical detection method required extra hardware for detection and sensing. Hence the size of the device is larger [71].

Recently, Optical cantilevers which are integrated waveguide cantilever sensors are proved to be promising solutions for portable sensors in the air and solution without the need for preliminary alignment or adjustment such as AFM-based optical detection methods while having a comparable sensitivity [71, 72]. The deflection of the cantilever is correlated to the optical intensity of the light travelling through the system to the cantilever (which serves as the output waveguide), when the cantilever is deflected less light is coupled to at the end waveguide thus the intensity of the output light is indicator of the amount of the cantilever deflection [69]. This concept of waveguide microcantilever has already been used for the development of Miniaturized pH Sensor [73].

2.3.2 Capacitive

2.3.2.1 Detection mechanism

In the capacitive detection mechanism, the electrically conductive cantilever serves as an electrode of a capacitor while the other electrode underneath is fixed [74]. The two electrodes are isolated from each other when the cantilever bends due to the attachment of analytes or force, it deflects changing the distance between the plates thus the value of the capacitance and the resonance frequency changes accordingly [75].

2.3.2.2 Advantages

- Simple.
- Electrostatic actuation and integrated detection.
- No need for an additional position sensing device.

2.3.2.3 Disadvantages

- less accurate than optical and piezoresistive sensing [67].
- The capacitive method does not work in electrolyte solution due to the generation of Faradic current between the capacitive plates and is therefore limited in its sensing applications.
- The interferometric methods work well for small displacements but are less sensitive in liquids [76].
- Complicated electronic circuits and fabrication processes.

2.3.3 Piezoelectric

2.3.3.1 Detection mechanism

This type of transducing is based on piezoelectric effect where an AC is applied to the cantilever which contains piezoelectric material such as lead zirconium titanate PZT or ZnO [77]. When the cantilever deflects, the current produced by the piezoelectric layer changes in accordance to stress change [75].

2.3.3.2 Advantages

- Low power consumption.
- Can be used for detection and actuation because the piezoelectric effect generates voltages when the cantilever bends [78].

2.3.3.3 Disadvantages

- Difficulty in miniaturization because the piezoelectric layer must remain thin compared with the total device thickness and careful processing is needed [71].

2.3.4 Piezoresistive

2.3.4.1 Detection mechanism

This sensing scheme is based on the piezoresistive effect [79], where a piezoresistive material such as doped silicon is incorporated in the microcantilever. When the microcantilever is deflected due to the attachments of analytes to the functionalized microcantilever surface, the integrated piezoresistor is strained resulting in a change in the resistivity. Using Wheatstone bridge circuit, this change in resistance can be sensed and a relationship between change in the resistance and the number of molecules detected can be established [80].

Due to its advantage of readout integration on the same chip, this method of microcantilever sensing became prominent [2,81,82].

2.3.4.2 Advantages

- Low cost.
- High sensitivity.
- The possibility of miniaturization.
- Integrated readout system onto the sensor chip thus does not require external detection devices.
- Works well in liquid environments.
- Multiple piezoresistive cantilevers can be microfabricated in an array-format, which considerably improves throughput and offers a cost effective approach to quantifying biomaterial mechanical properties [42].

- The Simple signal processing step.

2.3.4.3 Disadvantages

- Less sensitive when compared to optical sensors.
- The readout can be affected by the variation in the sensor's temperature.

2.3.5 Comparison

The aim of this study is to design a bio-MEMS biosensor that is simple, cheap, very sensitive and selective, easy to fabricate, easy to use, small and can work well in a liquid environment (blood sample for example).

Even though optical sensing is the most effective and widely used cantilever deflection measurement [83], It is not suitable for this study since it requires expensive and complex external hardware for sensing which conflicts with the miniature property of the intended sensor. In addition to that, optical sensing based microcantilever sensors are difficult to be fabricated and do not work in a liquid environment.

In the same way, Capacitive sensing mechanism also has the disadvantages of being complicated and it is not suitable for working in liquid environments [84]. On the other hand, piezoelectric possess the disadvantage requiring an electrode to the piezoelectric film which makes the sensor fabrication difficult due to the sticking problems.

Since piezoresistive method eliminates all the disadvantages of the techniques above at the same time fulfills the general biosensor requirements, it has been selected to be used in this study.

The following sections give the details of piezoresistive sensing mechanism theory.

2.4 Piezoresistive Microcantilever Theory

In this section, a brief introduction to the strain effects on crystal materials is introduced then the piezoresistance effect and theory behinds it is discussed. The section concludes with the theory of microcantilever-based piezoresistive sensors and the thermal noise effect.

2.4.1 Strain effect on crystal materials

When a crystal material is exposed to strain (fixed internal strain or external strain) this causes crystal deformation which results in changes in the band gaps thus changes its conductivity. The strain effects the carrier transport paths, hence result in significant changes the intrinsic carrier density of the material which is very important for intrinsic semiconductors. The strain altered bandgaps is the main cause of the piezoresistive effect [85].

Benefiting from these effects, strain has been used in many applications to semiconductor devices including: enhancement of electron devices such as Si and SiGe planar and nonplanar MOSFETs using fixed strain [86], the use of variable strain transducers such as discrete strain gauges [87] and integrated MEMS piezoresistive stress transducers [88] and in optoelectronic devices [89].

The strain is defined by 3 x 3 symmetric matrix, where strain coefficients $\varepsilon_{\alpha\beta}$ defines the lattice deformation in the x, y and z.

$$\varepsilon = \begin{pmatrix} \varepsilon_{xx} & \varepsilon_{xy} & \varepsilon_{xz} \\ \varepsilon_{yx} & \varepsilon_{yy} & \varepsilon_{yz} \\ \varepsilon_{zx} & \varepsilon_{zy} & \varepsilon_{zz} \end{pmatrix} \quad (2.7)$$

Another form of strain components is used where:

$$\begin{aligned} e_{xx} &= \varepsilon_{xx}; e_{yy} = \varepsilon_{yy}; e_{zz} = \varepsilon_{zz} \\ e_{xy} &= \hat{x}' \cdot \hat{y}' = \varepsilon_{xy} + \varepsilon_{yx} \\ e_{yz} &= y' \cdot \hat{z}' = \varepsilon_{yz} + \varepsilon_{zy} \\ e_{zx} &= \hat{z}' \cdot \hat{x}' = \varepsilon_{zx} + \varepsilon_{xz} \end{aligned} \quad (2.8)$$

It can also be written array form as:

$$e = \{e_{xx}, e_{yy}, e_{zz}, e_{yz}, e_{zx}, e_{xy}\} \quad (2.9)$$

Stress, which is the force in response to the strain in the unit area, is defined by a second-rank symmetric tensor which is written as $\tau_{\alpha\beta}$, $\alpha, \beta = x, y, z$. Stress and strain are related to each other using the elastic stiffness constants $C_{ij\alpha\beta}$ tensor which is fourth rank tensor [89].

$$\tau_{ij} = \sum_{\alpha\beta} C_{ij\alpha\beta} e_{\alpha\beta} \quad , i, j, \alpha, \beta = x, y, z, \quad (2.10)$$

Due to the symmetry of both the strain and the stress tensors:

$$C_{ij\alpha\beta} = C_{ji\alpha\beta} = C_{ij\beta\alpha} \quad (2.11)$$

By writing both strain and stress tensor as a six-component array as:

$$\begin{aligned} \mathbf{e} &= (e_{xx}, e_{yy}, e_{zz}, e_{yz}, e_{zx}, e_{xy}) \\ \boldsymbol{\tau} &= (\tau_{xx}, \tau_{yy}, \tau_{zz}, \tau_{yz}, \tau_{zx}, \tau_{xy}) \end{aligned} \quad (2.12)$$

The elastic stiffness tensor reduces to:

$$\tau_i = \sum_m C_{imem} \quad (2.13)$$

In cubic crystals, due to high symmetry this 6×6 matrix has a very simple form with only three independent components:

$$C_{ij} = \begin{pmatrix} C_{11} & C_{12} & C_{12} & 0 & 0 & 0 \\ C_{12} & C_{11} & C_{12} & 0 & 0 & 0 \\ C_{12} & C_{12} & C_{11} & 0 & 0 & 0 \\ 0 & 0 & 0 & C_{44} & 0 & 0 \\ 0 & 0 & 0 & 0 & C_{44} & 0 \\ 0 & 0 & 0 & 0 & 0 & C_{44} \end{pmatrix} \quad (2.14)$$

2.4.2 Piezoresistive effect

Piezoresistive effect is a property of metals and semiconductors. When these materials are exposed to stress their electrical resistivity changes accordingly [90]. This effect was discovered first in metals in 1856 by Lord Kelvin. In 1954 with the broad use of single crystal silicon in analog and digital circuits, Smith discovered and measured the piezoresistive effect in silicon and germanium [91].

The piezoresistivity is related to the stress by the piezoresistance coefficients (π coefficients) as following:

$$\frac{\Delta R}{R} = \pi T \quad (2.15)$$

Where R is the original resistance, ΔR is the change of resistance, and T is the applied mechanical stress. For a semiconductor sample with length l , width w , height h and resistivity ρ :

$$R = \rho \frac{l}{wh} \quad (2.16)$$

Thus $\Delta R/R$ can be expressed as

$$\frac{\Delta R}{R} = \left\{ \frac{\Delta l}{l} - \frac{\Delta w}{w} - \frac{\Delta h}{h} \right\} + \left\{ \frac{\Delta \rho}{\rho} \right\} \quad (2.17)$$

The first three terms of the RHS of (2.17) represents the geometrical change of the sample under stress, and the last term $\Delta\rho/\rho$ is the resistivity change due to stress.

Equation (2.17) can be used to describe the Gauge Factor (GF), which is defined as the ratio of the normalized resistance change with axial strain, by replacing the geometrical changes by the axial strain, $\varepsilon_{\text{axial}} = \Delta L/L$, the lateral strain, $\varepsilon_{\text{lateral}} = \Delta W/W = \Delta H/H$, and then replace both of them by the Poisson ratio, $\nu = -\varepsilon_{\text{lateral}}/\varepsilon_{\text{axial}}$, then the change in resistivity can be written as [92]:

$$\frac{\Delta R}{R} = (1 + 2\nu)\varepsilon_{\text{axial}} + \frac{\Delta \rho}{\rho} \quad (2.18)$$

Whereas gauge factor will be:

$$GF = \frac{\Delta R/R}{\varepsilon_{\text{axial}}} = (1 + 2\nu) + \frac{\frac{\Delta \rho}{\rho}}{\varepsilon_{\text{axial}}} \quad (2.19)$$

In contrast to in semiconductor materials, GF in metals is dominated by the geometric component making the conductivity component negligible. Thus GF in metals can be approximated as:

$$GF|_{\text{metals}} = \frac{\Delta R/R}{\varepsilon_{\text{axial}}} \simeq (1 + 2\nu) \quad (2.20)$$

Whereas in a crystalline cubic semiconductor, the symmetry of the diamond structure gets extensively affected by the deformation formed by strain thus the carrier transport is affected accordingly which makes the GF for semiconductors is dominated by the electronic component and can be described as:

$$GF|_{\text{semiconductors}} = \frac{\Delta R/R}{\varepsilon_{\text{axial}}} = \frac{\Delta \rho/\rho}{\varepsilon_{\text{axial}}} \quad (2.21)$$

The normalized resistivity change, $\Delta\rho/\rho$, is related to the stress by π_{ik} , the piezoresistance tensor.

$$\frac{\Delta \rho_i}{\rho} = \sum_{k=1}^6 \pi_{ik} \tau_k \quad (2.22)$$

where $i = 1, 2, \dots, 6$, π_{ik} is a 6×6 matrix. For cubic structures, due to high symmetry this matrix has three independent elements only:

$$\pi_{ij} = \begin{pmatrix} \pi_{11} & \pi_{12} & \pi_{12} & 0 & 0 & 0 \\ \pi_{12} & \pi_{11} & \pi_{12} & 0 & 0 & 0 \\ \pi_{12} & \pi_{12} & \pi_{11} & 0 & 0 & 0 \\ 0 & 0 & 0 & \pi_{44} & 0 & 0 \\ 0 & 0 & 0 & 0 & \pi_{44} & 0 \\ 0 & 0 & 0 & 0 & 0 & \pi_{44} \end{pmatrix} \quad (2.23)$$

Piezoresister needs to have passing current for actuation, but this current is not necessarily in the same direction of the stress. **Table 2.1** shows the normalized piezoresistance change for some stress and current directions.

Table 2.1. Normalized piezoresistance under some combination of stress and current directions [89].

Stress direction	Current direction	$\Delta\rho/\rho$
[100]	[100]	$T\pi_{11}$
[100]	[010]	$T\pi_{12}$
[110]	[110]	$T(\pi_{11} + \pi_{12} + \pi_{44})/2$
[110]	$[\bar{1}10]$	$T(\pi_{11} + \pi_{12} - \pi_{44})/2$
[111]	[111]	$T(\pi_{11} + 2\pi_{12} + 2\pi_{44})/2$

Using the normalized piezoresistance equation (2.22), The piezoresistance coefficients can be obtained for an arbitrary stress. In 1954 [91], Smith experimentally measured the piezoresistance coefficients of bulk Si and Ge for four stress and current configurations, shown in Fig. 2.1.

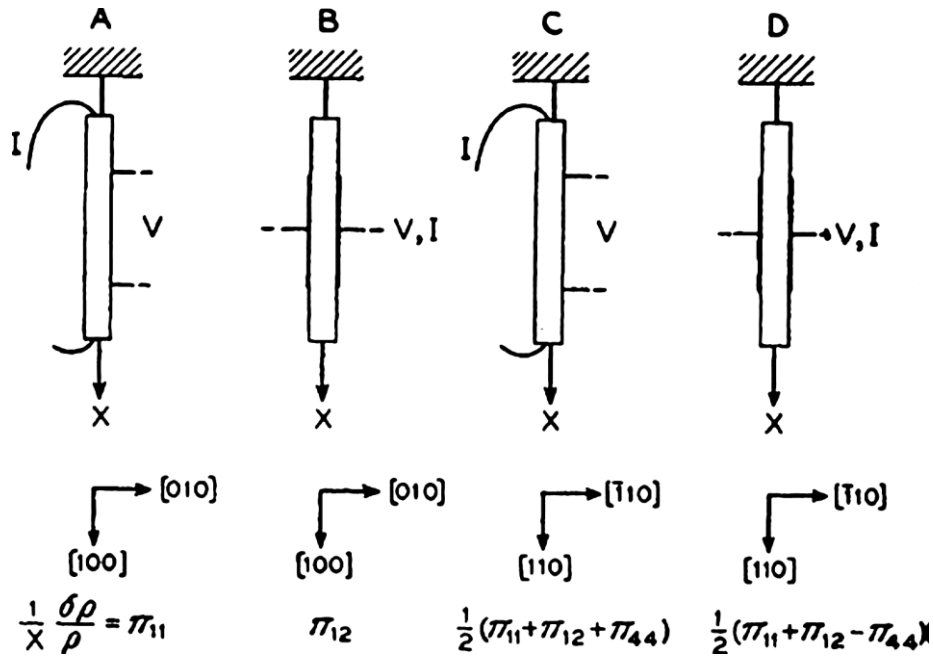


Figure 7.1 : Piezoresistance coefficients and corresponding stress-current configuration [47]

From these four configurations, the three independent π - coefficients of Si and Ge can be obtained as in **Table 2.2**.

Table 2.2. π -Coefficients for bulk Si and Ge (10^{-11}Pa^{-1}) [47].

	ρ_0 ($\Omega \cdot \text{cm}$)	π_{11}	π_{12}	π_{44}
n-Ge	16.6	-5.2	-5.5	-138.7
p-Ge	15.0	-10.6	5.0	98.6
n-Si	11.7	-102.2	53.7	-13.6
p-Si	7.8	6.6	-1.1	138.1

Not like the resistivity of the isotropic conductors which is independent of orientation, the piezoresistivity of strained anisotropic semiconductors (Si and Ge) has a strong dependency on the specific crystal direction. Since the material properties in cubic semiconductors are expressed in the coordinate system that is aligned with $\langle 100 \rangle$ crystal directions, when the piezoresistor is defined in any arbitrary direction the longitudinal and transverse π coefficients must be transformed to the new coordinate system to obtain the effective values; more details can be found in [89].

2.4.3 Microcantilever based piezoresistive sensors

In the piezoresistive microcantilever sensor, a piezoresistor is integrated into the cantilever. When the top of the sensor is exposed to force (stress), the resistivity of the piezoresistor changes accordingly. To obtain higher sensitivity for the same applied force (high output voltage for the same force), it is important to put the piezoresistor at a place that will be exposed to the maximum stress (near to the clamped end).

For crystalline semiconductors, the normalized resistivity change can be approximated as:

$$\frac{\Delta R}{R} \approx \pi_l T_l + \pi_t T_t \quad (2.24)$$

Where the first term is due to longitudinal stress (the current follows in the same direction of the applied stress) and the second term is due to the transverse stress (the current follows perpendicular to the direction of the applied stress). Figure (2.2) shows piezoresistor orientation in the two cases of longitudinal and transverse stress.

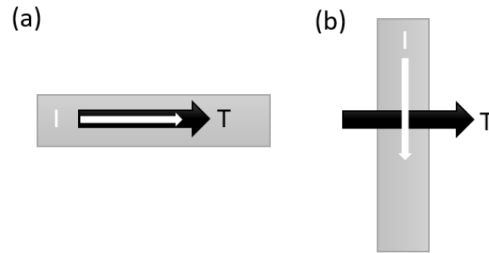


Figure 2.2: Two cases of rectangular piezoresistor orientations with respect to stress, T : (a) Longitudinal current, (b) transverse current

The total resistance can be expressed regarding the unstressed resistance is R and the change in the resistance as following:

$$R_{\text{total}} = R + \Delta R = R(1 + \pi_l T_l + \pi_t T_t) \quad (2.25)$$

When a current, I , passes through the piezoresistor, the total voltage can also be obtained using:

$$V_{\text{total}} = R_{\text{total}} I = RI + \Delta RI = V_{\text{offset}} + \Delta V \quad (2.26)$$

From (2.26), it can be seen that there is an offset in the voltage, V_{offset} , which is usually much larger than ΔV .

As mentioned in section (2.4.2), the resistivity is strongly dependent on crystal orientation. In some specific crystal directions, π_l and π_t are equal and opposite in Polarity. In such cases, when four piezoresistors are connected in Wheatstone bridge circuit (shown in fig (2.3)) the offset voltage will be zero. Thus the output voltage will be proportional to the input force [89].

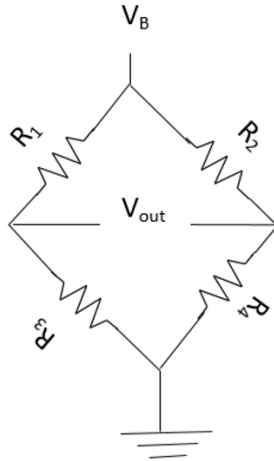


Figure 2.8 : Wheatstone Bridge

As can be seen in Figure 2.4, (100) p-Si approximately meet this condition in the $\langle 110 \rangle$ direction.

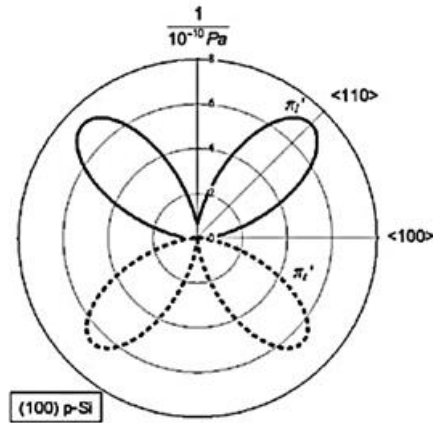


Figure 2.9 : Longitudinal and transverse π -coefficients for p-type Si in the (100) plane [48]

The piezoresistor of the microcantilever sensor is usually connected to three other fixed resistors using Wheatstone bridge, where the out voltage is described as following [93]:

$$V_{out} = \left[\frac{R_4}{R_4 + R_3} - \frac{R_2}{R_1 + R_2} \right] V_{in} \quad (2.27)$$

At the equilibrium, the output of the Wheatstone bridge should be zero, but when the resistivity changes due to the stress the output will not be zero.

2.4.4 Piezoresistance Temperature and Doping Dependency

On the one hand, since energy will be dissipated in the piezoresistive transducers due to the passing current, in consequence thermal noise is expected to be an issue.

On the other hand, the increase in the doping level of the piezoresister material can reduce this thermal noise effect but at the same time affects the π -coefficients thus the sensitivity. The bulk π -coefficients listed in Table (2.2) were obtained by for samples with relatively low doping concentrations. At high doping concentrations above 10^{18} cm^{-3} , the π -coefficients decrease shown in Figure 2.5.

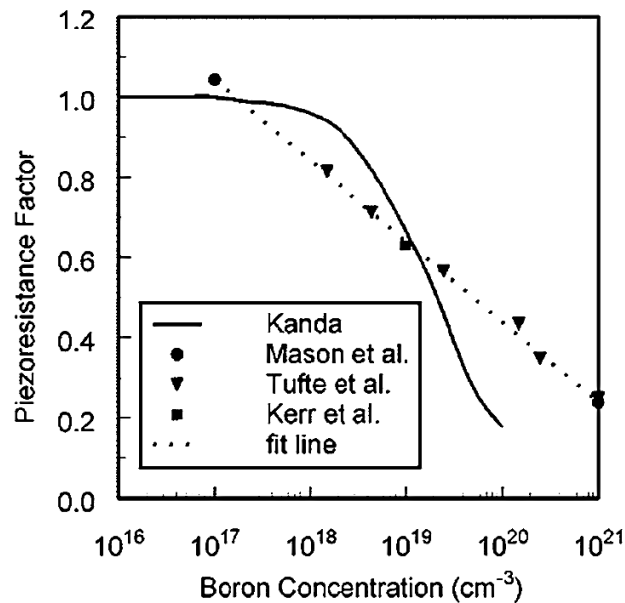


Figure 2.10 : Attenuation factor for bulk p-type Si piezoresistance coefficients as a function of boron concentration [94]

The temperature dependency can be compensated and corrected when combined with the doping effect on the piezoresistance by using the piezoresistance correction factor $P(N, T)$ [95]. But a trade-off must be made between the sensitivity and the temperature dependency.

3. SENSOR DESIGN AND SIMULATION

In Bio-MEMS applications, due to the low concentration of the analytes that need to be detected, minuscule detection signal results in the output of the sensor. In response to this, a need arisen for an optimized biosensor capable of giving high signal upon the attachment of small analytes to it; the ultimate goal is being able to convert the attachment of a single biomolecule into a measurable quantity.

For this purpose, highly sensitive MEMS microcantilevers based sensors have attracted lots of attention in the recent years to be used in biosensing applications because it is simple, cheap and performs well in liquid environments. However, the design of piezoresistive microcantilevers is not a straightforward problem due to coupling between the design parameters, constraints, process conditions, and performance. Using Finite Element Analysis (FEA), many studies have been conducted to change some of the sensor parameters especially dimensions and materials in such a way to find an optimized solution with enhanced sensitivity [96,97].

In this study, almost all the parameters that have a direct impact on the microcantilever-based piezoresistive sensor's sensitivity were varied using COMSOL Multiphysics 5.0, a commercial FEA tool, which resulted in an extremely sensitive sensor design that has almost 73.5 x times better sensitivity than the starting sensor.

3.1 General Optimization Procedure

Microcantilever-based biosensors gained lots of attention in recent years due to its promising sensitivity and high selectivity. Even though there are many publications in literature that concentrated on increasing the piezoresistive microcantilevers sensitivity, however still the resultant sensitivity enhancements are not good enough for practical applications. In addition to that, most of the prior works considered a

limited number of design and process parameters thus resulted in small sensitivity enhancement.

In this study, after a systematic analyzation of the effect of each design and process parameters on the sensitivity, a step-wise optimization approached has been developed in which almost all the design and process parameters were variated one at each step while fixing the others to get the maximum possible sensitivity at the end. At each step, the goal was to optimize the parameter in such a way that it maximizes and concentrates the stress on piezoresistors region for the same applied force thus get higher sensitivity. Later on, a range of forces was used to simulate the attachment of different numbers of molecules to the functionalized Gold layer and to calculate sensitivity regarding the change in the resistance/ force.

3.1.1 Optimization parameters

After the analyzation of the work found in literature, it was found that the parameters/approaches that be can be optimized/used to enhance the sensitivity of Piezoresistive microcantilever-based sensors are:

1. *Cantilever dimensions*: From equation (2.1) and equation (2.2), it can be seen that the deflection of the cantilever depends on the applied stress, cantilever's material Poisson's ratio and young's modulus, cantilever's length, width and thickness.
2. *Cantilever Material*: Different materials have different Poisson's ratio and young's modulus thus for the same applied force on the different cantilever stress, and deflection values will be obtained.
3. *Cantilever Shape*: Since the cantilever's shape also determines the stiffness of the cantilever. Thus the sensitivity changes by altering the cantilever shape.
4. *Piezoresistor's material*: different piezoresistive materials have different piezoresistive coefficients thus results into different sensitivity values ($\Delta R/R$).
5. *Piezoresistor's doping level*: many studies showed that increasing the doping level of the piezoresistor degrades the sensors sensitivity.
6. *Piezoresistor's Dimensions*: Piezoresistor's dimensions especially the thickness has a direct effect on the piezoresistive sensor's sensitivity.

7. *Piezoresistor's position*: to get the maximum sensitivity, the piezoresistor must be placed where the highest stress on the cantilever occurs upon deflection.
8. *Stress concentration Region's (SCR) shape and position*: Introducing some defects or holes in the cantilever can result in further sensitivity enhancement when its shape, dimensions, and position are optimized.

3.1.2 Optimization flowchart

The optimization of this piezoresistive microcantilever sensor was done in several steps, as shown in the flowchart in Figure 3.1. At each step, only one parameter was varied while the other parameters are kept fixed, and each variation was made in a different simulation. The best result of each optimization step was used throughout the following steps. In total, almost 46 different simulations were done to get the final optimized sensor.

Since the interactive forces that are used in biosensing applications are in the range of tens to hundreds of pN [98,99], the range from 25 to 250 pN was chosen to be used in this sensor. During all the simulations in the optimization process a total distributed force of 250 pN is applied on top of the Gold layer representing the attachment of the analytes to the sensor. Starting with a rectangular cantilever, the piezoresistor material and doping level were optimized in two steps. First, the piezoresistor material was varied (single crystal silicon and Poly-silicon) and the results were compared bearing in mind the ease of fabrication and the facilities available in ITUnano laboratory. Next, by changing the doping level and calculating the $\Delta R/R$ sensitivity, the doping level that will be used throughout the following simulations was determined.

Afterward, the cantilever material is varied to find the material that gives maximum stress and deflection for the same applied force. Again the best material for the cantilever structure was utilized in the following steps. Next, various cantilever shapes (Rectangular, Pi-shape, T-shape, Trapezoid, Stepped-Trapezoid and Triangular) were introduced, and for each shape the dimensions were varied bearing in mind the process and device limits. The results from all these simulations were compared to find the optimized shape which gives the maximum sensitivity.

Afterward, Stress Concentration Region (SCR) was introduced in the optimized structure in different locations and orientations seeking for further sensitivity enhancement.

After the final optimized sensor was obtained, the 25 to 250 pN force range was used to get the maximum stress and deflection for each and then from the results the change in resistance to force sensitivity was finally calculated.

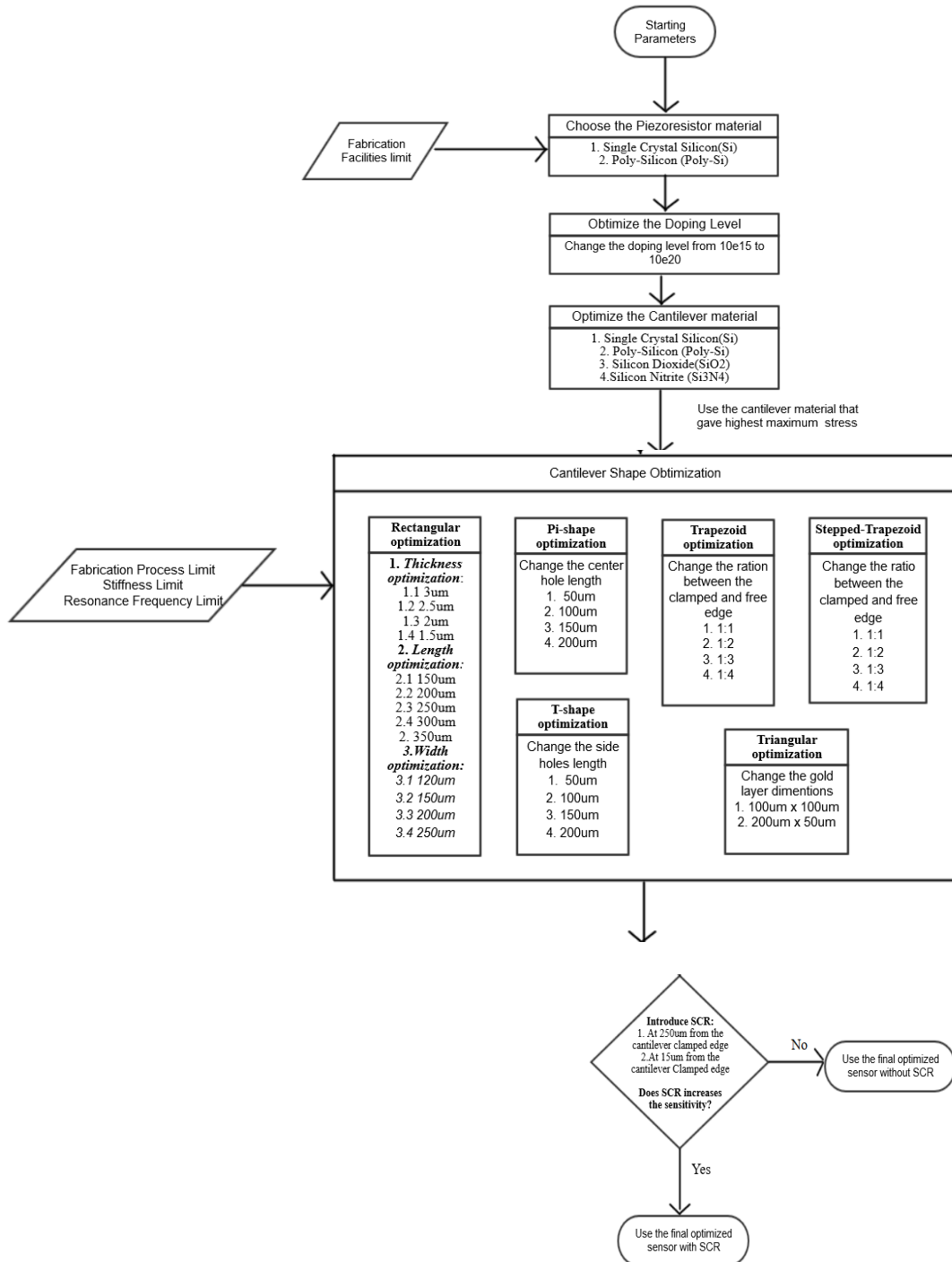


Figure 3.1 : Sensor Optimization procedure flowchart

3.2 Starting Piezoresistive Microcantilever

3.2.1 Sensor definition

As starting, a rectangular single crystal Silicon Microcantilever with dimensions ($200\mu m \times 120\mu m \times 1.5\mu m$) for length, width and thickness respectively was used. The different starting sensor parameters that were used are shown in Table 3.1 whereas Table 3.2 gives the different materials properties used throughout these simulations.

Table 3.1 Starting Sensor Specifications.

Parameter	Starting value
Cantilever shape	Rectangle
Cantilever material	Single Crystal Silicon (Si)
Cantilever Length (L)	200 μm
Cantilever Width (W)	120 μm
Cantilever Thickness (t)	3 μm
Gold layer Length (GL)	100 μm
Gold layer Width (GW)	100 μm
Gold Layer Thickness(Gt)	0.2 μm
Piezoresister Material	Polysilicon (Boron doped)
Piezoresister Length (PL)	20 μm
Piezoresister Width (PW)	5 μm
Piezoresister Thickness(Pt)	0.5 μm
Total Force exerted on the Gold layer (Ft)	250pN towards the ground
Piezoresister doping level (Pd)	$1 \times 10^{16} \text{ cm}^{-3}$
Input voltage (Vin)	1V

Table 3.2 Material properties.

Material	Poisson's ratio	Young Modulus	Density
Silicon Oxide (SiO ₂)	0.17	70 GPa	2200[kg/m ³]
Silicon Nitride (Si ₃ N ₄)	0.23	250 GPa	3100[kg/m ³]
Single Crystal Silicon (Si) [100]	0.28	170 GPa	2330[kg/m ³]
Polycrystalline silicon (Poly-Si)	0.22	160 GPa	2320[kg/m ³]
Gold	0.44	70 GPa	19300[kg/m ³]
P-Silicon (Boron doped) [101]	0.278	130 GPa	2330[kg/m ³]
P-Poly Silicon (Boron doped)	0.2	160 GPa	2320[kg/m ³]

On top of the cantilever, a $100\mu\text{m} \times 100\mu\text{m} \times 0.2\mu\text{m}$ Gold layer is used for the attachment of the analytes while $20\mu\text{m} \times 5\mu\text{m} \times 0.5\mu\text{m}$ rectangular polysilicon piezoresistor is used for the piezoresistive sensing. The piezoresistor used here have a uniform p-type dopant density of $1 \times 10^{16} \text{ cm}^{-3}$, a thickness of 400 nm and 1V excitation voltage (the interconnections are not simulated). The starting sensor is shown in Figure 3.2.

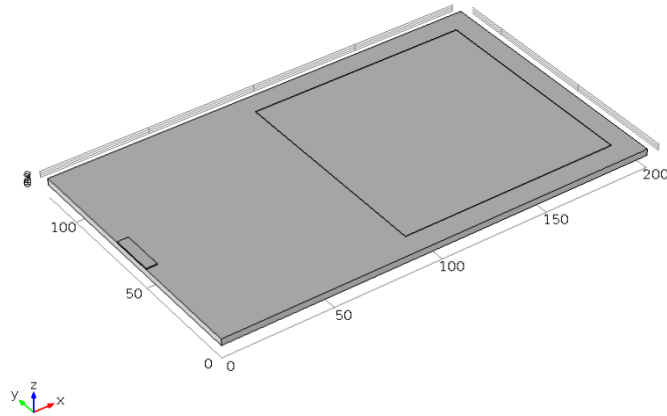


Figure 3.2 : Starting Sensor

From the fabrication perspective, The width of the starting cantilever is defined by adding $10\mu\text{m}$ offset to both sides of the $100\mu\text{m} \times 100\mu\text{m} \times 0.2\mu\text{m}$ Gold layer. Usually, microcantilevers length are in the range between $100 \mu\text{m}$ to $500 \mu\text{m}$ and the thickness in the range of $0.5 \mu\text{m}$ to $5 \mu\text{m}$, thus here the starting length was defined as double the length of the Gold layer and the thickness was selected to be $3 \mu\text{m}$ which is almost half of the range.

Since the dimensions of the piezoresistor will be fixed throughout the different simulations, $20 \mu\text{m}$ was selected as the piezoresistors length due to the space limit in the trapezoid and stepped-trapezoid structures. As presented in [7], it was the biosensor sensitivity is almost unaffected by the piezoresistors length.

3.2.2 Multiphysics setup

In this sensor design, two physics modules are used to define this sensor, “Piezoresistivity (domain currents)” and “Solid mechanics”. Piezoresistivity (domain currents) was used to define the piezoresistor by adding where piezoresistor doping

level was set to 10^{16} cm^{-1} . All the other parameters needed for the piezoresistor's definition are taken from the material.

In the Solid mechanics module, the cantilever is fixed at one end ($X = 0$) and a total force of 250pN was applied on top of the Gold layer.

3.2.3 Mesh and solver studies

Using the finite element analysis method, to achieve reliable results an acceptable element mesh must be used. In this sensor, a user-controlled mesh is employed in this simulation in which different mesh size are used in various regions of the sensor as shown in Figure 3.3; the edges of the Gold, piezoresistor, and cantilever are meshed using different fine triangular meshes with a minimum size equals to the thickness of each layer. The remaining of the sensor is meshed using fine free tetrahedral mesh.

Two solvers are used, the Stationary solver from which von Mises stress, deflection, and piezoresistor potential plots can be obtained and Eigenfrequency solver to get the eigenfrequencies of the sensor.

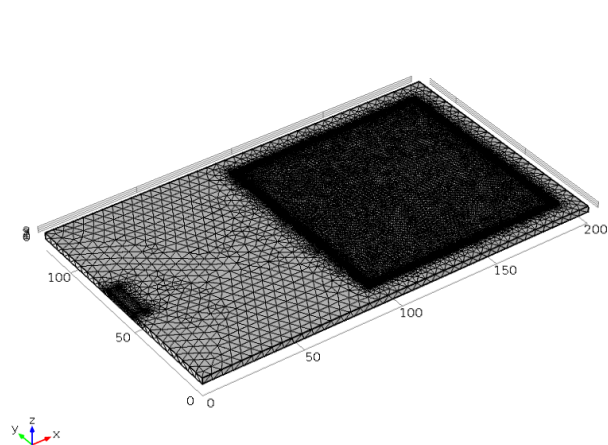


Figure 3.3 : Starting Sensor's mesh

3.3 Piezoresistor Material Selection

Since Silicon is the dominant material used in microfabrication, only silicon is utilized in this design. Two type of silicon is usually used as the piezoresistor material in piezoresistive sensors, single crystal silicon and Polycrystalline Silicon (Poly-Si). They have different properties that influence mechanical strength, sensitivity, and even manufacturability of the final sensor.

Since in both of them p-type (Boron-doped) gives higher sensitivity, only p-type Si and Poly-Si were used. Two different simulations to compare the results when Si and Poly-Si are used were done, From the obtained results and bearing in mind the fabrication facilities the sensor's piezoresistor material was defined and used in the following steps.

3.4 Choosing the Piezoresistor Doping level

Several researches in literature confirmed that increasing the doping level of the piezoresistor makes it almost temperature independent but at the same time reduces the sensors sensitivity thus a tradeoff must be done between the sensitivity and the thermal noise [102]. In this step, the doping density was varied from $1 \times 10^{15} \text{ cm}^{-3}$ to $1 \times 10^{20} \text{ cm}^{-3}$ to select the optimized doping level for this sensor.

3.5 Cantilever Material Optimization

The goal of this optimizing step is to choose the cantilever's material that gives the maximum deflection and maximum stress (thus maximum sensitivity) in response to the same applied force.

The most popular materials used for constructing microcantilevers are Single Crystal Silicon (Si), Polycrystalline silicon (Poly-Si), Silicon dioxide (SiO_2) and Silicon Nitride (Si_3N_4). Thus four simulations were made in this step where at each one of these materials were used as the cantilever's material. After best cantilever material had been defined in this optimization step, it was used throughout all the following steps.

3.6 Optimizing Cantilever Shape

Different cantilever shapes were used and varied in this step bearing in mind the fabrication process limit, the resonance frequency and stiffness.

3.6.1 Rectangular

3.6.1.1 Rectangular Cantilever Thickness Optimization

From equation (2.1) it is expected that the thinner cantilever is, the higher the deflection and sensitivity. Considering the fabrication process limits and the ratio

between the cantilever thickness and the piezoresistor thickness, the thickness of the cantilever has been given the values 3, 2.5, 2 and 1.5 μm and the simulation results were compared to choose the thickness which provides better sensitivity that will be used in the remaining steps.

3.6.1.2 Rectangular Cantilever Length Optimization

Again from equation (2.1), it is expected that the taller the cantilever is, the higher deflection and sensitivity. Since the length of the cantilever defines the stiffness and resonance frequency, it has been given the values 150, 200, 250, 300 and 350 μm and the simulation results were compared to choose the length which gives better sensitivity that will be used in the remaining steps.

3.6.1.3 Rectangular Cantilever Width Optimization

The smaller the cantilever width, the higher deflection and sensitivity results. But considering the used Gold layer width and offset limits mentioned before, it has been given the values 120, 150, 200 and 250 μm and the simulation results were compared to choose the design that provides better sensitivity which will represent the optimized rectangular shape microcantilever sensor.

3.6.2 Pi-shape from cantilever (Double legged)

The Pi-shape cantilever was obtained by inserting a hole in the middle of the final optimized rectangular cantilever (the hole width is one-third the optimized width), as shown in figure 3.4.a. Variations the hole length (50, 100, 150 and 200 μm) were made to find the optimized Pi-shaped microcantilever sensor structure. Finer meshes were used for this structure to avoid meshing errors, shown in figure 3.4.b.

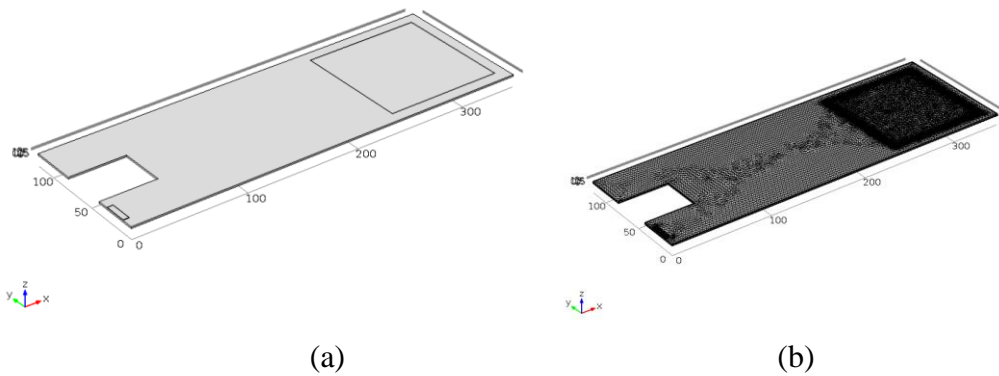


Figure 3.4 : Pi-Shape sensor (a) Structure (b) Mesh

3.6.3 T shape cantilever (one legged)

The T-shape cantilever was obtained by inserting two holes in both sides of the optimized rectangle (the hole width is one-third the optimized width), as shown in figure 3.5.a. Variations the hole lengths (50, 100, 150 and 200 μm) were made to find the optimized T-shaped microcantilever sensor structure. Finer meshes were used for this structure to avoid meshing errors, as shown in figure 3.5.b.

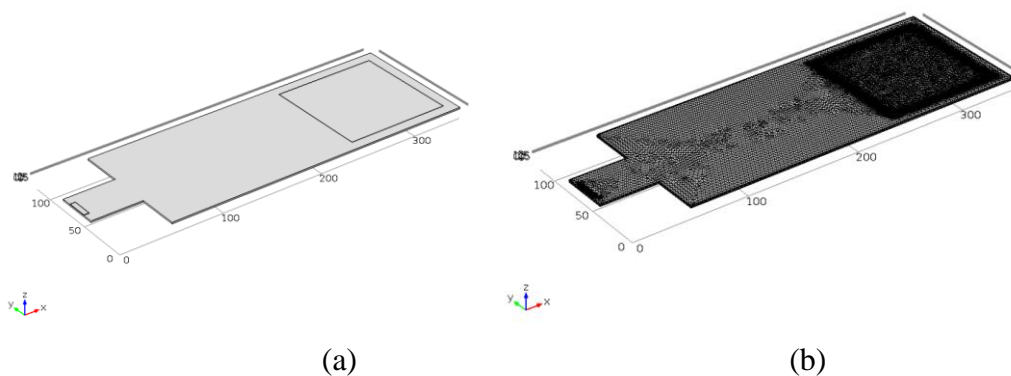


Figure 3.6 : T-Shape sensor (a) Structure (b) Mesh

3.6.4 Trapezoid shape cantilever

One of the unusually used cantilever forms is the trapezoid shape where the cantilever width is not fixed; it increases linearly from the clamped edge to the free edge with the increment of the cantilever length.

This structure was originally intruded in [103], but in this study, the ratio between the cantilever width was varied as 1:1,1:2, 1:3 and 1:4 while the width increases linearly in between, as shown in Figure 3.6. This results in changing the body center

point thus the sensitivity is expected to be enhanced. When the ratio between the clamped and free edge is 1:1, the structure is the same as the previously optimized rectangular cantilever.

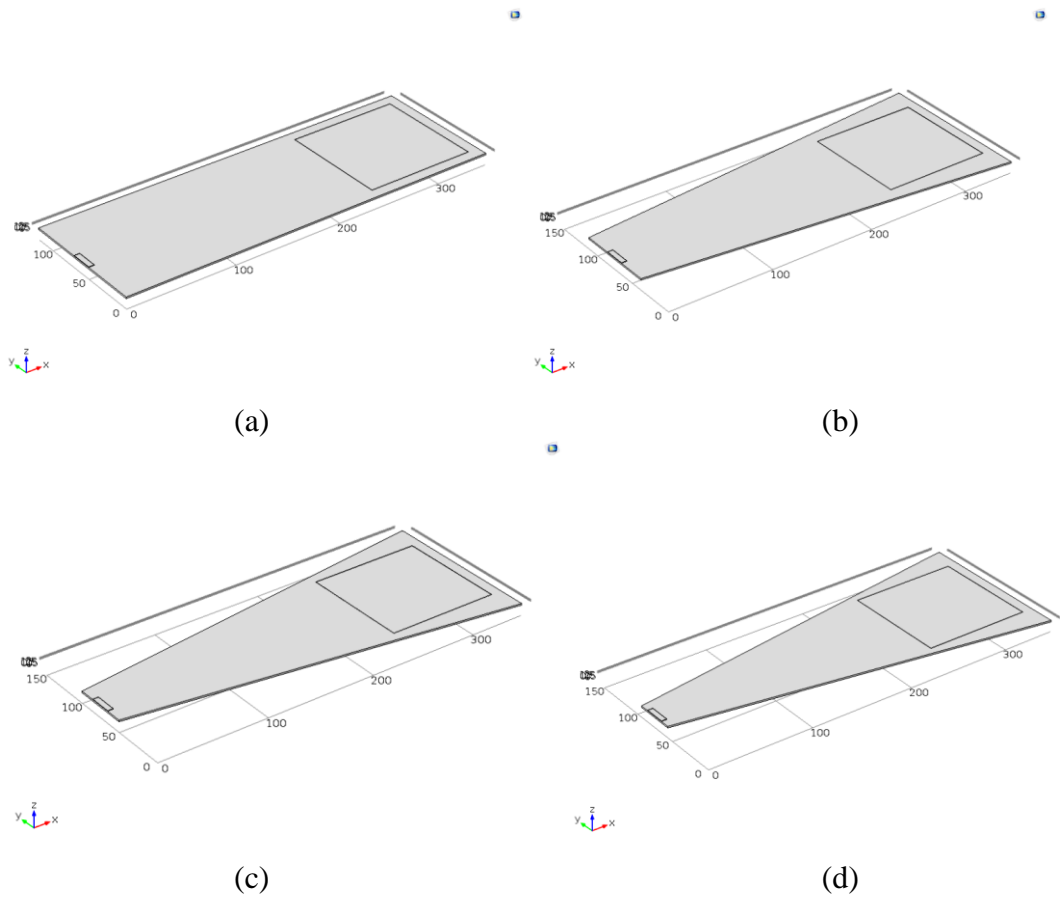
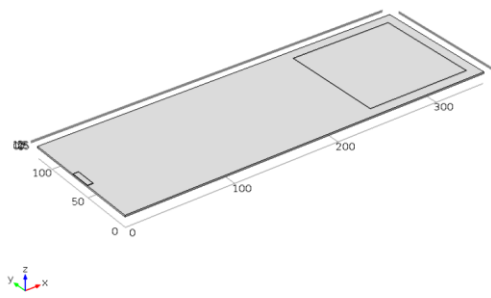


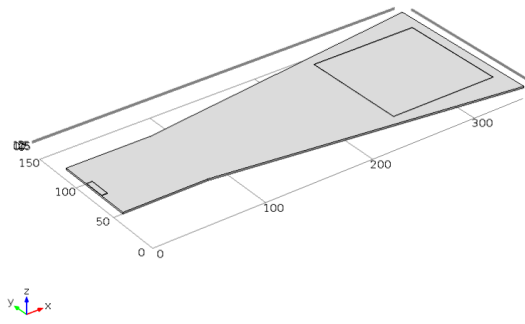
Figure 3.6 : Trapezoid Shape sensor (a) 1:1 (b) 1:2 (c) 1:3 and (d) 1:4

3.6.5 Stepped Trapezoid shape cantilever

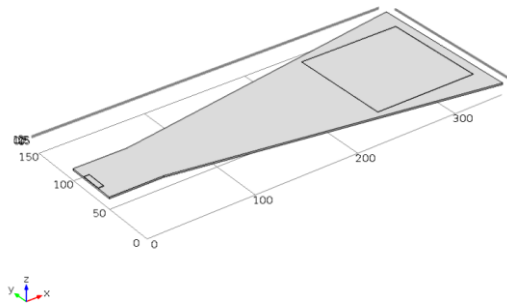
Another way to change the body center is by adding a square step near to the clamped cantilever edge after which the cantilever width starts to increase until it reaches the previously optimized cantilever width, as shown in Figure 3.7. Again variation in the ratio between the clamped edge width and the free edge width was made as 1:1, 1:2, 1:3 and 1:4. Which means that steps of $75\mu m \times 75\mu m$, $50\mu m \times 50\mu m$ and $37.5\mu m \times 37.5\mu m$ were added to the previous 1:2, 1:3 and 1:4 structures respectively.



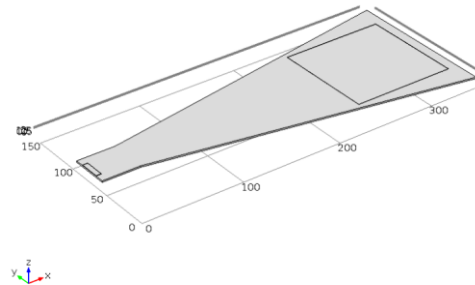
(a)



(b)



(c)



(d)

Figure 3.7 : Stepped-Trapezoid Shape sensor (a) 1:1 (b) 1:2 (c) 1:3 and (d) 1:4

3.6.6 Triangular shape cantilever

Another cantilever shape that is proposed is the triangular shape. To preserve the of Gold layer area, only two variations were possible for this structure. The first is by using $100\mu\text{m} \times 100\mu\text{m}$ Gold layer $20\mu\text{m}$ away from the clamped cantilever edge, whereas the other using a $200\mu\text{m} \times 50\mu\text{m}$ Gold layer $20\mu\text{m}$ away from the clamped edge. Both structures and meshes are shown in Figure 3.8.

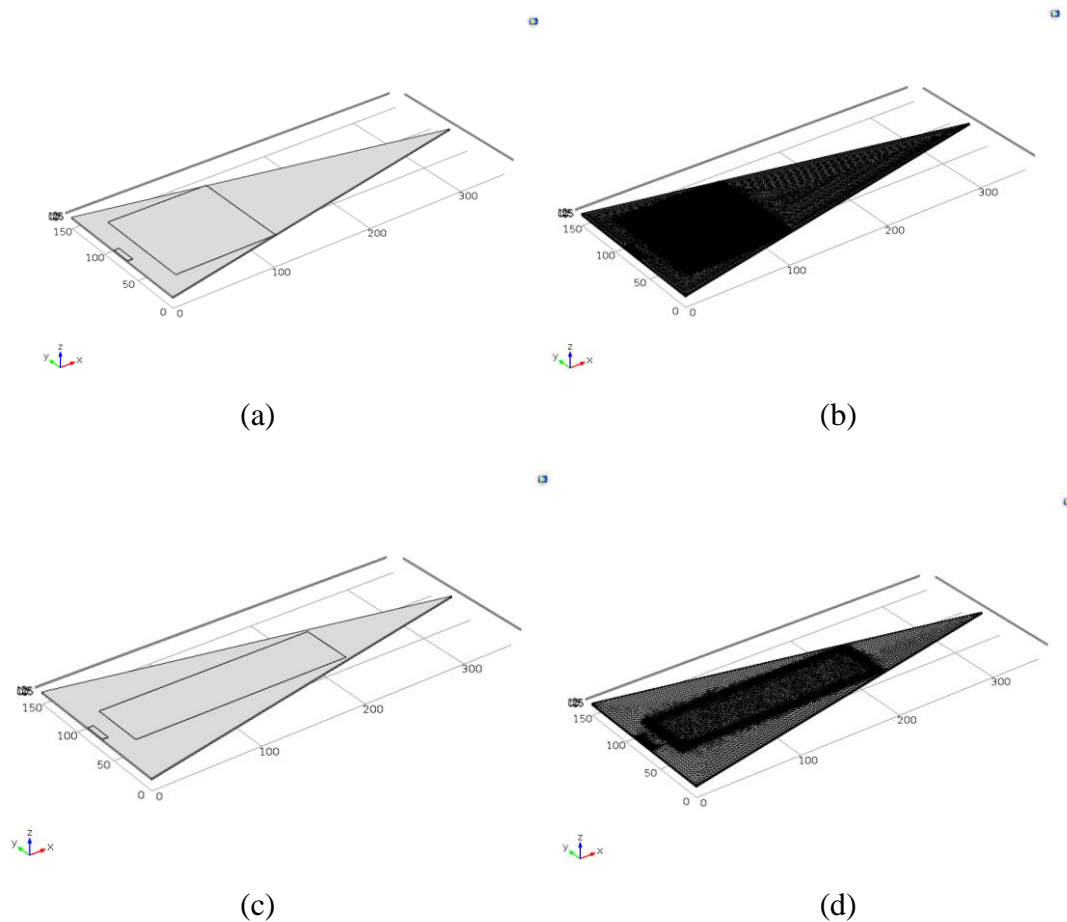


Figure 3.8 : Triangular Shape sensor (a) $100\mu\text{m}\times 100\mu\text{m}$ Gold layer (b) $100\mu\text{m}\times 100\mu\text{m}$ Gold layer mesh (c) $200\mu\text{m}\times 50\mu\text{m}$ Gold layer (d) $200\mu\text{m}\times 50\mu\text{m}$ Gold layer mesh

3.7 Stress Concentration Region

A new approach which has been proven to enhance the displacement, force and torque sensitivities of microcantilever-based sensors is to incorporate a Stress Concentration Region (SCR). SCR is a region in the structure that localizes the stress in that place in the cantilever. It can be done by either thinning the cantilever in a particular location [104, 105] or by incorporating a hole in the structure [106-108]. This approach became very attractive for the sensitivity enhancement since no extra high-tech equipment is needed to produce SCR, only etching and mask design.

If the SCR shape, dimensions, and position are optimized, it can result in sensor's sensitivity enhancement when compared with the case of no SCR. When a hole is used, different hole shapes can be utilized, but it has been confirmed in many studies that rectangular hole results into more sensitivity improvement than when other hole shapes were used [109,110].

Due to the expected difficulty of the fabrication when the thickness reducing SCR method is used, in this study a rectangular hole has been used as an SCR. After variation in the SCR length was made, a $30\mu\text{m}\times 10\mu\text{m}$ rectangular hole was defined as the SCR that will be used in this design. The location and orientation of the SCR were varied to find the optimum place for the SCR which results in an increase in the cantilever stress.

3.8 Range of Force

In this work, the attachment of the biomolecules is simulated using a distributed force applied on top of the Gold layer. After the final sensor design is obtained, the 25 to 250 pN force range was used to get the maximum stress and deflection for each and then from the results the sensitivity regarding the change in the resistance/ force was calculated.

3.9 Fabrication

The fabrication of this sensor will be realized starting with Double-Side Polished (DSP) silicon wafer (Figure 3.9.a).

Using Low-Pressure Chemical Vapor Deposition (LPCVD), silane (SiH_4) and Oxygen (O_2) will be used to cover both sides of the wafer will be with $1.5\mu\text{m}$ Silicon Dioxide (SiO_2), the reaction is given in equation 3.1 (Figure 3.9.b).



Next, a $0.5\mu\text{m}$ layer of polysilicon will be deposited on the top of the wafer from the decomposition of tetraethylorthosilicate (TEOS; $\text{Si}(\text{OC}_2\text{H}_5)_4$) in LPCVD process as given in equation 3.2.



The polysilicon layer will be patterned using lithography (mask 1, Figure 3.10.a) and dry etched in Chlorine Based Reactive Ion Etching (RIE) to define the piezoresistor shape (Figure 3.9.c). Then, the piezoresistor will be doped with Boron using Ion Implantation.

To define the Gold layer for the analytes attachment, a reversed AZ 1514H positive photoresist mask will be used first using lithography (mask 2, Figure 3.10.b).

Afterward, using sputtering a very thin layer of chromium (Cr) followed by the 200 nm thick Gold (Au) layer will be deposited on top of the wafer (Figure 3.9.d). Using Acetone, the excess Gold will be removed by Lift-off technique (Figure 3.e). For the connections, aluminum wires will be fabricated using reversed AZ 1514H positive photoresist mask (lithography process using mask 3, Figure 3.10.c) followed the deposition of Aluminum using by electron beam evaporation (Figure 3.9.f). Again, the excess Aluminum will be removed by the Lift-off technique using Acetone (Figure 3.9.g). To define the SiO₂ cantilever shape, photoresist mask will be needed to define the cantilever shape on the front side (lithography using mask 4, Figure 3.10.d) then using Buffered Oxide Etchant (B.O.E.), a mix of Fluorhydric Acid (HF) and Ammonium Fluoride (NH₄F), the SiO₂ in the front side will be patterned whereas the SiO₂ in the back side will be completely removed (Figure 3.9.h).

Using LPCVD (from silane (SiH₄) and ammonia (NH₃)), Silicon Nitride (Si₃N₄) will be deposited on both sides of the wafer. Afterward, the back side will be patterned using lithography to define the opening (Mask 5, Figure 3.10.3), the sensor at this stage is shown in Figure 3.9.i. The cantilever will finally be released by etching the silicon using Tetramethylammonium hydroxide (TMAH) and then Si₃N₄ will be removed using Orthophosphoric acid (H₃PO₄). The H₃PO₄ etching selectivity of Si₃N₄ over SiO₂ can be enhanced using different ways among which adding of Si(OH)₄ to H₃PO₄ in the presence of NH₄F and NH₄HF₂ gives an etch selectivity greater than 10⁴. Since H₃PO₄ might etch the Al and Au layer, the etching time of Si₃N₄ must be controlled very precisely.

The final sensor cross section is shown in Figure 3.9.j. The masks used in this fabrication process for a single sensor is shown in Figure 3.10.

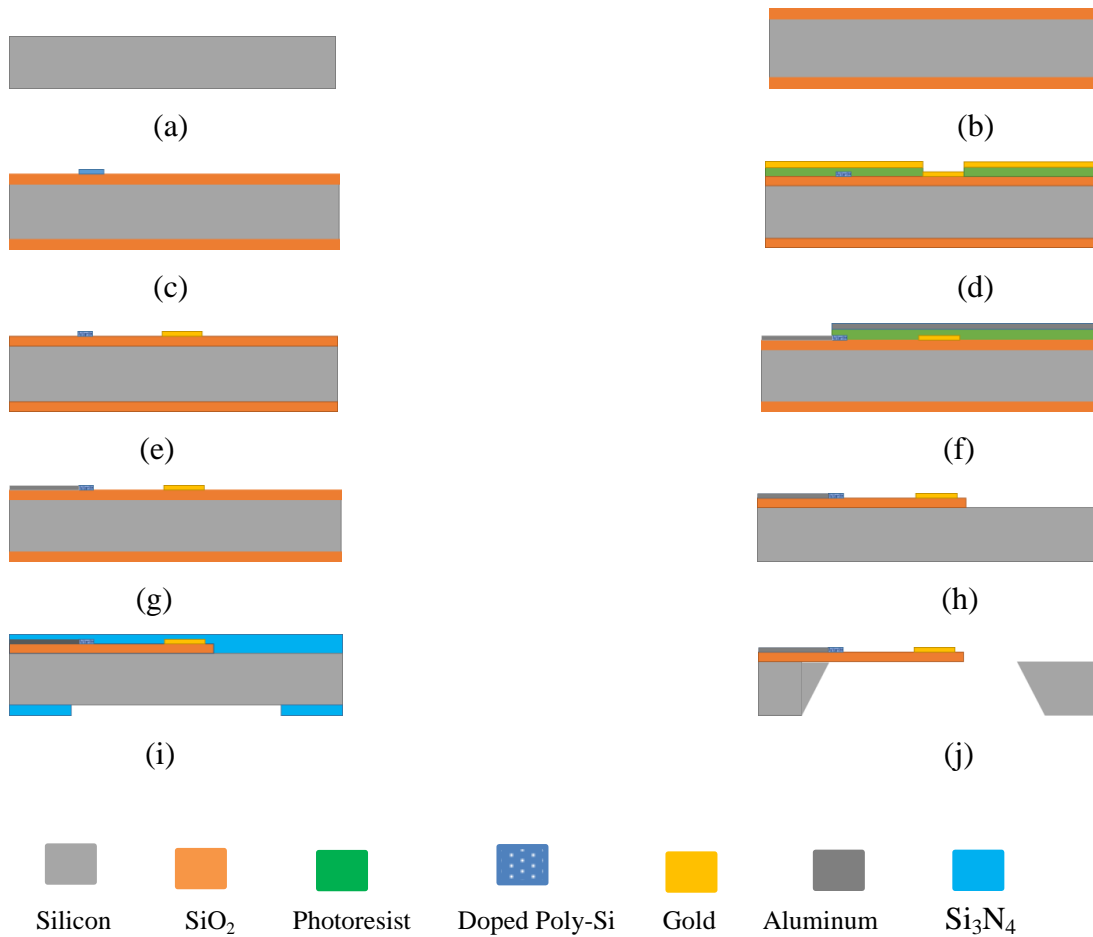


Figure 3.9 : Cross-section view of the Sensor Fabrication sequence : (a) DSP wafer (b) Wafer covered with SiO₂ on both sides (c) Polysilicon deposition and patterning (d) Reversed photoresist and Gold deposition (e) Gold Lift-off (f) Reversed photoresist and Aluminum deposition (g)Aluminum Lift-off, (h) SiO₂ patterning (i) Si₃N₄ deposition and patterning (j) Final sensor cross section

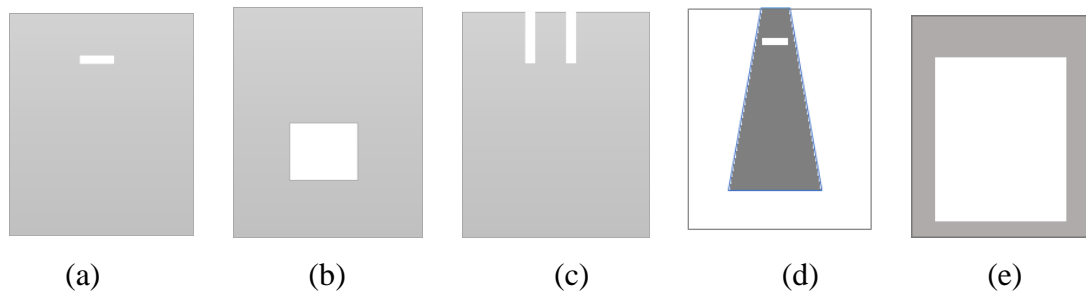


Figure 3.10 : Fabrication Masks (a) Piezoresistor mask (b) Gold mask (c) Aluminum connections mask (d) Cantilever shape mask (e) Cantilever holes backside mask

4. RESULTS AND DISCUSSION

In this chapter, the results obtained from the different piezoresistor microcantilever biosensor simulations are presented and discussed to find the sensor design that gave the highest sensitivity.

4.1 Starting Sensor

As mentioned in section 3.2.3, from the Stationary solver, von Mises stress, deflection, and piezoresistor potential plots were obtained, as shown in Figure 4.1.

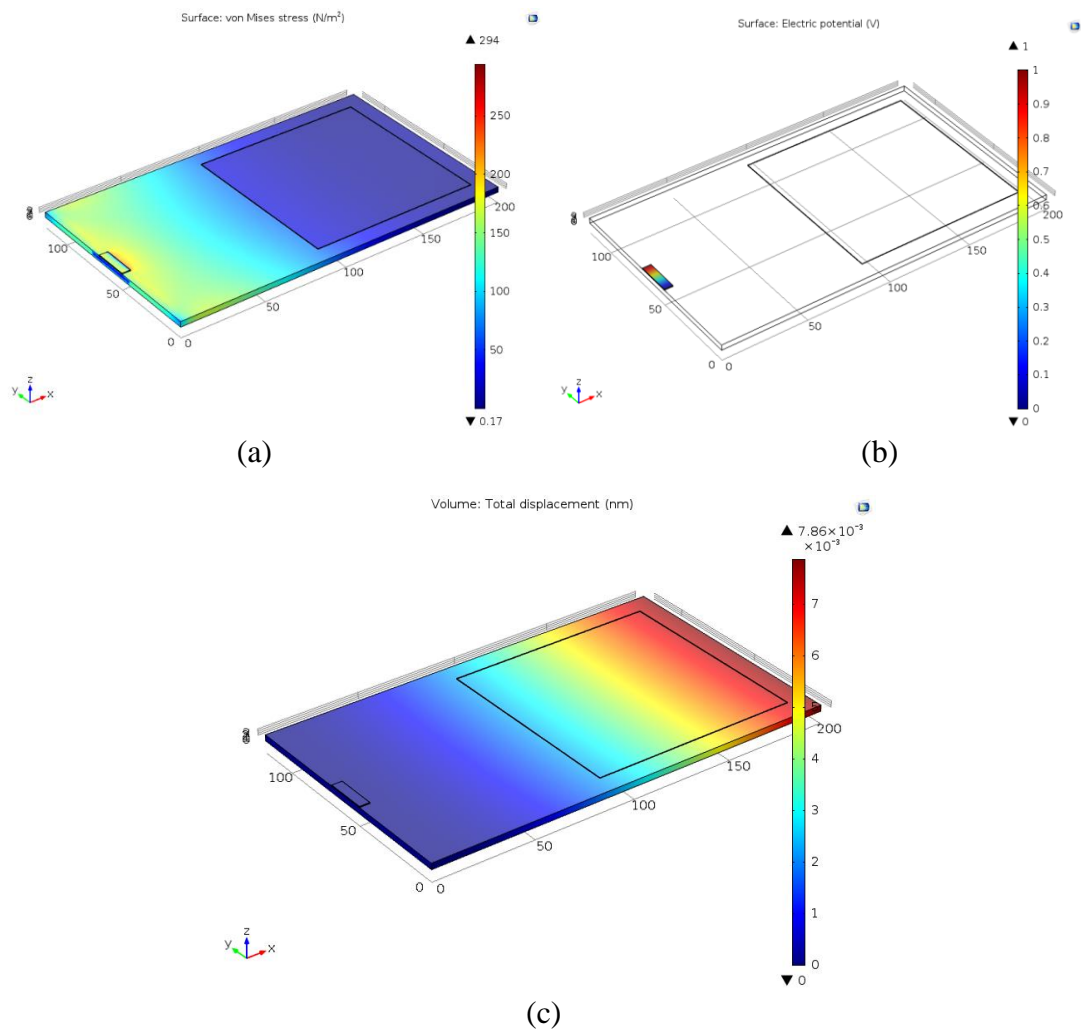


Figure 4.1 : Starting Sensor Results (a) Von Mises stress plot, (b) Piezoresistor potential plot and (c) Deflection plot

Using the Eigenfrequency solver, the first six eigenfrequencies of the starting sensor were found to be 91.535KHz, 0.3543MHz, 0.6096MHz, 1.239MHz, 1.749MHz and 1.9129MHz.

Since the piezoresistor sensor in this design is a transverse piezoresistor (the piezoresistor experiences stress in perpendicular to the current flow direction), [112], the $\Delta R/R$ sensor sensitivity is calculated using equation (4.1) by assuming the transverse stress is equals to the maximum von mises stress and the longitudinal stress equals to zero. Table 4.1 presents the longitudinal (π_l) and transverse piezoresistive coefficients (π_t) of a Polysilicon material.

$$\text{Sensitivity } (\Delta R/R) = \pi_t \sigma_{max} \quad (4.1)$$

Table 4.1 : longitudinal (π_l) and transverse piezoresistive coefficients (π_t) of a Polysilicon material [113].

Wafer Type	$\pi_l (10^{-11} Pa^{-1})$	$\pi_t (10^{-11} Pa^{-1})$
n-type	-45.4	34.5
p-type	58.8	-18.5

It was found that for the starting sensor, $\Delta R/R$ equals to $-5.4 \times 10^{-8} \Omega/\Omega$, the minus sign refers to the fact that the resistance decreases with stress because it is the transverse orientation. Using global evaluation, the current passing through the piezoresistor and its resistance were also calculated. Table 4.2 presents the results of the starting sensor simulation.

Table 4.2 : The Starting Sensor Simulation Results.

Property	Value
Input Voltage	1 V
Current passing through the Piezoresister	0.21440 mA
Resistance of the piezoresister	4.6642 K Ω
Maximum Von Mises stress	294 N/m^2
Maximum deflection	0.00786 nm
Sensitivity $(\Delta R/R) = \pi_t \sigma_{max}$	$-5.4 \times 10^{-8} \Omega/\Omega$

4.2 Piezoresistor Material Selection

From the Stationery solver, it was found that the maximum von Mises stress plot for single crystal silicon is 278 N/m^2 whereas when polysilicon was used as the piezoresistor material it is 294 N/m^2 but in both cases the, maximum deflection is the same (0.00786 nm). Figure 4.2 shows the maximum von mises stress plot in both cases. The single crystal silicon piezoresistor used here is oriented to be at 45° to the die edge, and so lies in the $\langle 110 \rangle$ direction of the crystal.

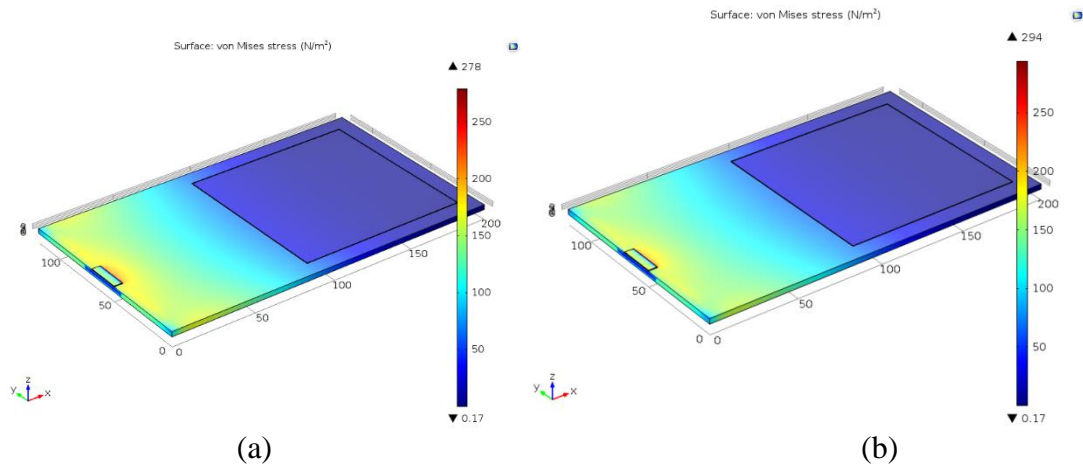


Figure 4.2 : Von Mises stress plot (a) Single crystal silicon piezoresistor (b) Polysilicon piezoresistor

Using equation (4.1), the $\Delta R/R$ sensitivity in both cases was calculated and found to be -1.84×10^{-7} and -5.4×10^{-8} for the single crystal silicon and polysilicon cases respectively (The values of the longitudinal (π_l) and transverse piezoresistive coefficients (π_t) of a silicon $\langle 100 \rangle$ wafer for a doping level of 10^{16} cm^{-3} shown in table 4.3).

Even though the $\Delta R/R$ sensitivity is higher in the case of single crystal silicon, for this sensor design polysilicon has been chosen because it's sensitivity does not depend on the crystal orientation, the sensor fabrication is easier, cheaper and can be realized in ITUnano laboratory.

Table 4.3 : Longitudinal (π_l) and transverse piezoresistive coefficients (π_t) of a silicon $\langle 100 \rangle$ wafer for a doping level of 10^{16} cm^{-3} [114].

Wafer Type	$\pi_l (10^{-11} Pa^{-1})$	$\pi_t (10^{-11} Pa^{-1})$	Orientation
n-type	-31.6	-17.16	$\langle 110 \rangle$
p-type	71.8	-66.3	$\langle 110 \rangle$

4.3 Choosing the Piezoresistor Doping Level

As mentioned in section 3.1, the sensitivity of the piezoresistive sensor decreases with the increasing of the doping level. At the same time, the high doping level makes the sensor almost temperature independent thus a tradeoff between the optimal cantilever performance and the thermal noise immunity must be done.

For this purpose, the doping level of the Boron doped polysilicon piezoresistor was varied in the range between $1 \times 10^{15} \text{ cm}^{-3}$ to $1 \times 10^{20} \text{ cm}^{-3}$. Using the plot obtained from Kanda's model in Figure 4.3, The piezoresistance factor (P) of p-type silicon for each dopant concentration at 300K was determined.

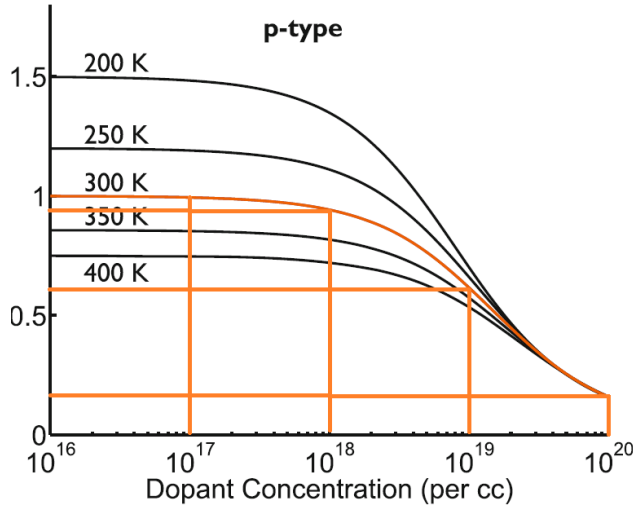


Figure 4.3 : The piezoresistance factor of p-type silicon plotted as a function of dopant concentration for several operating temperatures [115]

Afterward, the transverse piezoresistive coefficient for each doping level was calculated using equation 4.2, as shown in Table 4.4.

$$\pi(N, T) = P(N, T)\pi^{ref} \quad (4.2)$$

where π_{ref} is the value of the piezoresistive coefficient of interest for lightly doped silicon (10^{16} cm^{-3}) at 300 K. Using this equation, all of the piezoresistive coefficients (π_{11} , π_{12} , π_{44} , π_l and π_t) can be scaled linearly using the piezoresistance factor.

Table 4.4: Polysilicon Transverse piezoresistance coefficient (π_t) for different doping level calculated from the piezoresistance factor (P) plot (T=300K).

Doping Level	10^{15} 1/cm^3	10^{16} 1/cm^3	10^{17} 1/cm^3	10^{18} 1/cm^3	10^{19} 1/cm^3	10^{20} 1/cm^3
piezoresistance factor (P)	1	1	1	0.95	0.6	0.2
Poly-Si Transverse Piezoresistance coefficient π_t (10^{-11} Pa^{-1})	-18.5	-18.5	-18.5	-17.58	-11.1	-3.7

From the simulation results, the maximum von Mises stress, maximum deflection and the resistance of the piezoresistance for each doping level was determined. Then, the sensitivity in each case was calculated using equation 4.1. The results of this optimization step are presented in Table 4.5. The sensitivity is plotted against different doping levels in Figure 4.4.

Table 4.5: Simulation Results when Different Piezoresistor Doping levels were used.

Property	Doping Level					
	10^{15} 1/cm^3	10^{16} 1/cm^3	10^{17} 1/cm^3	10^{18} 1/cm^3	10^{19} 1/cm^3	10^{20} 1/cm^3
Resistance (Ω)	1.0532 $\times 10^6$	1.1627 $\times 10^5$	19252	4664	820.27	92.727
Maximum Von Mises stress (N/m^2)	294	294	294	294	294	294
Maximum deflection (nm)	0.00786	0.00786	0.00786	0.00786	0.00786	0.00786
Sensitivity $(\Delta R/R) = \pi_T \sigma_{max}$	-5.4×10^{-8}	-5.4×10^{-8}	-5.4×10^{-8}	-5.1×10^{-8}	-3.2×10^{-8}	-1×10^{-8}

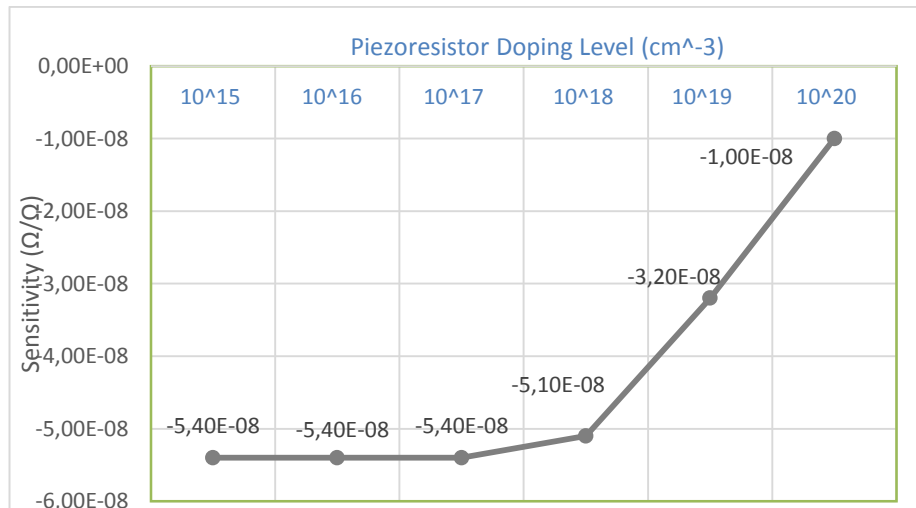


Figure 4.4 : The $\Delta R/R$ Sensitivity of the sensor when Different Doping Level was used for the p-type Polysilicon piezoresistor

From the results, it can be seen that using 10^{18} 1/cm^3 doping level it is high enough to reduce the thermal noise effect, at the same time the sensitivity does not be affected that much. Thus this doping level chosen and used throughout the following simulations.

4.4 Cantilever Material Optimization

As expected, different cantilever materials gave different maximum deflection and stress values as shown in Table 4.6. It can be seen that Silicon Dioxide (SiO_2) gave the highest maximum deflection and stress values because of its low young's modulus values compared to the other materials.

Table 4.6: Simulation results when Different Cantilever materials were used.

Property	Cantilever Material			
	Si	Poly-Si	SiO_2	Si_3N_4
Maximum Von Mises stress (N/m^2)	294	309	566	270
Maximum deflection (nm)	0.00786	0.0085	0.02	0.00545
Sensitivity ($\Delta R/R$) = $\pi_T \sigma_{max}$	-5.4×10^{-8}	-6.1×10^{-8}	-9.9×10^{-8}	-5.3×10^{-8}

The difference between the results of different cantilever materials is better represented graphically in Figure 4.5.

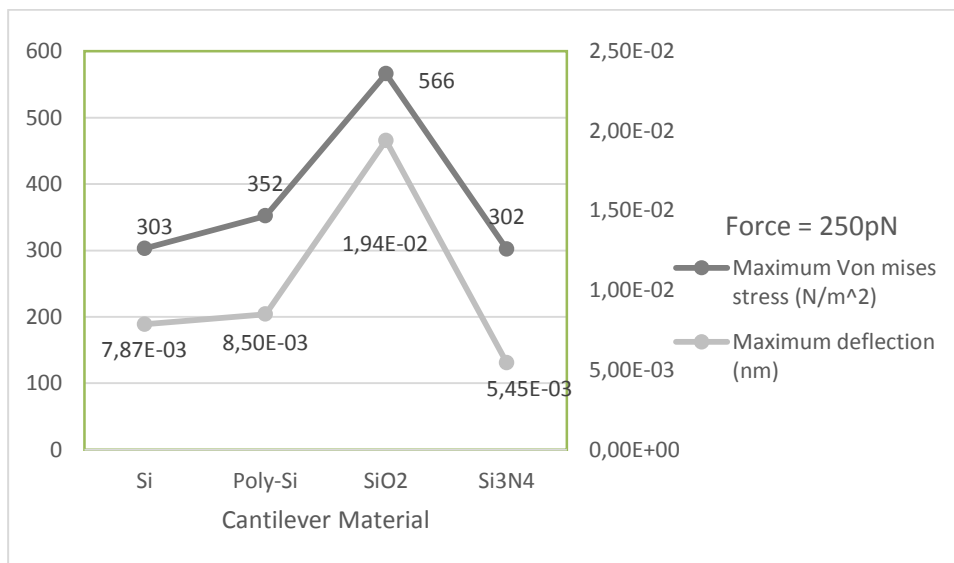


Figure 4.5 : Maximum Von Mises Stress and Maximum deflection values for various cantilever materials

It was found that SiO₂ resulted into almost 2.5x higher deflection and 1.7x higher sensitivity when compared to single crystal silicon (the starting cantilever material) case thus SiO₂ has been selected as the cantilever material for this biosensor and it is used in the following optimization steps. Figure 4.6 is the graph that presents the calculated sensitivity ($\Delta R/R$) values for the different cantilever material.

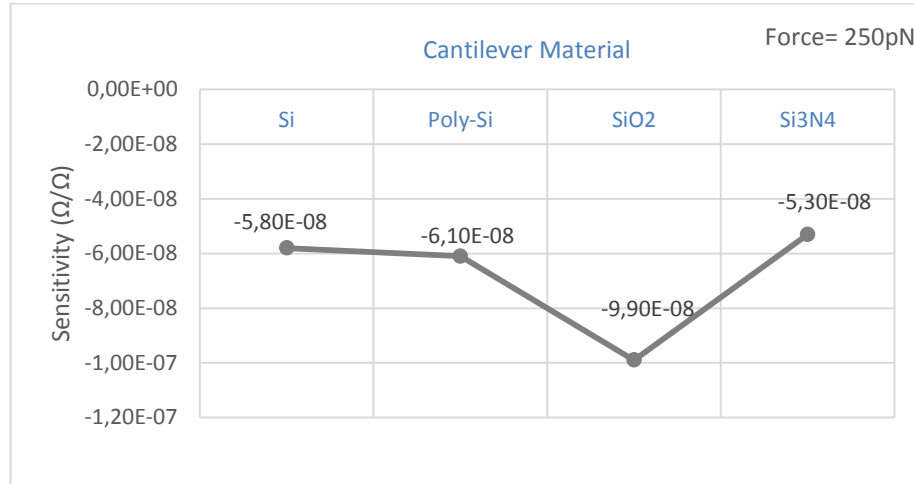


Figure 4.6 : The $\Delta R/R$ Sensitivity of the Sensor when the Cantilever was Built from Different Materials

4.5 Optimizing Cantilever Shape

4.5.1 Rectangular

4.5.1.1 Rectangular cantilever thickness optimization

When the cantilever thickness was varied between 3 μ m and 1.5 μ m, it was found that as the cantilever thickness decreases, the sensitivity increases. From the results shown in Table 4.7, it can be seen that using 1.5 μ m thick cantilever gave the highest sensitivity which is more than 4x times higher than the 1.5 μ m thick cantilever. Thus, 1.5 μ m was chosen to be the final optimized cantilever thickness.

Table 4.7: Simulation results when Different Cantilever thicknesses were used.

Property	Cantilever Thickness			
	3 μ m	2.5 μ m	2 μ m	1.5 μ m
Maximum Von Mises stress (N/m^2)	566	797	1287	2329
Maximum deflection ($n\ m$)	0.02	0.03	0.06	0.15
Sensitivity ($\Delta R/R$) =	-9.9	-1.4	-2.26	-4.09
$\pi_T \sigma_{max}$	$\times 10^{-8}$	$\times 10^{-7}$	$\times 10^{-7}$	$\times 10^{-7}$

The difference in performance for various cantilever thicknesses is more visible graphically in Figure 4.7 And Figure 4.8.

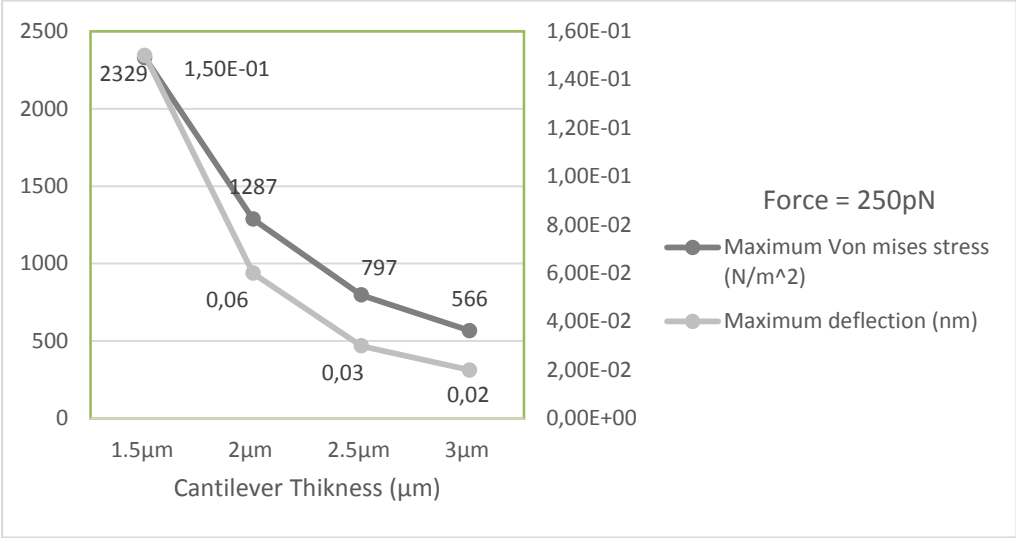


Figure 4.7 : Maximum Von Mises Stress and Maximum Deflection Values for Different Rectangular Cantilever Thicknesses

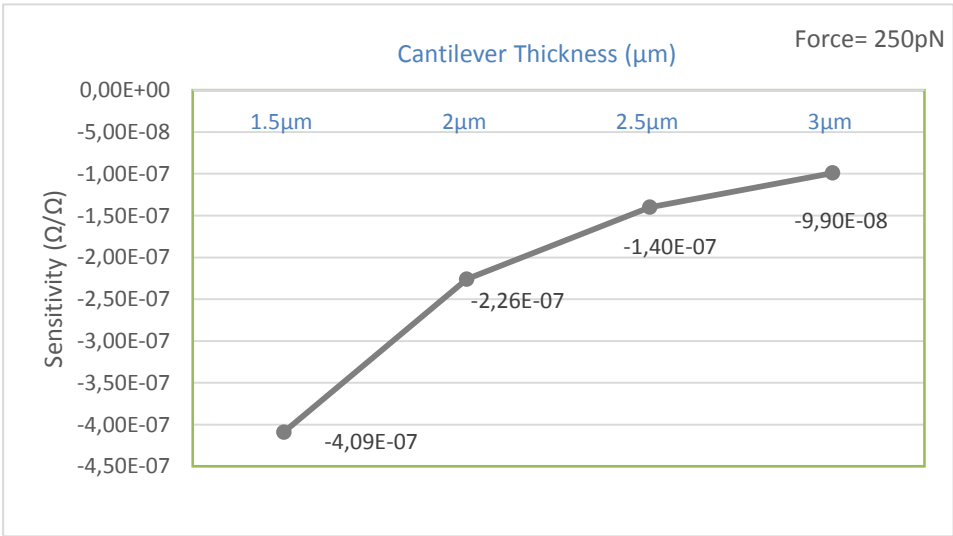


Figure 4.8 : The $\Delta R/R$ Sensitivity of the Sensor when for Different Cantilever Thicknesses

4.5.1.2 Rectangular cantilever length optimization

When the cantilever length was varied between 150μm to 350μm, it was found that as the cantilever length increases, the sensitivity increases. From the results shown in Table 4.8, it can be seen that using 350μm length cantilever gave the highest sensitivity which is almost 3.5x higher than the 150μm length cantilever. Thus, 350μm was chosen to be the final optimized cantilever length.

Table 4.8: Simulation Results when Different Cantilever Lengths were Used.

Property	Cantilever Length				
	150 μm	200 μm	250 μm	300 μm	350 μm
Maximum Von Mises stress (N/m^2)	1640	2329	3035	4603	5618
Maximum deflection (nm)	0.05	0.15	0.35	0.65	1.1
Sensitivity ($\Delta R/R$) = $\pi_T \sigma_{max}$	-2.88 $\times 10^{-7}$	-4.09 $\times 10^{-7}$	-5.33 $\times 10^{-7}$	-8.09 $\times 10^{-7}$	-9.87 $\times 10^{-7}$

The difference in results obtained when different cantilever lengths were used is more visible graphically in Figure 4.9 And Figure 4.10.

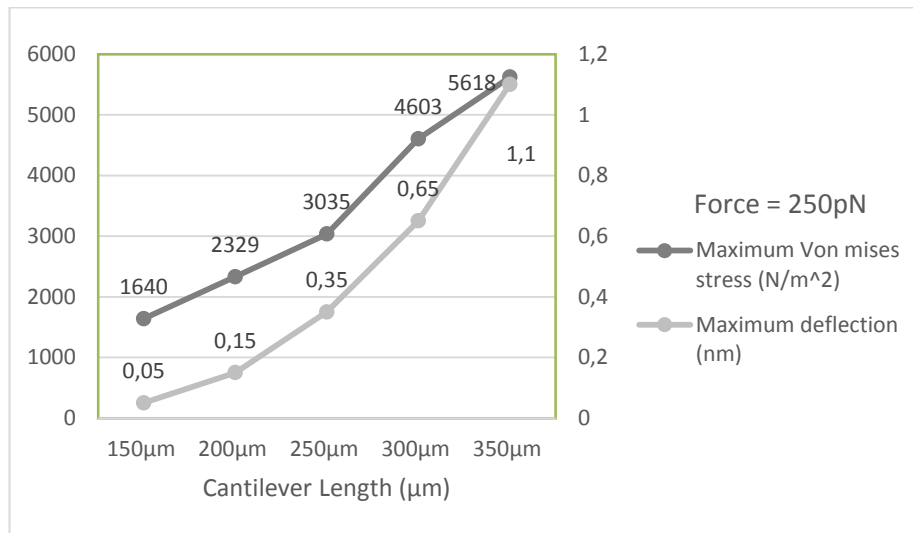


Figure 4.9 : Maximum Von Mises Stress and Maximum Deflection Values for Different Rectangular Cantilever Lengths

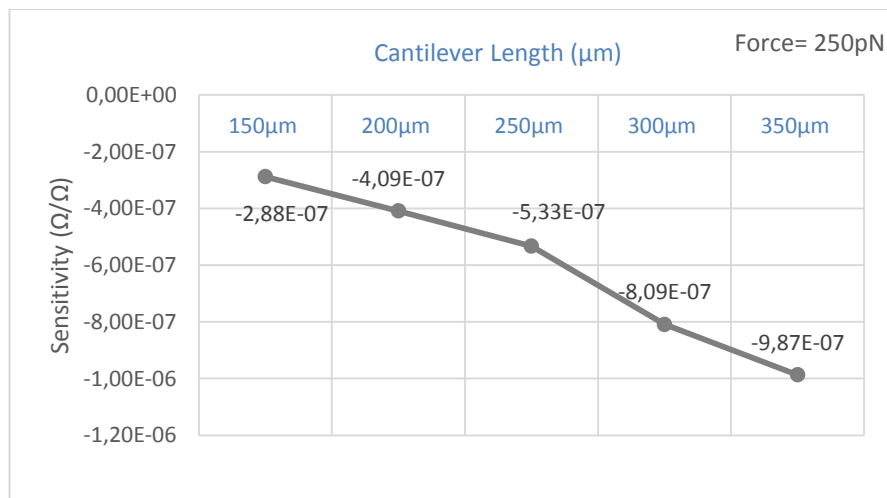


Figure 4.10 : The $\Delta R/R$ Sensitivity of the Sensor for Different Rectangular Cantilever Lengths

4.5.1.3 Rectangular Cantilever Width Optimization

When the cantilever width was varied between 120 μm and 250 μm , it was found that as the cantilever width increases, the sensitivity decreases. From the results shown in Table 4.9, it can be seen that using 120 μm width cantilever gave the highest sensitivity which is almost 2.4x higher than the 250 μm width cantilever. Thus, 120 μm was chosen to be the final optimized cantilever width.

Table 4.9: Simulation Results when Different Cantilever Widths were used.

Property	Cantilever Width			
	120 μm	150 μm	200 μm	250 μm
Maximum Von Mises stress (N/m^2)	5618	4212	3394	2376
Maximum deflection (nm)	1.1	0.88	0.66	0.53
Sensitivity ($\Delta R/R$) = $\pi_T \sigma_{max}$	-9.87×10^{-7}	-7.4×10^{-7}	-5.96×10^{-7}	-4.17×10^{-7}

The difference in performance when different cantilever thickness are used is more evident when shown graphically in Figure 11. And Figure 12.

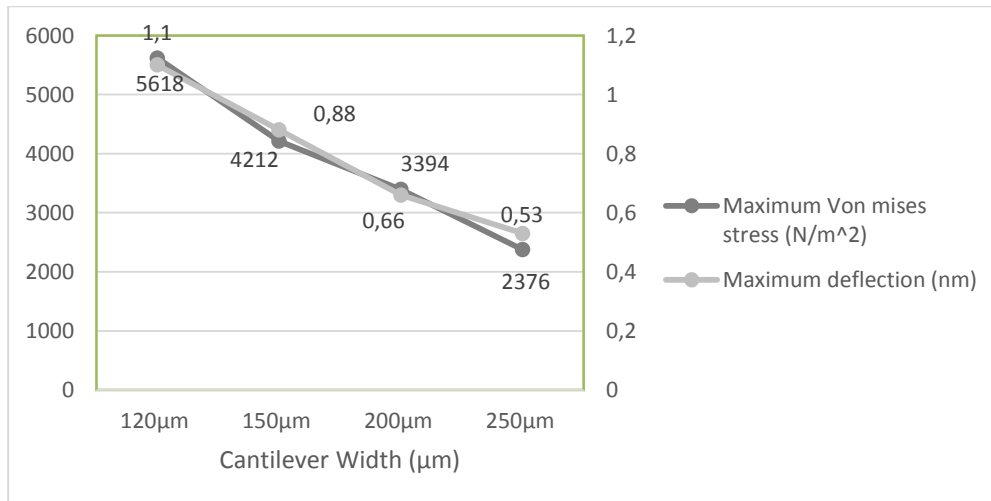


Figure 4.11 : Maximum Von Mises Stress and Maximum Deflection Values for Different Rectangular Cantilever Widths

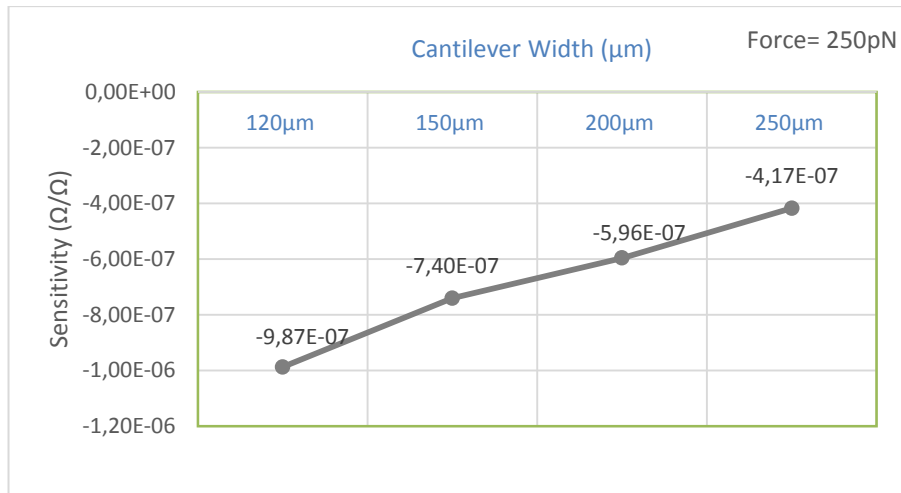


Figure 4.12 : The $\Delta R/R$ Sensitivity of the Sensor for Different Rectangular Cantilever Widths

Using Eigenfrequency solver, the first six eigenfrequencies of the final optimized rectangular sensor ($350\mu m \times 120\mu m \times 1.5\mu m$) were found to be 8.75KHz, 61.58KHz, 66.6KHz, 0.189MHz, 0.22MHz and 0.39MHz. The von mises stress and deflection plots for this sensor are shown in Figure 4.13.

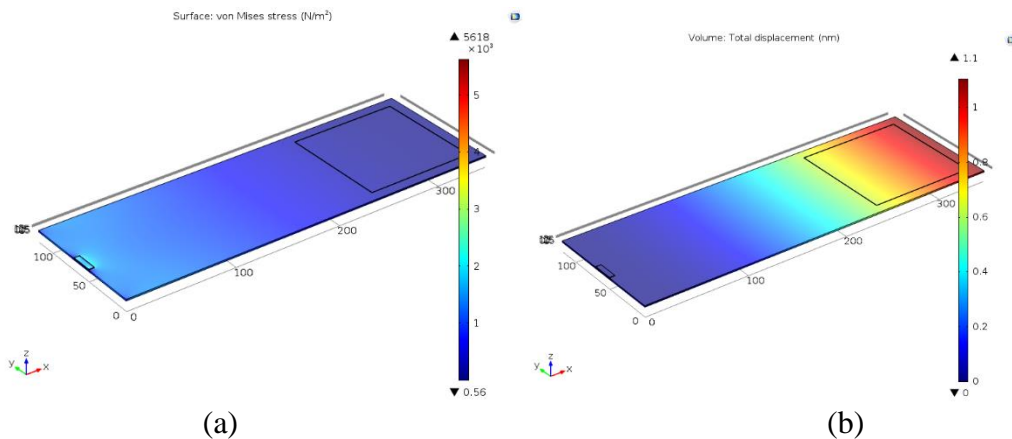


Figure 4.13 : Optimized Rectangular Cantilever (a) Von Mises stress plot, (b) Deflection Plot

4.5.2 Pi shape cantilever (Double legged)

From the results obtained from the different Pi-shaped cantilevers (presented in Table 4.10), it can be seen that using $50\mu m$ length hole gave the highest maximum von Mises stress and highest sensitivity. Thus, this design was chosen to be the optimized Pi-Shape cantilever design.

Table 4.10: Simulation Results for Pi-shape cantilever variations.

Property	Middle Hole Length			
	50μm	100μm	150μm	200μm

Maximum Von Mises stress (N/m^2)	4656	4430	4611	4541
Maximum deflection (nm)	1.36	1.51	1.6	1.64
Sensitivity ($\Delta R/R$) =	-8.18	-7.78	-8.1	-7.98
	$\times 10^{-7}$	$\times 10^{-7}$	$\times 10^{-7}$	$\times 10^{-7}$
$\pi_T \sigma_{max}$				

Using Eigenfrequency solver, the first six eigenfrequencies of the optimized Pi-shape sensor were found to be 7.8KHz, 60.3KHz, 63.2KHz, 0.184MHz, 0.215MHz and 0.369MHz. The von Mises stress and deflection plots for this sensor are shown in Figure 4.14.

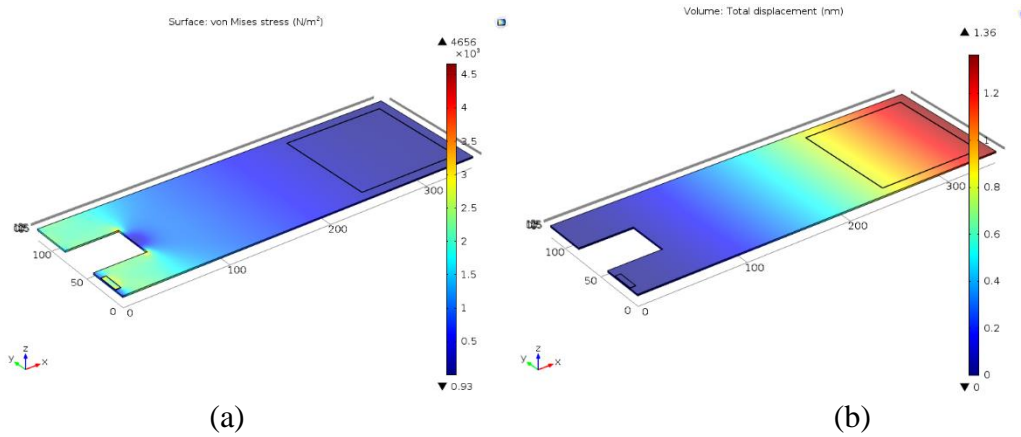


Figure 4.14 : Optimized Pi-shape Cantilever (a) Von Mises stress plot, (b) Deflection Plot

4.5.3 T shape cantilever (one legged)

From the results obtained from the different T-shaped cantilevers (presented in Table 4.11), it can be seen that using 100 μ m length side hole gave the highest maximum von Mises stress and highest sensitivity. Thus, this design was chosen to be the optimized T-Shape cantilever design.

Table 4.11: Simulation Results for T-shape cantilever variations.

Property	Side Holes Length			
	50 μ m	100 μ m	150 μ m	200 μ m
Maximum Von Mises stress (N/m^2)	8453	8921	8332	8909
Maximum deflection (nm)	2.08	2.66	3.02	3.2
Sensitivity ($\Delta R/R$) =	-1.49	-1.568	-1.46	-1.566
	$\times 10^{-6}$	$\times 10^{-6}$	$\times 10^{-6}$	$\times 10^{-6}$
$\pi_T \sigma_{max}$				

Using Eigenfrequency solver, the first six eigenfrequencies of the starting sensor were found to be 5.5KHz, 40.86KHz, 57.8KHz, 0.146MHz, 0.174MHz and

0.199MHz. The von Mises stress and deflection plots for this sensor are shown in Figure 4.15.

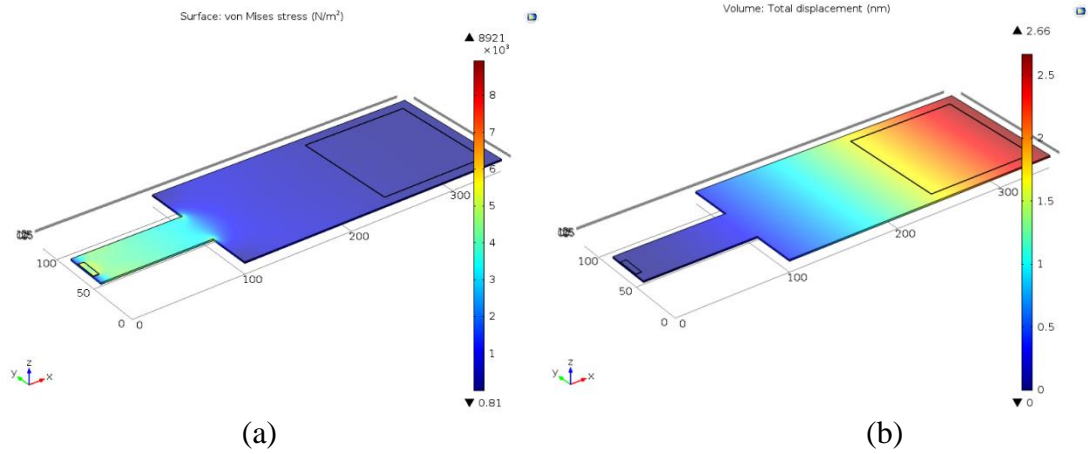


Figure 4.15 : Optimized T-shape Cantilever (a) Von Mises stress plot, (b) Deflection Plots

4.5.4 Trapezoid shape cantilever

From the results obtained from the different trapezoid shaped cantilevers (in Table 4.12), it can be seen that the structure with 1:4 ratio between the clamped cantilever edge to the free edge gave the highest maximum von Mises stress and highest sensitivity which. Which have almost 2.5x times more sensitivity than the 1:1 case (the optimized rectangular cantilever). Thus, this design was chosen to be the optimized trapezoid shape cantilever design.

Table 4.12: Simulation Results for Trapezoid Shape Cantilever variations.

Property	Ratio of Clamped cantilever end to the other free end			
	1:1	1:2	1:3	1:4
Maximum Von Mises stress (N/m^2)	5618	8065	11900	14300
Maximum deflection (nm)	1.1	1.46	1.9	2.25
Sensitivity ($\Delta R/R$) = $\pi_T \sigma_{max}$	-9.87×10^{-7}	-1.42×10^{-6}	-2.09×10^{-6}	-2.5×10^{-6}

The difference between the results obtained for different ratios is clearer in the graphs in Figure 4.16. And Figure 4.17.

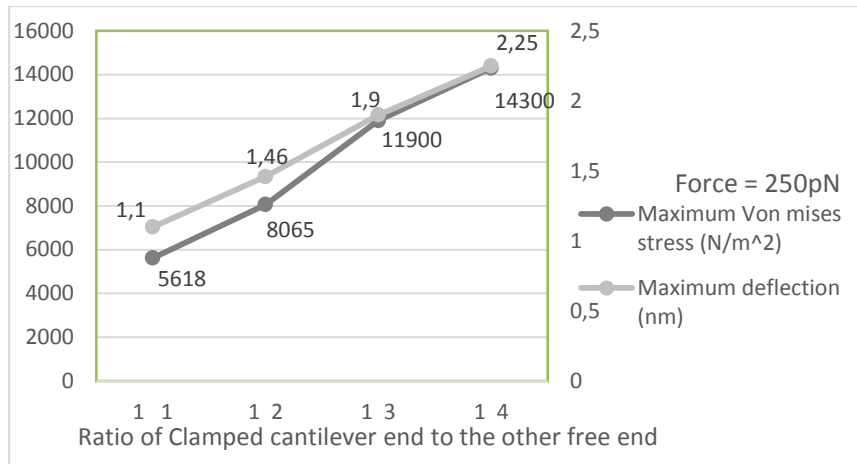


Figure 4.16 : Maximum Von Mises Stress and Maximum Deflection Values for Different Trapezoid cantilevers designs

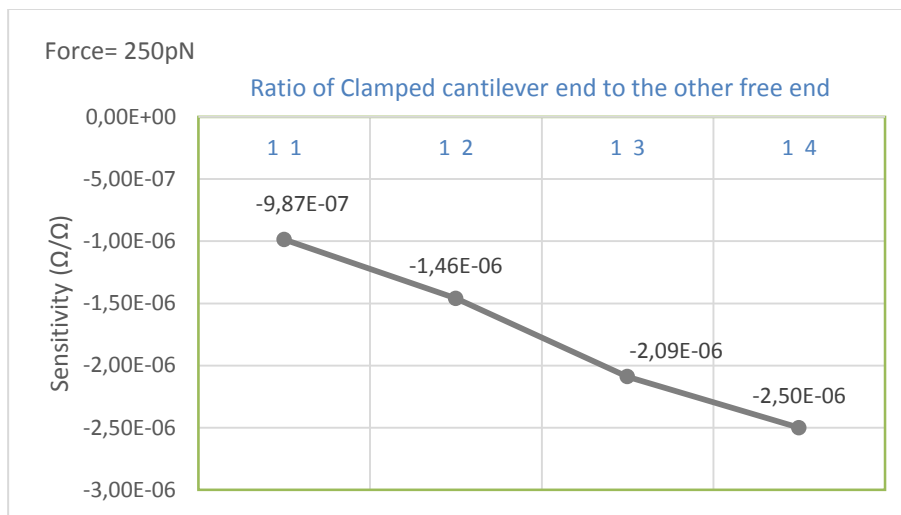


Figure 4.17 : The $\frac{\Delta R}{R}$ Sensitivity of the Sensor for Different Trapezoid cantilevers designs

Using Eigenfrequency solver, the first six eigenfrequencies of the starting sensor were found to be 5.92KHz, 44KHz, 59KHz, 0.183MHz, 0.188MHz and 0.252MHz. The von Mises stress and deflection plots for the optimized trapezoid sensor are shown in Figure 4.18.

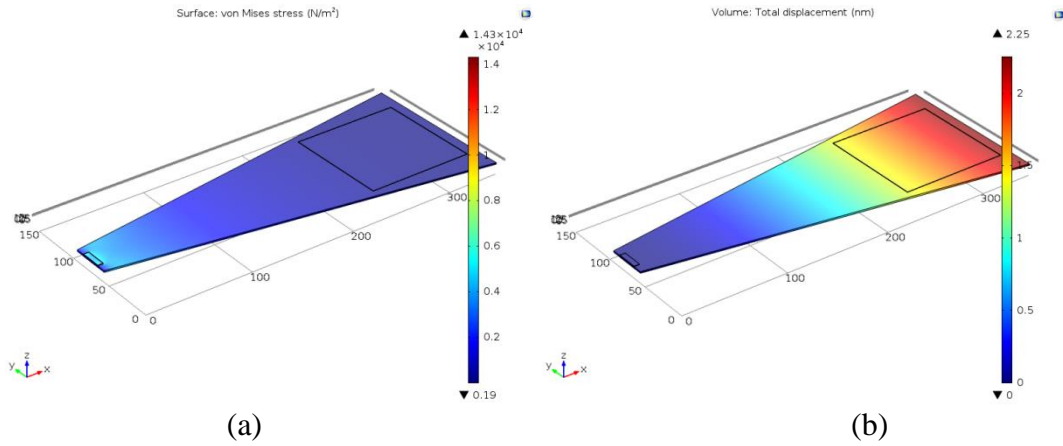


Figure 4.18 : Optimized Trapezoid Cantilever (a) Von Mises stress plot, (b) Deflection Plot

4.5.5 Stepped Trapezoid shape cantilever

From the results obtained from the different stepped-trapezoid shaped cantilevers (presented in Table 4.13), it can be seen that the structure with 1:4 ratio between the clamped cantilever edge to the free edge gave the highest maximum von Mises stress and highest sensitivity which is almost 2.5x times greater than the 1:1 case (the optimized rectangular cantilever). Thus, this design was chosen to be the optimized stepped-trapezoid shape cantilever design.

Table 4.13: Simulation Results for Stepped-Trapezoid Shape Cantilever variations.

Property	Ratio of Clamped cantilever end to the other free end			
	1:1	1:2	1:3	1:4
Maximum Von Mises stress (N/m^2)	5618	8327	12700	13700
Maximum deflection (nm)	1.1	1.63	2.2	2.66
Sensitivity ($\Delta R/R$) =	-9.87×10^{-7}	-1.46×10^{-6}	-2.23×10^{-6}	-2.41×10^{-6}
$\pi_T \sigma_{max}$				

The difference between the obtained results for different ratios is more evident when shown graphically in Figure 4.19. And Figure 4.20.

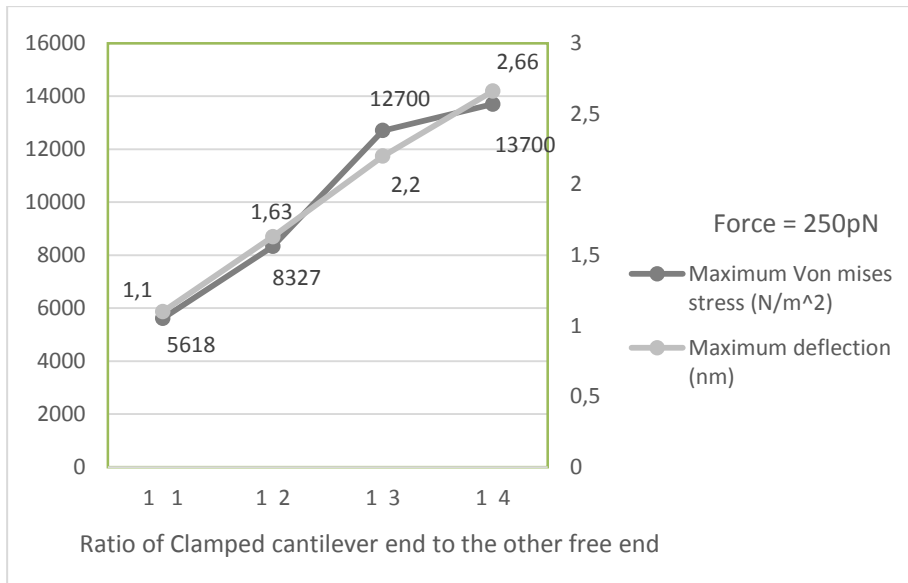


Figure 4.19 : Maximum Von Mises Stress and Maximum Deflection Values for Different Stepped-Trapezoid cantilevers designs

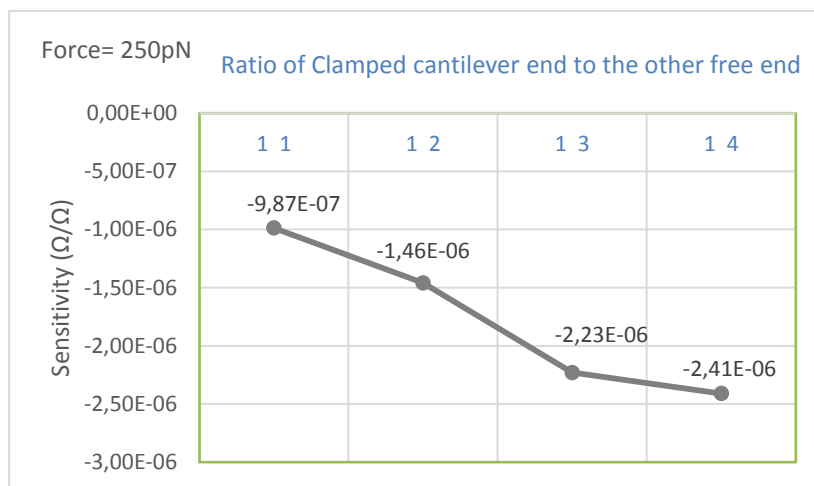


Figure 4.20 : The $\frac{\Delta R}{R}$ Sensitivity of the Sensor for Different Stepped-Trapezoid cantilevers designs

Using Eigenfrequency solver, the first six eigenfrequencies of the starting sensor were found to be 5.48KHz, 42KHz, 58.5KHz, 0.15MHz, 0.184MHz and 0.267MHz. The von Mises stress and deflection plots for the optimized trapezoid sensor are shown in Figure 4.21.

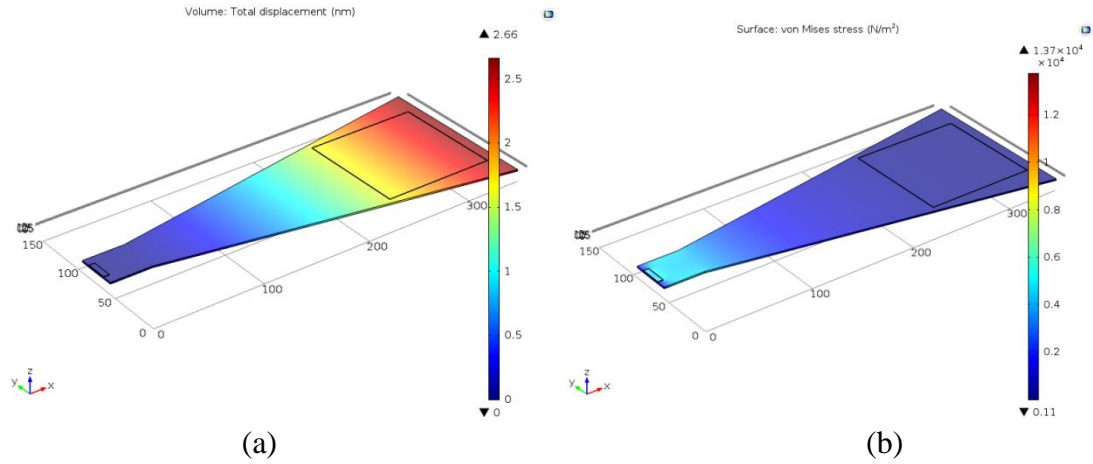


Figure 4.21 : Optimized Stepped-Trapezoid Cantilever (a) Von Mises stress plot, (b) Deflection Plot

4.5.6 Triangular shape cantilever

From the results obtained from the different triangular shaped cantilevers (presented in Table 4.14), it can be seen that the structure $200\mu m \times 50\mu m$ Gold layer $20\mu m$ away from the clamped edge gave the highest maximum von mises stress and highest sensitivity which is almost 1.8x times higher than the $100\mu m \times 100\mu m$ Gold layer case. Thus, it was chosen to be the optimized triangular shape cantilever design.

Table 4.14: Simulation Results for Triangular Shape Cantilever variations.

Property	Gold Layer Dimensions	
	$100\mu m * 100\mu m$	$200\mu m * 50\mu m$
Maximum Von Mises stress (N/m^2)	1149	2027
Maximum deflection (nm)	0.07	0.23
Sensitivity ($\Delta R/R$) =	-2.01×10^{-7}	-3.56×10^{-7}
$\pi_T \sigma_{max}$		

Using Eigenfrequency solver, the first six eigenfrequencies of the optimized triangular sensor were found to be 21.7KHz, 93.6KHz, 0.186MHz, 0.219MHz, 0.414MHz and 0.465MHz. The von Mises stress and deflection plots for the optimized trapezoid sensor are shown in Figure 4.22.

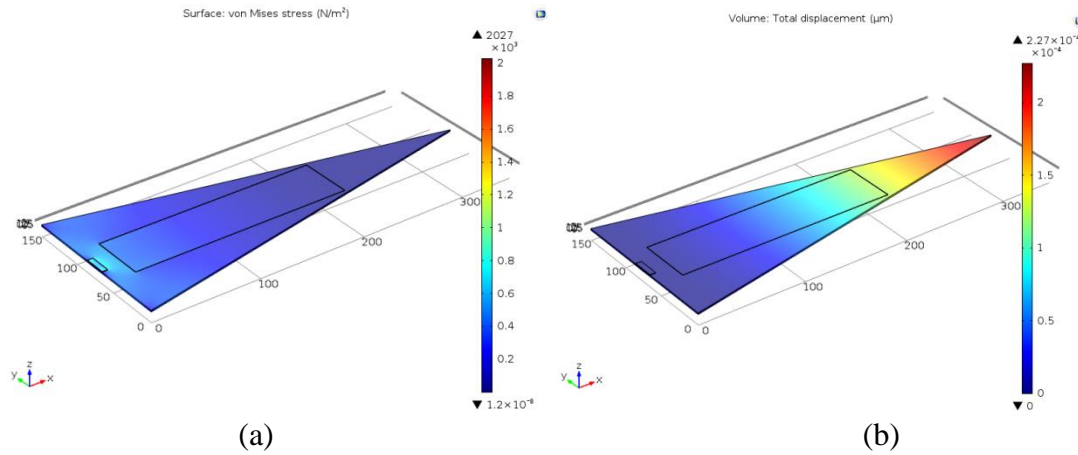


Figure 4.22 : Optimized Triangular Cantilever (a) Von Mises stress plot, (b) Deflection Plot

4.6 Comparison between different shapes

The goal of this optimization step was to change the cantilever shape and optimize each shape to get the design that gives the highest sensitivity when the same amount of force is applied. The results of the different optimized shapes are presented in Table 4.15.

Table 4.15: Comparison between the Simulation Results for the Different Cantilever Shapes.

Property	Cantilever Shape						
	Start	Rectangle	Pi Shape	T Shape	Trapezoid	S. Trapezoid	Triangular
Maximum Von Mises stress (N/m^2)	294	5618	4656	8921	14300	13700	2027
Maximum deflection (nm)	0.00786	1.1	1.36	2.66	2.25	2.66	0.23
Sensitivity ($\Delta R/R$) = $\pi_t \sigma_{max}$	-5.4×10^{-8}	-9.87×10^{-7}	-8.18×10^{-7}	-1.568×10^{-6}	-2.5×10^{-6}	-2.41×10^{-6}	-3.56×10^{-7}

From Table 4.15, it can be seen that when the different rectangular cantilever dimensions were optimized (length, width and thickness) the sensitivity increased 18.3x folds. In addition to that, adding two side holes to the structure increased the sensitivity by 1.6 factor (T-shape).

Comparing the trapezoid and stepped-trapezoid structure, for the same applied force, the trapezoid gave higher maximum von Mises stress whereas the stepped trapezoid gave the highest maximum deflection. Overall, when all the shape result are

compared to each other, it can be seen that optimized trapezoidal microcantilever design gave the highest sensitivity which is more than 46x times greater than the starting sensor sensitivity, the results can be compared more easily looking at the graphs shown in Figure 4.23 and Figure 4.24.

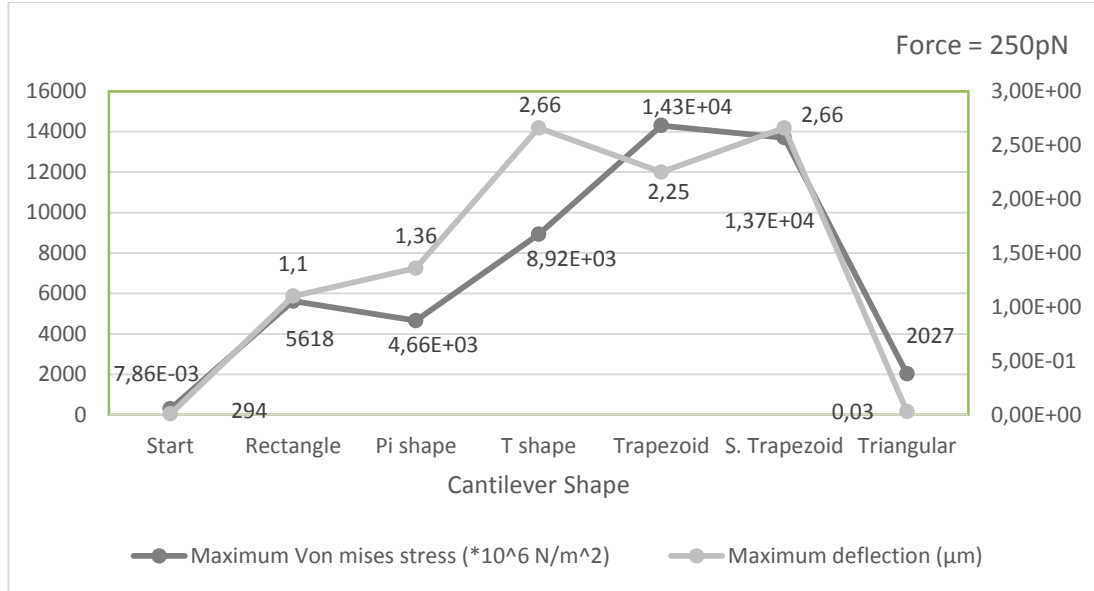


Figure 4.23 : Maximum Von Mises Stress and Maximum Deflection Values for Different Cantilever shapes

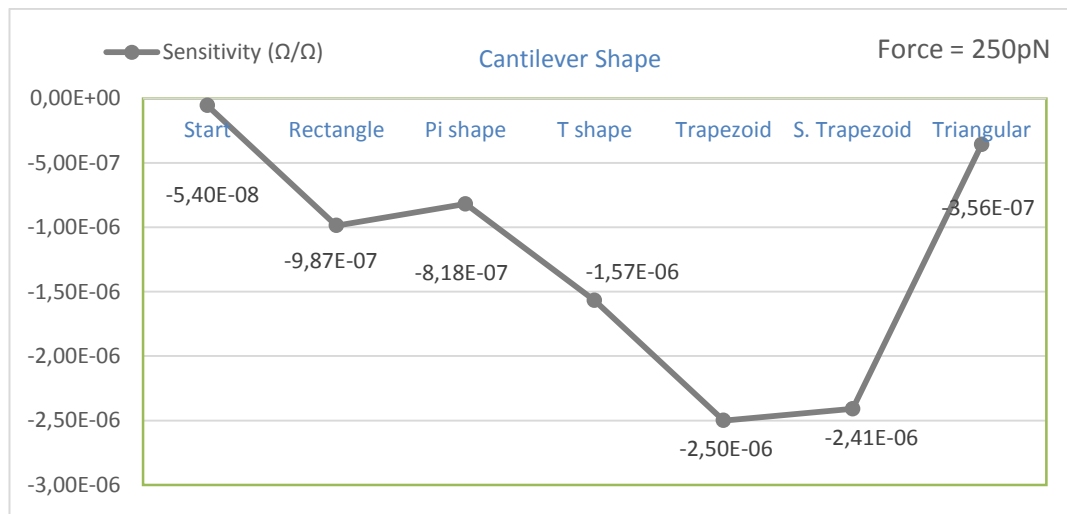


Figure 4.24 : The $\frac{\Delta R}{R}$ Sensitivity of the Sensor for Different Cantilever shapes

4.7 Stress Concentration Region (SCR)

As can be seen from Table 4.16, when the $30\mu \times 10\mu$ SCR rectangular hole was placed 15μ away from the clamped cantilever edge, shown in Figure 4.25, it resulted in almost 1.6x times sensitivity which is the best sensitivity value compared to the other positions.

Table 4.16: Effect of Adding Stress Concentration Region (SCR) at different positions.

Property	Without SCR	Using SCR at 15 μ m	Using SCR at 65 μ m	Using SCR at 115 μ m	Using SCR at 165 μ m
Maximum Von Mises stress (N/m^2)	14300	22600	14900	14000	12800
Sensitivity ($\Delta R/R$) = $\pi_t \sigma_{max}$	-2.5 $\times 10^{-6}$	-3.97 $\times 10^{-6}$	-2.62 $\times 10^{-6}$	-2.46 $\times 10^{-6}$	-1.28 $\times 10^{-6}$

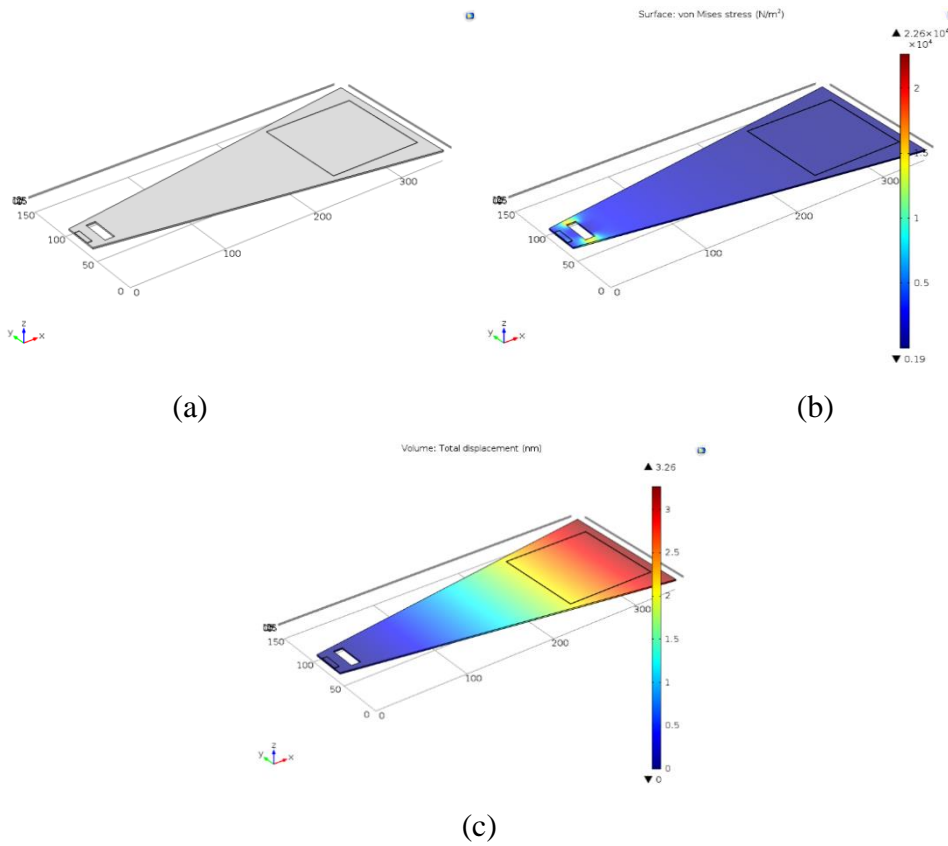


Figure 4.25 : Final Optimized Sensor (a) Geometry, (b) Von Mises stress plot and (C) Deflection Plot

When the SCR hole orientation was changed 90 degrees, as shown in Figure 4.26, it resulted into $-2.71e-6$ sensitivity which is less than the other orientation. Thus the first design was chosen to be the final optimized sensor design. When compared to the starting sensor, this final sensor design has 73.5 times better sensitivity.

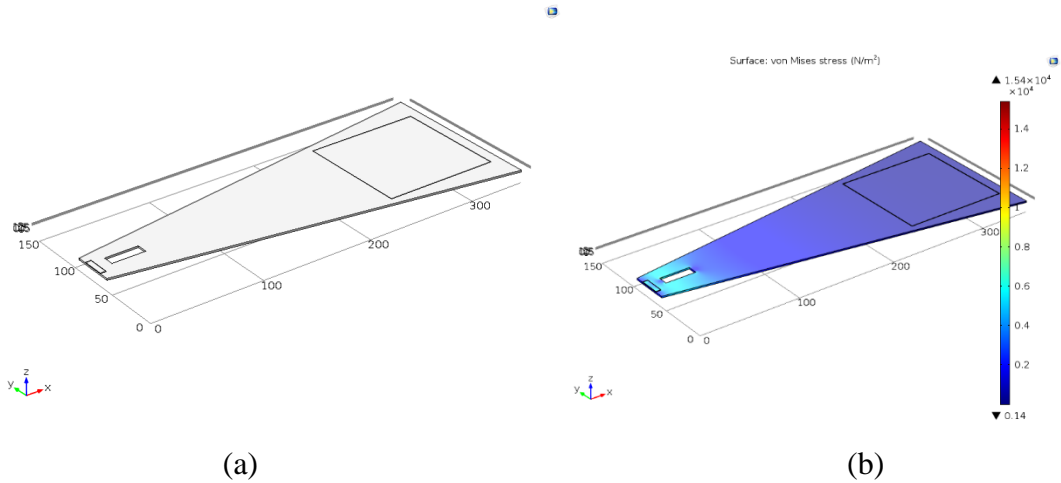


Figure 4.26 : Trapezoid Cantilever with 90 degrees Oriented SCR hole (a) Geometry
(b) Von Mises Stress Plot

Using Eigenfrequency solver, the first six eigenfrequencies of the final sensor were found to be 4.86KHz, 42.66KHz, 54.73KHz, 0.16MHz, 0.17MHz and 0.248MHz and their mode shapes are presented in Figure 4.27.

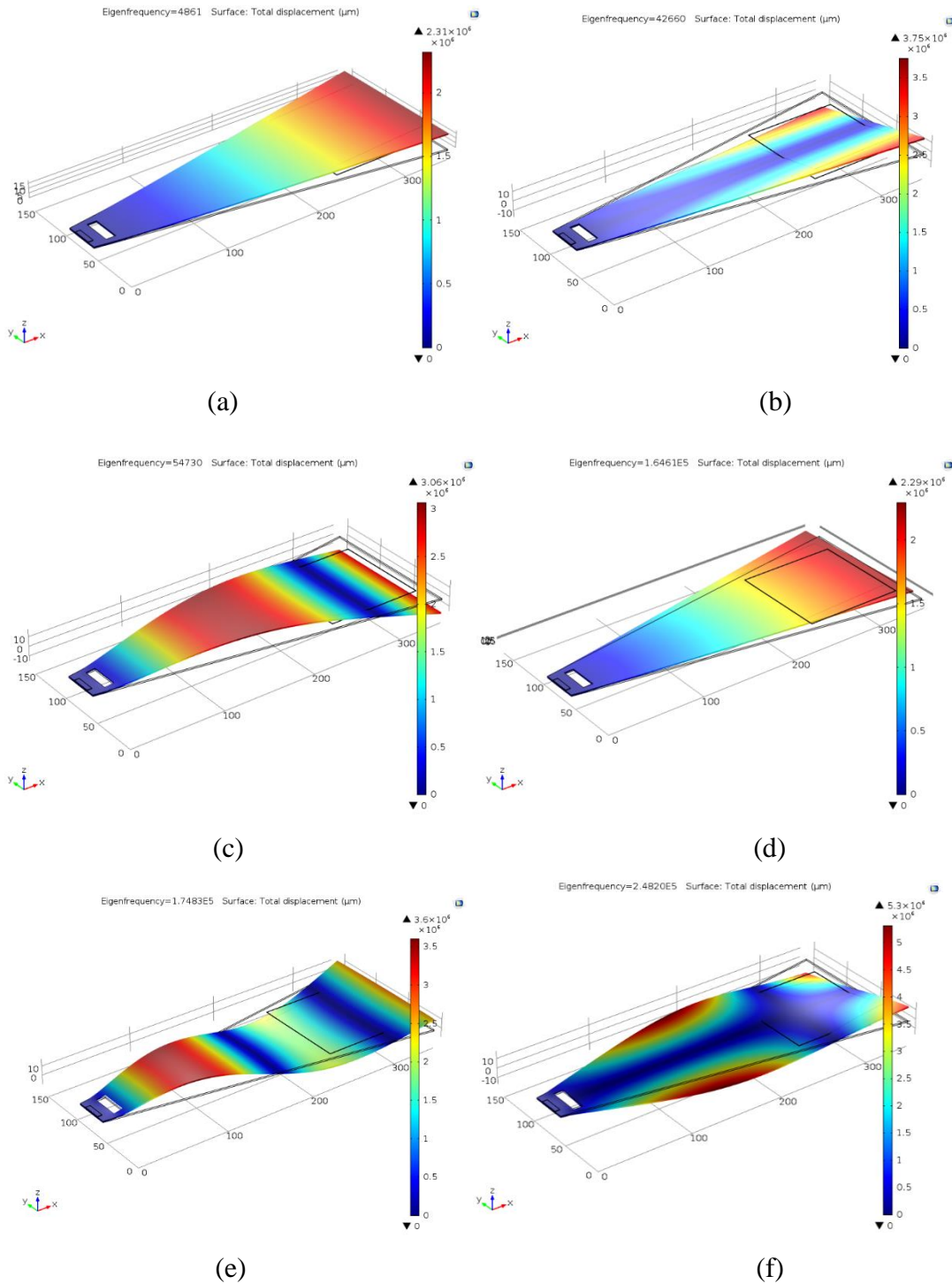


Figure 4.27 : Final Optimized Sensor Mode Shapes (a) 4.86KHz, (b) 42.66KHz, (c)54.73KHz, (d) 0.16MHz, (e) 0.17MHz and (f) 0.248MHz

4.8 Final Sensor Design

As mentioned in section 3.1, the range of forces between 25 to 250 pN was used to get the maximum stress and deflection for each and then from the results the mechanical sensitivity regarding the change in the resistance/ force will finally be calculated; the simulation results are presented in Table 4.17.

Table 4.17: Optimized Sensor results when Different Forces Are Applied.

Property	25pN	50pN	100pN	150pN	200pN	250pN
Maximum Von Mises stress (N/m^2)	2262	4525	9049	13600	18100	22600
Maximum deflection (nm)	0.33	0.65	1.3	1.96	2.61	3.26
Sensitivity ($\Delta R/R$) = $\pi_t \sigma_{max}$	-3.97×10^{-7}	-7.95×10^{-7}	-1.59×10^{-6}	-2.39×10^{-6}	-3.18×10^{-6}	-3.97×10^{-6}

As it can be seen from the $\Delta R/R$ Sensitivity graph shown in Figure 4.28, the normalized change in the resistance increases linearly with the linear increase of the applied force which complies with Hook's law.

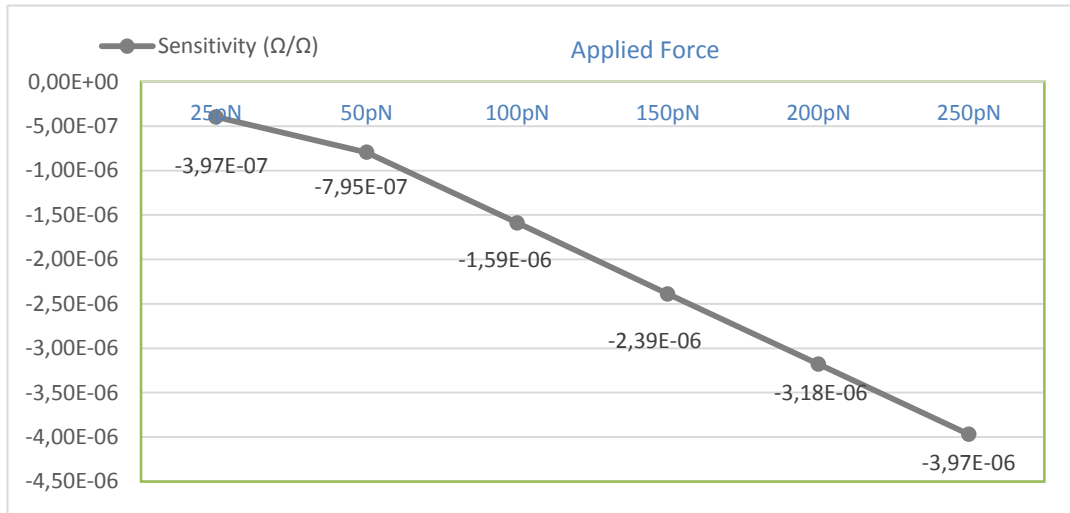


Figure 4.28 : The $\Delta R/R$ Sensitivity of the Sensor for Different Cantilever shapes

From the obtained results, the mechanical sensitivity in terms of the normalized resistance change to the applied force was calculated using equation 4.3 and found that it equals to $-1.5 \times 10^{-8} \Omega/\Omega/pN$. This means for each 1pN ($10^{-10}g$) biomolecules attach to this biosensor, the piezoresistor resistivity will decrease by $1.5 \times 10^{-8} \Omega$.

$$\text{Sensitivity} = \frac{\Delta R/R}{F} = \frac{-7.95 \times 10^{-7}}{50pN} = -1.5 \times 10^{-8} \Omega/\Omega/pN \quad (4.3)$$

This change in resistance can be translated into a change in voltage by configuring the biosensor in the Whinstone bridge circuit shown in Figure 4.29 below where R is fixed resistor, and the input voltage is 1V.

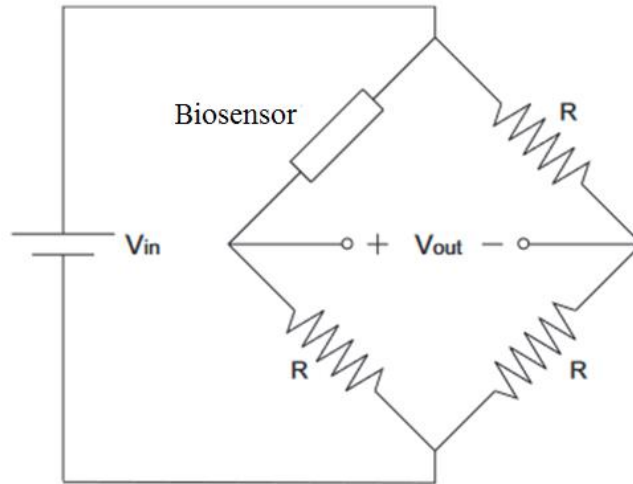


Figure 4.29 : The biosensor's Whinstone bridge circuit

When this microcantilever sensor is functionalized by coating it with different molecules of bio-elements such as enzyme, antigen and antibody, it will be to detect various bio-molecules in a complex sample.

4.9 Comparison with Prior Works Available in Open Literature

Many works found in literature focused on improving the sensitivity of piezoresistive cantilevers. However, in contrast to our approach most of the previous works considered optimizing a a limited number of design and process parameters that minor sensitivity enhancements were obtained.

In [116], when a 250pN force applied to the 1.5 μm thick microcantilever sensor with 0.4 thick single crystal silicon piezoresistor and 0.6 thick single crystal silicon piezoresistor, the $\Delta R/R$ sensitivity of the sensor was 0.3×10^{-6} and 0.25×10^{-6} respectively, whereas our 1.5 μm thick microcantilever sensor with 0.5 polysilicon piezoresistor results into 3.97×10^{-6} sensitivity which is 10 times higher sensitivity for the same applied force.

A similar sensor that was previously presented by the same group in [117] had enhanced sensitivity due to the incorporated SCR (using thinning technique) to a 1 μm thick microcantilever sensor with 0.2 thick single crystal silicon piezoresistor. When a 250pN force is applied to the final optimized sensor, the $\Delta R/R$ sensitivity of the sensor was found to be 5.2×10^{-6} . Whereas when the same force is applied to our 1.5 μm thick microcantilever sensor with 0.5 polysilicon piezoresistor, it gave

3.97×10^{-6} sensitivity. As mentioned before, thinning the cantilever thickness and the piezoresistor thickness enhances the sensitivity but in our case higher thickness fabrication limit was considered which justifies the lower sensitivity result compared to that design. But when $1\mu\text{m}$ is used for this sensor design it gives 1.01×10^{-5} sensitivity which is 2x times higher than their sensor and 187x times better than the starting sensor.

In the [118], SCR approach was also used by incorporating a rectangular SCR $20\mu\text{m}$ away from the $1\mu\text{m}$ thick clamped silicon dioxide cantilever edge, whereas the piezoresistor is a $0.2\mu\text{m}$ C-shaped single crystal silicon. When a 250nN force is applied to that sensor, the sensitivity was 1.75×10^{-4} . For the same force, the $\Delta R/R$ sensitivity of our sensor was found to be 3.97×10^{-3} which is almost 23 times higher.

In [119], the final optimized sensor was $1.5\mu\text{m}$ thick Trapezoidal Slotted-shaped silicon oxide microcantilever. When $1.923 \times 10^{-10}\text{N}$ force was applied to that sensor; it resulted into $2.463 \times 10^{-8} \Delta R/R$ sensitivity but when the same force was applied to the sensor design presented in this study, the $\Delta R/R$ sensitivity was found to be 3.97×10^{-6} which is 161 times higher.

5. CONCLUSIONS, RECOMMENDATIONS AND FUTURE WORK

5.1 Conclusions

In this study, finite element analysis tool (COMSOL Multiphysics) was used to get a highly sensitive MEMS microcantilevers based biosensor. The sensor optimization procedure was done using a step-wise optimization approached in which almost all the design and process parameters were varied and optimized one at each step while fixing the others.

During the rectangular shape microcantilever optimization step, it was found that the cantilever thickness has the highest effect on the sensor sensitivity. In addition to that, after the different rectangular microcantilever dimensions were optimized (length, width and thickness), the sensitivity increased 18.3x folds. Also, adding two side holes to the rectangular cantilever structure increased the sensitivity by 1.6 factor (T-shape). Overall, for the same applied force, the trapezoid-shaped microcantilever design gave higher maximum von Mises stress whereas the stepped-trapezoid shaped gave the highest maximum deflection.

The impact of the SCR was also analyzed; it was found that introducing a $30\mu \times 10\mu\text{m}$ SCR rectangular hole to the optimized trapezoid structure $15\mu\text{m}$ away from the clamped cantilever edge, resulted in almost 1.6x times sensitivity enhancement which gave the best sensitivity value compared to the other positions.

When compared to the starting sensor, the final sensor design has 73.5x times better $\Delta R/R$ sensitivity which is more sensitive than the other sensor designs available in literature. In terms of the normalized change in resistance to the applied force the final sensor sensitivity equals to $^{-1.5 \times 10^{-8} \Omega/\Omega/pN}$. This means that for each 1pN ($10^{-10}g$) biomolecules attach to this biosensor, the piezoresistor resistivity will decrease by $1.5 \times 10^{-8}\Omega$.

5.2 Recommendations and Future Work

- As a future work, the fabrication sequence presented in section 3.9 will be used to fabricate the sensor and compare the results with simulation results.
- As seen from the simulation results, the cantilever thickness, and the piezoresistor thickness readily affects the sensor sensitivity. In this design 1.5 μm and 0.5 μm were set as the lowest thickness limit for the silicon dioxide cantilever and the polysilicon piezoresistor. Using thinner layers of these materials for the same design will result in a further increase in the sensitivity.
- As shown in section 4.2, when a single crystal silicon based piezoresistor was used instead of the polysilicon based piezoresistor, the resulting $\Delta R/R$ sensor sensitivity was more than three times higher. Thus, using single crystal silicon as the piezoresistor material for the same optimized sensor design presented in this study is expected to result in a more sensitive sensor.
- Since the trapezoid shaped microcantilever gave higher maximum von Mises stress whereas the stepped-trapezoid shaped microcantilever gave the highest maximum deflection for the same applied force, it is recommended to use this a trapezoid shaped microcantilever when the sensing technique is piezoresistive whereas step-trapezoid shaped microcantilever is recommended when optical sensing is used.
- A microcantilever array can be made from several microcantilevers of the design presented here and functionalized differently to detect several biological species at the same time.

REFERENCES

- [1] **D. Morton Jr. and J. Gabriel**, *Electronics: The Life Story of a Technology*, 1st ed. JHU Press, 2007.
- [2] "**BioMEMS Market Size, Share | Industry Report, 2023**", *Gminsights*. Retrieved November 20, 2016, from: <https://www.gminsights.com/industry-analysis/biom>.
- [3] **S. Clerc and B. Roussel**, "BioMEMS: Microsystems for Healthcare Applications 2016", Yole Development, France, 2016.
- [4] **T. James, M. Mannoor and D. Ivanov**, "BioMEMS –Advancing the Frontiers of Medicine", *Sensors*, vol. 8, no. 9, pp. 6077-6107, 2008.
- [5] **G. Whitesides**, "The origins and the future of microfluidics," *Nature*, vol. 442, no. 7101, pp. 368-373, 2006.
- [6] **Bio-MEMS**. *Wikipedia*. Accessed: 19 November, 2016, <https://en.wikipedia.org/wiki/Bio-MEMS>.
- [7] **R. Bashir**, "BioMEMS: state-of-the-art in detection, opportunities, and prospects," *Advanced Drug Delivery Reviews*, vol. 56, no. 11, pp. 1565-1586, 2004.
- [8] **J. Stetter and W. Penrose**, "Understanding Chemical Sensors and Chemical Sensor Arrays (Electronic Noses): Past, Present, and Future," *Sensors Update*, vol. 10, no. 1, pp. 189-229, 2002.
- [9] **H. Baltes**, *Enabling Technologies for MEMS and Nanodevices*, 1st ed. Weinheim [Germany]: Wiley, 2013.
- [10] **Protein microarray**. *Wikipedia*. Accessed: 14 November, 2016, https://en.wikipedia.org/wiki/Protein_microarray.
- [11] **E. Seibel, C. Brown, J. Dornitz and M. Kimmey**, "Scanning Single Fiber Endoscopy: A New Platform Technology for Integrated Laser Imaging, Diagnosis, and Future Therapies," *Gastrointestinal Endoscopy Clinics of North America*, vol. 18, no. 3, pp. 467-478, 2008.
- [12] **A. Moglia, A. Mencassi, M. Schurr and P. Dario**, "Wireless capsule endoscopy: from diagnostic devices to multipurpose robotic systems," *Biomedical Microdevices*, vol. 9, no. 2, pp. 235-243, 2006.
- [13] **G. Pan and L. Wang**, "Swallowable Wireless Capsule Endoscopy: Progress and Technical Challenges," *Gastroenterology Research and Practice*, vol. 2012, pp. 1-9, 2012.

- [14] **X. Huang, S. Li, E. Davis, D. Li, Q. Wang and Q. Lin**, "A MEMS Dielectric Affinity Glucose Biosensor," *Journal of Microelectromechanical Systems*, vol. 23, no. 1, pp. 14-20, 2014.
- [15] **L. Andrus, R. Unruh, N. Wisniewski and M. McShane**, "Characterization of Lactate Sensors Based on Lactate Oxidase and Palladium Benzoporphyrin Immobilized in Hydrogels," *Biosensors*, vol. 5, no. 3, pp. 398-416, 2015.
- [16] **MEMS BASED CONTINUOUS ALCOHOL MONITORING DEVICE**. *Small Business Innovation Research (SBIR)*. Accessed: November 14, 2016, <https://www.sbir.gov/sbirsearch/detail/269742>.
- [17] **Sandia National Laboratories: Licensing/Technology Transfer Rapid Automated Point-of-Care System (RapiDx)**, Ip.sandia. Retrieved November 14, 2016, from: <https://ip.sandia.gov/technology.do/techID=81>.
- [18] **New Research: The Argus II Retinal Prosthesis (Bionic Eye) Is Safe, Effective, and Improves Visual Function**, VisionAware. Retrieved November 14, 2016 from: <http://www.visionaware.org/blog/visionaware-blog/new-research-the-argus-ii-retinal-prosthesis-bionic-eye-is-safe-effective-and-improves-visual-function/12>.
- [19] **E. E. NUXOLL and R. A. SIEGEL**, "BioMEMS Devices for Drug Delivery," *IEEE ENGINEERING IN MEDICINE AND BIOLOGY MAGAZINE*, no. 0739-51750925002009, 2009.
- [20] **MiniMed Paradigm REAL-Time 522/722 Insulin Pump User Guide | Medtronic Diabetes**, Medtronicdiabetes. Retrieved November 14, 2016 from: <http://www.medtronicdiabetes.com/download-library/minimed-522-722>.
- [21] **R. Jivani, G. Lakhtaria, D. Patadiya, L. Patel, N. Jivani and B. Jhala**, "Biomedical microelectromechanical systems (BioMEMS): Revolution in drug delivery and analytical techniques," *Saudi Pharmaceutical Journal*, vol. 24, no. 1, pp. 1-20, 2016.
- [22] **C. Bettinger, J. Borenstein and S. Tao**, *Microfluidic cell culture systems*, 1st ed. Norwich, N.Y.: William Andrew, 2012.
- [23] **J. Borenstein and G. Vunjak-Novakovic**, "Engineering Tissue with BioMEMS," *IEEE Pulse*, vol. 2, no. 6, pp. 28-34, 2011.8
- [24] **M. HajjHassan, V. Chodavarapu and S. Musallam**, "NeuroMEMS: Neural Probe Microtechnologies," *Sensors*, vol. 8, no. 10, pp. 6704-6726, 2008.
- [25] **da Vinci Surgery | Robotic-Assisted Surgery**, Davincisurgery. Retrieved November 14, 2016 from: <http://www.davincisurgery.com/>.
- [26] **A. Perestrelo, A. Águas, A. Rainer and G. Forte**, "Microfluidic Organ/Body-on-a-Chip Devices at the Convergence of Biology and Microengineering," *Sensors*, vol. 15, no. 12, pp. 31142-31170, 2015.

- [27] **Biosensor - definition of a biosensor in English from the Oxford Dictionary**, Oxford dictionaries Retrieved September 02, 2016 from: <http://www.oxforddictionaries.com/definition/english/biosensor>.
- [28] **Biosensor**, Wikipedia. Retrieved November 20, 2016 from: <https://en.wikipedia.org/wiki/Biosensor>.
- [29] **Biosensor**, The Free Dictionary. Retrieved September 02, 2016 from: <http://medical-dictionary.thefreedictionary.com/biosensor>.
- [30] **K. Narsaiah, S. Jha, R. Bhardwaj, R. Sharma and R. Kumar**, "Optical biosensors for food quality and safety assurance—a review," *Journal of Food Science and Technology*, vol. 49, no. 4, pp. 383-406, 2011.
- [31] **A. Boisen, S. Dohn, S. Keller, S. Schmid and M. Tenje**, "Cantilever-like micromechanical sensors," *Reports on Progress in Physics*, vol. 74, no. 3, p. 036101, 2011.
- [32] **P. Gopinath, V. Anitha and S. Mastani**, "Microcantilever based Biosensor for Disease Detection Applications," *JOMB*, vol. 4, no. 4, pp. 307-311, 2015.
- [33] **P. Mehrotra**, "Biosensors and their applications – A review," *Journal of oral biology and craniofacial research*, vol. 6, 2016.
- [34] **R. Datar, S. Kim, S. Jeon, P. Hesketh, S. Manalis, A. Boisen and T. Thundat**, "Cantilever Sensors: Nanomechanical Tools for Diagnostics," *MRS Bulletin*, vol. 34, no. 06, pp. 449-454, 2009.
- [35] **X. Li, H. Yu, X. Gan, X. Xia, P. Xu, J. Li, M. Liu and Y. Li**, "Integrated MEMS/NEMS Resonant Cantilevers for Ultrasensitive Biological Detection," *Journal of Sensors*, vol. 2009, pp. 1-10, 2009.
- [36] **Grand View Research** .(2015) . *Biosensors Market Research Report* (Report ID: 978-1-68038-321-8).
- [37] **Shengbo Sang, Wendong Zhang, Yuan Zhao**, (2013), *State Of The Art In Biosensors - General Aspects*, Chapter4 : Review on the Design Art of Biosensors, InTech.
- [38] **R. Datar, S. Kim, S. Jeon, P. Hesketh, S. Manalis, A. Boisen and T. Thundat**, "Cantilever Sensors: Nanomechanical Tools for Diagnostics", *MRS Bull.*, vol. 34, no. 06, pp. 449-454, 2009.
- [39] **D. Khushalani, V. Dubey, P. Bheley, J. Kalambe, R. Pande and R. Patrikar**, "Design optimization & fabrication of micro cantilever for switching application", *Sensors and Actuators A: Physical*, vol. 225, pp. 1-7, 2015.
- [40] **V. Kumar, M. Mahdavi, X. Guo, E. Mehdizadeh and S. Pourkamali**, "Ultra sensitive lorentz force MEMS magnetometer with pico-tesla limit of detection", in *IEEE International Conference on Micro Electro Mechanical Systems (MEMS)*, 2015.
- [41] **S. Vashist and H. Holthöfer**, "Microcantilevers for Sensing Applications", *Measurement and Control*, vol. 43, no. 3, pp. 84-88, 2010.

- [42] **B. Sheeparamatti, M. Hebbal, R. Sheeparamatti, V. Math and J. Kadadevaramath**, "Simulation of Biosensor using FEM", in International MEMS Conference 2006, 2006, pp. Conference Series 34 (2006) 241–246.
- [43] **G. Shekhawat and V. Dravid**, "Biosensors: Microcantilevers to lift biomolecules", *Nature Nanotech*, vol. 10, no. 10, pp. 830-831, 2015.
- [44] **M. Martyniuk**, "Towards MEMS-based chem/bio sensing arrays with on-chip optical read-out", *PRZEGLĄD ELEKTROTECHNICZNY*, vol. 1, no. 10, pp. 235-238, 2015.
- [45] **H. Lang, J. Ramseyer, W. Grange, T. Braun, D. Schmid, P. Hunziker, C. Jung, M. Hegner and C. Gerber**, "An Artificial Nose Based on Microcantilever Array Sensors", *J. Phys.: Conf. Ser.*, vol. 61, pp. 663-667, 2007.
- [46] **R. Ma, P. Chou, Y. Wang, T. Hsueh, L. Fu and C. Lee**, "A microcantilever-based gas flow sensor for flow rate and direction detection", *Microsystem Technologies*, vol. 15, no. 8, pp. 1201-1205, 2008.
- [47] **C. Huang, H. Hsueh, Y. Huang, H. Liao, H. Tsai, Y. Juang, T. Lin, S. Lu and C. Lin**, "A fully integrated wireless CMOS microcantilever lab chip for detection of DNA from Hepatitis B virus (HBV)", *Sensors and Actuators B: Chemical*, vol. 181, pp. 867-873, 2013.
- [48] **O. Cakmak, E. Ermek, N. Kilinc, I. Baris, I. Kavakli, G. Yaralioglu and H. Urey**, "MICROCANTILEVER BASED LOC SYSTEM FOR COAGULATION MEASUREMENTS", in 18th International Conference on Miniaturized Systems for Chemistry and Life Sciences, San Antonio, Texas, USA, 2014.
- [49] **Gopinath , V. R. Anitha, and S. Aruna Mastani** 'Microcantilever Based Biosensor For Disease Detection Applications'. *Journal of Medical and Bioengineering* 4 (2015).
- [50] **Chaudhary, M. and A. Gupta**, Microcantilever-based sensors. *Defence Science Journal*, 2009. 59(6): p. 634.
- [51] **G. G. Stoney**, "The tension of metallic films deposited by electrolysis *Proc. Roy. Soc. A*, vol. 82, no. 553, pp. 172–175, 1909.
- [52] **Cantilever**. *Wikipedia*. Accessed: September, 2016, <https://en.wikipedia.org/wiki/Cantilever>.
- [53] **J. Tamayo, J. J. Ruz, V. Pini, P. Kosaka, and M. Calleja**, "Quantification of the surface stress in microcantilever biosensors: Revisiting Stoney's equation," *Nanotechnology*, vol. 23, no. 47, p. 475702, 2012.
- [54] **K.-U. Kirstein, Y. Li, M. Zimmermann, C. Vancura, T. Volden, W. H. Song, J. Lichtenberg, and A. Hierlemann**, 'Cantilever-Based Biosensors In CMOS Technology'. *Design, Automation And Test In Europe*, 2005. *Proceedings. IEEE*, 2005.
- [55] **S. Koev, R. Fernandes, W. Bentley and R. Ghodssi**, "A Cantilever Sensor With an Integrated Optical Readout for Detection of Enzymatically Produced Homocysteine", *IEEE Trans. Biomed. Circuits Syst.*, vol. 3, no. 6, pp. 415-423, 2009.

- [56] **Jun Li, F. Albri, R. Maier, Wenmiao Shu, Jining Sun, D. Hand and W. MacPherson**, "A Micro-Machined Optical Fiber Cantilever as a Miniaturized pH Sensor", *IEEE Sensors J.*, vol. 15, no. 12, pp. 7221-7228, 2015.
- [57] **Ghatkesar, Murali K., et al.** "Real-time mass sensing by nanomechanical resonators in fluid." *Sensors*, 2004. Proceedings of IEEE. IEEE, 2004.
- [58] **Bhushan, Bharat.** *Springer Handbook Of Nanotechnology*. Berlin: Springer, 2006
- [59] **Thompson, M.J. D.A. Horsley** 'Lorentz Force MEMS Magnetometer'. Hilton Head, 2010.
- [60] **Dahai Ren , Lingqi Wu , Meizhi Yan, Mingyang Cui, Zheng You and Muzhi Hu** 'Design And Analyses Of A MEMS Based Resonant Magnetometer'. *Sensors* 9.9 (2009): 6951-6966.
- [61] **Lorentz force.** *Encyclopedia Britannica*. Accessed: September 28, 2016, <https://global.britannica.com/science/Lorentz-force>.
- [62] **Lorentz force.** *Wikipedia*. Accessed: September 28, 2016, https://en.wikipedia.org/wiki/Lorentz_force.
- [63] **Varun Kumar, Mohammad Mahdavi, Xiaobo Guo, Emad Mehdizadeh and Siavash Pourkamali** 'Ultra Sensitive Lorentz Force MEMS Magnetometer With Pico-Tesla Limit Of Detection'. 28Th IEEE International Conference On Micro Electro Mechanical Systems (MEMS), Estoril: IEEE, 2015.
- [64] **Golebiowski, Jacek.** 'Microelectromechanical Transducer With Optical Readout For Magnetic Flux Density Measurements'. *Przegląd Elektrotechniczny* 2012.
- [65] **Thompson, M.J., M. Li, and D.A. Horsley.** 'Low Power 3-Axis Lorentz Force Navigation Magnetometer'. IEEE 24Th International Conference On Micro Electro Mechanical Systems (MEMS), Cancun: IEEE, 2011.
- [66] **Ziegler, Christiane.** 'Cantilever-Based Biosensors'. *Analytical and Bioanalytical Chemistry* 379.Issue 7-8 (2004): 946-959.
- [67] **P. Sangeetha and A. Vimala Juliet**, "Biosensor for Tuberculosis detection using MEMS device", in 3rd International Conference on Electronics, Biomedical Engineering and its Applications (ICEBEA'2013), Hong Kong (China), 2013.
- [68] **J. Kalambe and R. Patrikar**, "Design of Microcantilever-Based Biosensor with Digital Feedback Control Circuit", *Journal of Sensors*, vol. 2012, pp. 1-9, 2012.
- [69] **M. Nordström, D. Zauner, M. Calleja, J. Hübner and A. Boisen**, "Integrated optical readout for miniaturization of cantilever-based sensor system", *Appl. Phys. Lett.*, vol. 91, no. 10, p. 103512, 2007.
- [70] **E. Hwu, H. Liao, F. Bosco, C. Chen, S. Keller, A. Boisen and K. Huang**, "An Astigmatic Detection System for Polymeric Cantilever-Based Sensors", *Journal of Sensors*, vol. 2012, pp. 1-7, 2012.

- [71] **K. Zinoviev, C. Dominguez, J. Plaza, V. Busto and L. Lechuga**, "A novel optical waveguide microcantilever sensor for the detection of nanomechanical forces", *J. Lightwave Technol.*, vol. 24, no. 5, pp. 2132-2138, 2006.
- [72] **S. Koev, R. Fernandes, W. Bentley and R. Ghodssi**, "A Cantilever Sensor With an Integrated Optical Readout for Detection of Enzymatically Produced Homocysteine", *IEEE Trans. Biomed. Circuits Syst.*, vol. 3, no. 6, pp. 415-423, 2009.
- [73] **Jun Li, F. Albri, R. Maier, Wenmiao Shu, Jining Sun, D. Hand and W. MacPherson**, "A Micro-Machined Optical Fiber Cantilever as a Miniaturized pH Sensor", *IEEE Sensors J.*, vol. 15, no. 12, pp. 7221-7228, 2015.
- [74] **O. Sidek, M. Miskam, H. Khaleed, M. Alias and S. Mohd**, "Optimal Design of Capacitive Micro Cantilever Beam Accelerometer", *Modern Applied Science*, vol. 3, no. 9, 2009.
- [75] **T. Sarath, D. Chakradhar Rao, Y. G. S. S Sai Charan and S. Annaiah Durai**, "Design and Simulation of MEMS Cantilever based Capacitive Sensor", in *National Conference on Science, Engineering and Technology (NCSET – 2016)*, 2016.
- [76] **J. Kalambe and R. Patrikar**, "Design of Microcantilever-Based Biosensor with Digital Feedback Control Circuit", *Journal of Sensors*, vol. 2012, pp. 1-9, 2012.
- [77] **A. Arnau** (2008) *Piezoelectric transducers and applications*. New York: Springer.
- [78] **S. Faegh, N. Jalili and S. Sridhar**, "A Self-Sensing Piezoelectric MicroCantilever Biosensor for Detection of Ultrasmall Adsorbed Masses: Theory and Experiments", *Sensors*, vol. 13, no. 5, pp. 6089-6108, 2013.
- [79] **Piezoresistive effect**. *Wikipedia*. Accessed: September 28, 2016, https://en.wikipedia.org/wiki/Piezoresistive_effect.
- [80] **S. R, P. JM and P. Deep**, "DESIGN of MICRO CANTILEVER BEAM for VAPOUR DETECTION USING COMSOL MULTI PHYSICS SOFTWARE", *International Journal of Engineering and Technology (IJET)*, vol. 7, no. 3, 2015.
- [81] **R. Ab. Rahim, B. Bais and B. Yeop Majlis**, "Design and Analysis of MEMS Piezoresistive SiO₂ Can tilever\$based Sensor with Stress Concentration Region for Biosensing Applications", in *IEEE International Conference on Semiconductor Electronics (ICSE 2008)*, Johor, Malaysia, 2008.
- [82] **N. Korlina Madzhi and A. Ahmad**, "Design Simulation and Analysis of Polysiliconbased CMOS Micromachined Piezoresistive Microcantilever for Glucose Sensing", in the *World Congress on Engineering (WCE)*, London. UK, 2012.

- [83] **D. Parsediya, J. Singh and P. Kankar**, "Simulation and Analysis of Highly Sensitive MEMS Cantilever Designs for "in vivo Label Free" Biosensing", *Procedia Technology*, vol. 14, pp. 85-92, 2014.
- [84] **S. S. and V. Juliet A.**, "Piezoresistive MEMS Cantilever based CO₂ Gas Sensor", *International Journal of Computer Applications*, vol. 49, no. 18, pp. 6-10, 2012.
- [85] **S. Manzeli, A. Allain, A. Ghadimi and A. Kis**, "Piezoresistivity and Strain-induced Band Gap Tuning in Atomically Thin MoS₂", *Nano Letters*, vol. 15, no. 8, pp. 5330-5335, 2015.
- [86] **Strain engineering**. *Wikipedia*. Accessed: October 05, 2016, https://en.wikipedia.org/wiki/Strain_engineering.
- [87] **Strain Gauges : Electrical Instrumentation Signals - Electronics Textbook**. *All about circuits*. Accessed: October 05, 2016, <http://www.allaboutcircuits.com/textbook/direct-current/chpt-9/strain-gauges/>.
- [88] **S. Meti, K. B. Balavald and B. G. Sheeparmatti**, "MEMS Piezoresistive Pressure Sensor: A Survey", Shwetha Meti et.al. *Int. Journal of Engineering Research and Applications*, vol. 6, no. 4, 2016.
- [89] **Y. Sun, S. Thompson and T. Nishida**, *Strain effect in semiconductors*. New York: Springer, 2010.
- [90] **K. Naeli**, "Optimization of Piezoresistive Cantilevers for Static and Dynamic Sensing Applications", Ph.D, Georgia Institute of Technology, 2009.
- [91] **C. Smith**, "Piezoresistance Effect in Germanium and Silicon", *Physical Review*, vol. 94, no. 1, pp. 42-49, 1954.
- [92] **S. Dyer**, *Survey of instrumentation and measurement*. New York: Wiley, 2001.
- [93] **Measuring Strain with Strain Gages**. *National Instruments*. Accessed: October 05, 2016, <http://www.ni.com/white-paper/3642/en/>.
- [94] **J. Harkey and T. Kenny**, "1/f noise considerations for the design and process optimization of piezoresistive cantilevers", *Journal of Microelectromechanical Systems*, vol. 9, no. 2, pp. 226-235, 2000.
- [95] **V. Lindroos**, *Handbook of silicon based MEMS materials and technologies*. Amsterdam: William Andrew/Elsevier, 2010.
- [96] **V. Mounika Reddy and G. Sunil Kumar**, "Design And Analysis of Microcantilevers With Various Shapes. Using COMSOL Multiphysics Software", *International Journal of Emerging Technology and Advanced Engineering*, vol. 3, no. 3, 2013.
- [97] **S. Arora, A. Arora and P. George**, "Design Of Mems Based Microcantilever Using Comsol Multiphysics", *International Journal of Applied Engineering Research*, vol. 7, no. 11, 2012.
- [98] **G. Villanueva, G. Rius, J. Montserrat, F. Perez-Murano and J. Bausells**, "Piezoresistive Microcantilevers for Biomolecular Force Detection," in *2007 Spanish Conference on Electron Devices*, 2007.

- [99] **R. Ab. Rahim, B. Bais and B. Yeop Majlis**, "Design and analysis of MEMS piezoresistive SiO₂ cantilever-based sensor with stress concentration region for biosensing applications", in ICSE 2008. IEEE International Conference on Semiconductor Electronics, 2008.
- [100] **B. Ashok Kumar and K. Srinivasa Rao**, "PIEZORESISTIVE CANTILEVER BASED MEMS BIO-SENSOR", Journal of Mechanics and MEMS (J M M), vol. 8, no. 2, 2016.
- [101] **V. Chivukula, M. Wang, H. Ji, A. Khaliq, J. Fang and K. Varahramyan**, "Simulation of SiO₂-based piezoresistive microcantilevers", Sensors and Actuators A: Physical, vol. 125, no. 2, pp. 526-533, 2006.
- [102] **M. Ansari and B. Gangadhara**, "Piezoresistivity and its Applications in Nanomechanical Sensors," in International Conference on Advances in Manufacturing and Materials Engineering, ICAMME 2014, Mangalore, Karnataka, India, 2014.
- [103] **B. Abdelaziz, K. Fouad and S. Kemouche**, "The Effect of Temperature and Doping Level on the Characteristics of Piezoresistive Pressure Sensor," Journal of Sensor Technology, vol. 4, 2014.
- [104] **D. Kishore Parsediya, J. Singh and P. Kumar Kankar**, "Simulation and analysis of highly sensitive MEMS cantilever designs for "in vivo label-free" biosensing," Procedia Technology, vol. 14, 2014.
- [105] **H. Hawari, Y. Wahab, M. Azmi, A. Shakaff, U. Hashim and S. Johari**, "Design and Analysis of Various Microcantilever Shapes for MEMS-Based Sensing," Journal of Physics: Conference Series 495, 2014.
- [106] **A. Gupta, R. Bashir, G. Neudeck and M. McElfresh**, "Design of piezoresistive silicon cantilevers with stress concentration region (SCR) for scanning probe microscopy (SPM) applications," in International Conference on Modeling and Simulation of Microsystems - MSM 2000, United States, 2000.
- [107] **Sh Mohd Firdaus, Husna Omar and Ishak Abd Azid**. (2012). Finite Element Analysis - New Trends and Developments. *Chapter 11: High Sensitive Piezoresistive Cantilever MEMS Based Sensor by Introducing Stress Concentration Region (SCR)*. InTech.
- [108] **X. Zhang, M. Yang, K. Vafai and C. S. Ozkan**, "Design and Analysis of Microcantilevers for Biosensing Applications," Journal of Laboratory Automation, vol. 8, no. 2, 2003.
- [109] **I. Ethem SACU and M. ALCI**, "DESIGN OF A BASIC PIEZORESISTIVE MICROCANTILEVER BIOSENSOR," Istanbul University- Journal of Electrical and Electronics Engineering (IU-JEEE), vol. 13, no. 2, 2013.
- [110] **B. Ashok Kumar and K. Srinivasa Rao**, "PIEZORESISTIVE CANTILEVER BASED MEMS BIO-SENSOR," Journal of Mechanics and MEMS (JMM), vol. 8, no. 2, 2016.
- [111] **S. Subhashini and A. Vimala Juliet**, "Piezoresistive Mems Cantilever-based Co₂ Gas Sensor", International Journal of Computer Applications, vol. 49, no. 18, 2012.

- [112] **S. Senturia, *Microsystem Design, 1st ed.* Boston, MA: Springer US, 2002.**
- [113] **B. David William,** "Micromechanics of integrated sensors and the planar processed pressure transducer", Ph.D, Material science, University of Wisconsin-Madison, 1988.
- [114] **K. Madhavi, M. Krishna and C. Chandrasekhara,** "Design of a Piezoresistive Micro Pressure Sensor using Finite Element Analysis," International Journal of Computer Applications, vol. 70, no. 3, 2013.
- [115] **J. Doll and B. Pruitt,** Piezoresistor design and applications, 1st ed. 2013.
- [116] **B. Bais, R. Ab Rahim and B. Yeop Majlis,** "Finite Element and System Level Analyses of Piezoresistive Microcantilever for Biosensing Applications", Australian Journal of Basic and Applied Sciences, vol. 5, no. 12, 2011.
- [117] **R. Ab. Rahim, B. Bais and B. Yeop Majlis,** "Design and analysis of MEMS piezoresistive SiO₂ cantilever-based sensor with stress concentration region for biosensing applications", in ICSE 2008. IEEE International Conference on Semiconductor Electronics, 2008.
- [118] **I. SACU and M. ALCI,** "DESIGN OF A BASIC PIEZORESISTIVE MICROCANTILEVER BIOSENSOR", I. E. SACU and M. ALCI/ IU-JEEE, vol. 13, no. 2, 2013.
- [119] **A. Swami and P. Agarwal,** "Design And Analysis of Microcantilevers Type Sensor With Different Shape of Piezoresistive Patch", International Journal of Emerging Trends in Electrical and Electronics, vol. 11, no. 2, 2015.

CURRICULUM VITAE



Name Surname : Amal Ahmed
Place and Date of Birth : Sudan 07/02/1990
E-Mail : ahmeda@itu.edu.tr

EDUCATION

- **B.Sc.** : 2011, University of Khartoum, Faculty of Engineering, Electrical and Electronics Engineering Department.

PROFESSIONAL EXPERIENCE AND REWARDS:

- 2011: Awarded from Schlumberger Company for outstanding achievement in the 2010/2011 Academic Year.
- August 2011 – September 2013: Electronics Research and Development Engineer – U of K CubeSat project
- March 2013 – June 2013: Part-Time Teaching Assistant, University of Khartoum
- 2013-now: Turkey Burslari Full Scholarship holder to study master in Nano-Science and Nano-Engineering at Istanbul Technical University (ITU) after completing the first year studying the Turkish language.
- February 2014 – Now: Full-Time Teaching Assistant, University of Khartoum
- November 2014 – June 2015: Arabic Electrical Circuits translator #101091, Professional Education Organization International (PEOI) (Volunteer)
- 2016 Best Delegate Award in my participation in Fatih University Model United Nations Conference (FUMUN2016).